The Effect and Prevention of Trace Metal Contaminants on CO_2 Reduction by Heterogenous Copper Catalyst

by

Kwan Yee Leung

A dissertation submitted in partial fulfillment
of the requirements for the degree of
Doctor of Philosophy
(Chemistry)
in the University of Michigan
2020

Doctoral Committee:

Assistant Professor Charles McCrory, Chair
Professor Stephen Maldonado
Associate Professor Paul Zimmerman
Professor Rachel Goldman

Kwan Yee Leung

kwanle@umich.edu

ORCID iD: 0000-0002-5292-4569

Dedication

This edition of *The Effect and Prevention of Trace Metal Contaminants on CO_2 Reduction by Heterogeneous Copper Catalyst* is dedicated to those who provided unconditional support throughout my graduate journey. I would like to dedicate my work to my parents, who were extremely supportive of my decisions, and my sister, who encouraged me in her own way. I especially thank our family cat Elly for being incredibly patient whenever I seek comfort through hugging and petting her.

To my great friends Mani, Estra, Aleesha, Alice, Jimmy, Yan, and Charlotte, thank you for allowing me to express my emotions for hours on end about my life. I also want to mention my remarkable long-term teachers in elementary school, Ms. Ho and Ms. Ma. I could not have completed my education without the foundation established by them. My academic success is attributed to them. I dedicate my work to all my amazing friends and lifetime teachers.

Finally, I would like to dedicate this work to all Brothers and Sisters, or my "Hands and Feet", who share a common goal with me. Through my graduate journey, I hope to show them that dedication and persistence is the key to achieving a goal. I will always remember all of you in my heart. May our goal becomes reality in the near future.

Acknowledgements

This dissertation could not be completed without the immense help and support that I received in many ways in the past 5 years. I thank my advisor, Professor Charles McCrory, for being a great mentor in providing guidance, not only about being a graduate student, but also about long term goals in our lives. I also want to thank Professor Stephen Maldonado for deepening my understanding of electrochemistry. My research would be significantly delayed without the advice given by Professor Paul Zimmerman in my candidacy exam. I also thank Professor Rachel Goldman for providing a new perspective on the definition of trace metal, which helped me reshape the scope of my research. My successful PhD career would not happen without my undergraduate training in electrochemistry by Professor Anne Co from The Ohio State University, and I sincerely thank her.

Other than faculties, the staff members in the Department of Chemistry also played an important role in my PhD study. I thank James Windak for the help with the measurement and interpretation of ICP-MS data, and Roy Wentz for the help with the design and construction of the custom glassware used in all of my experiments. Aside from research, the expertise from my Graduate Coordinators Liz Oxford and Katie Foster as well as Student Service Manager Heather Hanosh allowed me to smoothly proceed my graduate school career. I thank them for always making sure I had the proper resources and reminding me about deadlines.

A successful graduate journey always comes with a group of awesome teammates. I thank the entire McCrory lab for everyone's effort to start a new lab from scratch. The group provide a

comforting yet inspiring environment for my everyday life in the University of Michigan, and I am truly grateful for having this motivating family in my research career. I also want to thank April, Molly, Sarah, and Bernadette from the Department of Chemistry. They are always happy to listen to my worries and struggles and are always excited when I share positive news happened during my graduate life. In addition to mental support, they would always give fresh perspectives about science whenever we discuss our research projects. Through conversations with them, who conduct research in a related yet distinctly different science topic, I was able to sharpen my communication skills in exchanging scientific ideas with chemists in various research areas. I cannot appreciate more for the friendship, both in personal life and in my science career, that we developed in the last few years.

One of my other memorable accomplishments in my graduate career is my achievements in teaching, consulting, and education development. Teaching and education were a completely new field to me when I joined the University of Michigan and ultimately became my most passionate subject during my graduate experience. I thank Dr. Carol Ann Castañeda and Dr. Alex Poniatowski for the opportunity of becoming a Graduate Student Mentor. I would like to especially acknowledge and thank the Center for Research in Learning and Teaching, Dr. Nicole Tuttle, and Dr. Ronit Ajlen for giving me the opportunity to become a Graduate Student Instructional Consultant. Finally, I thank Professor Ginger Shultz, Jeff, and Eleni from the Shultz group for organizing the instructional coaching program and giving me the chance to become an instructional coach. Through my roles as a GSM, a GSIC, and an instructional coach, I learned many valuable lessons about teaching. Not only did I learned how to effectively communicate and help manage a large team of fellow instructors from being a GSM, the role of GSIC and instructional coach continuously taught me countless lessons on best practices in teaching and creating an inclusive

learning environment. More importantly, I learned crucial skills on conducting classroom observations and teaching consultations particularly on classroom interaction. I also acquired the skills to assist instructors to continuously improve and reshape their teaching strategies as well as teaching goals through my position as an instructional coach. All lessons and skills I learned from these experiences have a remarkable impact on my view of my career and personal life.

At last, I would also like to thank Hawkeye the Wellness Dog, who is a source of great comfort at some of my most difficult moments.

From the bottom of my heart, I thank everyone along the way who encouraged me and provided support that led to my success and accomplishment.

Table of Contents

Dedication ii

Acknowledgements iii

List of Tables ix

List of Figures xiv

List of Equations xxiii

Abstract xxiv

Chapter 1: Research Motivation of CO_2 Reduction at Cu Electrodes: Factors Influencing Activity and Product Distribution 1

1.1 Introduction to problem: CO_2RR on Cu electrodes 1

1.2 Applied Potential 3

1.3 CO_2 Concentration, Bulk and Local pH, and Buffer Capacity 9

1.4 Effect of Electrolyte Cation on Product Distribution 23

1.5 Porous and Nanostructured Cu Catalysts 25

1.6 Research Motivation and Trace Metal Contamination 28

1.7 References 35

Chapter 2: Effect and Prevention of Trace Ag Contamination from Ag/AgCl Reference Electrodes on CO_2 Reduction Product Distributions at Polycrystalline Copper Electrodes 49

2.1 Preface 49

2.2 Introduction 49

2.3 Experimental 51

2.4 Result and Discussion 59

2.5 Conclusion 80

2.6 References 81

Chapter 3: Effect of Trace Metal Contaminants and Material Pre-treatments on Product Distribution of CO_2 Reduction by Heterogeneous Copper Catalyst 84

3.1 Preface 84

3.2 Introduction 84

3.3 Experimental 88

3.4 Results and Discussion 91

3.5 Conclusion 114

3.6 References 116

Chapter 4: Conclusion and Future Outlook on Methods to Mitigate Trace Metal Contamination 121

4.1 Preface 121

4.2 Conclusion and Summary 121

4.3 Future outlook 123

4.4 References 132

Appendix 134

List of Tables

Table 0-1 Product Faradaic efficiencies of Cu CO_2RR under standard conditions, using double-junction Ag/AgCl/KCl(sat.) 136

Table 0-2 Product Faradaic Efficiencies of Cu CO_2RR, Single-Junction Ag/AgCl/KCl(sat.) ... 137

Table 0-3 Amount of Ag^+ leached from Ag/AgCl/KCl(sat.) under no polarization in water for 24 h. Limit of quantification is 0.5 ppb. 137

Table 0-4 Baseline amount of possible Ag^+ contamination in acidic solutions used in the studies. Limit of quantification is 0.5 ppb. 139

Table 0-5 Baseline amount of possible Ag^+ contamination in electrochemical cell components. Solid samples were etched by 10 mL of 1 M trace metal grade HNO_3. Limit of quantification is 5 ng in 10 mL sample..... 139

Table 0-6 Ag^+ concentration in electrolyte (0.1 M H_2SO_4) in working chamber under polarization after Ni HER. Limit of quantification is 0.5 ppb. 139

Table 0-7 Ag^+ deposited on Ni foil under polarization after Ni HER. Limit of quantification is 5 ng in 10 mL sample..... 140

Table 0-8 Amount of Ag^+ deposited on 99.999% Cu foil during CO_2RR. Limit of quantification is 5 ng in 10 mL sample..... 140

Table 0-9 Product Faradaic efficiencies of long-term Cu CO2RR, potential between –1.600 and –1.630 V vs Ag/AgCl/KCl(sat.)..... 140

Table 0-10 Amount of Ag^+ deposited on 99.999% Cu foil during long-term (12 h) CO_2RR. Limit of quantification is 5 ng in 10 mL sample. 141

Table 0-11 Product Faradaic efficiencies of Cu CO2RR using double frit with Ag titration, potential between –1.570 and –1.610 V vs Ag/AgCl. 141

Table 0-12 Ag^+ deposited on Cu foil after CO_2RR under Ag^+ titration with externally added Ag^+. Limit of quantification is 5 ng in 10 mL sample. 142

Table 0-13 Baseline amount of possible metal contamination in ppb in acidic solutions used in the studies. Limit of quantification is 0.5 ppb. 143

Table 0-14 Baseline amount of possible metal contamination in ng in electrochemical cell components. Solid samples were etched by 10 mL of 1 M trace metal grade HNO_3. Limit of quantification is 5 ng in 10 mL sample (50 ng for Fe). 143

Table 0-15 Metal etched in ng from membranes and auxiliary electrodes. Solid samples were etched by 10 mL of 1 M trace metal grade HNO_3. Limit of quantification is 5 ng in 10 mL sample (50 ng for Fe). 144

Table 0-16 Product Faradaic efficiencies of Cu CO_2RR under standard conditions + different membrane/auxiliary electrode, using double-junction Ag/AgCl/KCl(sat.), potential range –1.55 V to – 1.61 V vs Ag/AgCl. 144

Table 0-17 Metal present in working and auxiliary chambers after Ni HER using different membrane/auxiliary electrodes. Limit of quantification is 0.5 ppb. 145

Table 0-18 Metal etched in ng from Ni after HER using different membrane/auxiliary electrodes. Solid samples were etched by 10 mL of 1 M trace metal grade HNO_3. Limit of quantification is 5 ng in 10 mL sample (50 ng for Fe). 146

Table 0-19 Product Faradaic efficiencies of Cu CO_2RR under standard conditions + 99.95% Cu, using double-junction Ag/AgCl/KCl(sat.) 147

Table 0-20 Product Faradaic efficiencies of Cu CO_2RR under standard conditions + 99.8% Cu, using double-junction Ag/AgCl/KCl(sat.) 148

Table 0-21 Metal etched in ng from different purity Cu foil before and CO_2RR under standard condition. Solid samples were etched by 10 mL of 1 M trace metal grade HNO_3. Limit of quantification is 5 ng in 10 mL sample (50 ng for Fe). 150

Table 0-22 Product Faradaic efficiencies of Cu CO_2RR under standard conditions + resin-treated trace metal grade Na_2CO3, using double-junction Ag/AgCl/KCl(sat.) 150

Table 0-23 Product Faradaic efficiencies of Cu CO_2RR under standard conditions + untreated trace metal grade Na_2CO3, using double-junction Ag/AgCl/KCl(sat.) 151

Table 0-24 Product Faradaic efficiencies of Cu CO_2RR under standard conditions + resin-treated BioXtra grade $NaHCO_3$, using double-junction Ag/AgCl/KCl(sat.) 151

Table 0-25 Product Faradaic efficiencies of Cu CO_2RR under standard conditions + untreated BioXtra grade $NaHCO_3$, using double-junction Ag/AgCl/KCl(sat.) 152

Table 0-26 Product Faradaic efficiencies of Cu CO_2RR under standard conditions + pre-electrolysis HPLC grade $NaHCO_3$, using double-junction Ag/AgCl/KCl(sat.) 152

Table 0-27 Product Faradaic efficiencies of Cu CO_2RR under standard conditions + untreated HPLC grade $NaHCO_3$, using double-junction Ag/AgCl/KCl(sat.) 153

Table 0-28 Product Faradaic efficiencies of Cu CO_2RR under standard conditions + resin-treated ACS grade $NaHCO_3$, using double-junction Ag/AgCl/KCl(sat.) 153

Table 0-29 Product Faradaic efficiencies of Cu CO_2RR under standard conditions + untreated ACS grade $NaHCO_3$, using double-junction Ag/AgCl/KCl(sat.) 154

Table 0-30 Metal etched in ng from 99.999% Cu foil after CO_2RR under standard condition + different purity and pre-treatment of bicarbonate electrolyte. Solid samples were etched by 10 mL of 1 M trace metal grade HNO_3. Limit of quantification is 5 ng in 10 mL sample (50 ng for Fe). 156

Table 0-31 Product Faradaic efficiencies of CO_2RR using glassy carbon electrodes under 0.1 M untreated BioXtra grade $KHCO_3$, with Nafion as the membrane and carbon rod as the auxiliary electrode. 157

Table 0-32 Product Faradaic efficiencies of CO_2RR using glassy carbon electrodes with 0.04% P4VP under 0.1 M untreated BioXtra grade $KHCO_3$, with Nafion as the membrane and carbon rod as the auxiliary electrode. 157

Table 0-33 Product Faradaic efficiencies of Au CO_2RR under 0.1 M untreated BioXtra grade $KHCO_3$, with Nafion as the membrane and carbon rod as the auxiliary electrode. 157

Table 0-34 Product Faradaic efficiencies of Au CO_2RR with 0.04% P4VP under 0.1 M untreated BioXtra grade $KHCO_3$, with Nafion as the membrane and carbon rod as the auxiliary electrode. 157

Table 0-35 Product Faradaic efficiencies of Au CO_2RR with 0.1% P4VP under 0.1 M untreated BioXtra grade $KHCO_3$, with Nafion as the membrane and carbon rod as the auxiliary electrode. 158

Table 0-36 Product Faradaic efficiencies of Au CO_2RR with 1.0% P4VP under 0.1 M untreated BioXtra grade $KHCO_3$, with Nafion as the membrane and carbon rod as the auxiliary electrode. 158

Table 0-37 Product Faradaic efficiencies of CO_2RR using glassy carbon electrodes with 0.04% P4VP and 0.02% Au under 0.1 M untreated BioXtra grade $KHCO_3$, with Nafion as the membrane and carbon rod as the auxiliary electrode. 158

Table 0-38 Product Faradaic efficiencies of CO_2RR using glassy carbon electrodes with 0.04% P4VP and 0.16% Au under 0.1 M untreated BioXtra grade $KHCO_3$, with Nafion as the membrane and carbon rod as the auxiliary electrode. 158

Table 0-39 Product Faradaic efficiencies of CO_2RR using glassy carbon electrodes with 0.04% P4VP and 0.32% Au under 0.1 M untreated BioXtra grade $KHCO_3$, with Nafion as the membrane and carbon rod as the auxiliary electrode. 159

List of Figures

Figure 1-1 The product distribution of Cu catalyzed CO_2RR under different applied potentials.[11] Republished with permission of the Royal Society of Chemistry (Great Britain), from Energy Environ. Sci., 2012, 5, 7050–7059; permission conveyed through Copyright Clearance Center, Inc. 4

Figure 1-2 The product distribution of the Ag-catalyzed CO_2RR under different applied potentials.[24] Republished with permission of the Royal Society of Chemistry (Great Britain), from Phys. Chem. Chem. Phys., 2014,16, 13814-13819*;* permission conveyed through Copyright Clearance Center, Inc. 7

Figure 1-3 The product distribution of the Au-catalyzed CO_2RR under different applied potentials.[25] Republished with permission of the Royal Society of Chemistry (Great Britain), from Phys. Chem. Chem. Phys., 2017, 19, 15856*;* permission conveyed through Copyright Clearance Center, Inc. 8

Figure 1-4 Product distribution of the Cu CO_2RR under various CO_2 pressure.[26] Republished with permission of IOP Publishing, Ltd, from Electrochimica Acta, 2006, 51, 4880*;* permission conveyed through Copyright Clearance Center, Inc. 10

Figure 1-5 The calculated change in local pH in different electrolyte concentration with a $KHCO_3$ buffer solution at 50 A/m^2 and 150 A/m^2 current densities, assuming the boundary layer thickness of 0.01 cm.[27] Republished with permission of Springer Nature, from Journal of Applied

Electrochemistry, 2006, 36, 161; permission conveyed through Copyright Clearance Center, Inc. 13

Figure 1-6 (top) Local pH at the electrode surface, and (bottom) local CO_2 concentration at the electrode surface as a function of time at 2.5, 5, and 10 mA/cm^2 current densities in a bicarbonate buffer.[20] Adapted with permission from *ACS Catal.* 2017, 7, 12, 8467-8479. Copyright 2017 American Chemical Society. 14

Figure 1-7 (a) Illustration of mass transport of CO_2 and H^+ species during CO_2RR at the surface of a metal electrode, and (b) the concentration gradient of CO_2 and H^+ near the electrode surface.[14] Reprinted with permission from Yingshuo Liu, Kwan Yee Leung, Samuel E. Michaud, Taylor L. Soucy & Charles C. L. McCrory. *Comments on Inorganic Chemistry*, 2019. 15

Figure 1-8 (top) The product distribution of Cu nanoparticle catalyzed CO_2RR using different concentration of bicarbonate buffers, and (bottom) under different CO_2 pressure.[19] Adapted with permission. 19

Figure 1-9 Possible mechanism for CO_2RR basic on the pH-dependence observed for the formation of products such as CH_4 and CH_3OH, and pH-independence observed for the formation of C_2H_4. Reprinted with permission.[19] 21

Figure 1-10 Partial current densities of CO_2RR products (H_2, CO, $COOH^-$, CH_4, C_2H_4, and EtOH) as a function of electrolyte cations.[49] As the size of the electrolyte cation increases, there is increased production of HCOOH and the C_2 products C_2H_4 and CH_3CH_2OH. Adapted with permission from J. Am. Chem. Soc. 2017, 139, 11277−11287. Copyright (2017) American Chemical Society. 24

Figure 1-11 (a) Top down and (b) cross-sectional SEM images of a mesostructured Ag film with ~200 nm voids interconnected by ~50 nm diameter channels. (c) H_2 production shown here as a specific current density j_{H2}, decreases with increasing roughness factor, and (d) CO production increases with increasing roughness factor.[52] Adapted with permission. 26

Figure 1-12 SEM images showing (a) electropolished Cu surface (b) nanoparticles covered Cu surface (c) sputtered Cu surface, and (bottom) the CO_2RR product distribution using these surfaces.[15] Adapted with permission of Royal Society of Chemistry (Great Britain), from Phys. Chem. Chem. Phys., 2012, 14, 76–81*;* permission conveyed through Copyright Clearance Center, Inc. 27

Figure 1-13 Design of the forced convective electrochemical flow cell, used in the initially proposed research..... 30

Figure 1-14 Product distribution of the initial preliminary data of Cu CO_2RR, with a saturated calomel electrode (SCE) as the reference electrode. 31

Figure 1-15 Faradaic efficiencies of (A) CH_4 (B) CO (C) C_2H_4 and (D) H_2 of the Cu CO_2RR over time when the bicarbonate electrolyte was untreated (black), pre-treated with EDTA (red), and pre-treated with chelating resin (blue).[73] Reprinted with permission from *ACS Catal.* 2015, 5, 7, 4479-4484. Copyright (2015) American Chemical Society. 33

Figure 2-1 Product distributions for CO_2RR at Cu electrodes using (a-b) single junction Ag/AgCl/KCl(sat.) reference electrodes and (c-d) double junction Ag/AgCl/KCl(sat.)/$NaHCO_3$(0.1 M) reference electrodes. (a) and (c) show the full product distribution range (0-100% Faradaic efficiency) and highlight relative H_2 and CH_4 production. (b)

and (d) zoom in to the 0-8% Faradaic efficiency range and highlight relative CO, HCOOH, and C_2H_4 production. 61

Figure 2-2 Average values of the product distributions for CO_2RR at Cu electrodes in 20 mV intervals using (a-b) single junction Ag/AgCl/KCl(sat.) reference electrodes and (c-d) double junction Ag/AgCl/KCl(sat.)/$NaHCO_3$(0.1 M) reference electrodes. (a) and (c) show the full product distribution range (0-100% Faradaic efficiency) and highlight relative H_2 and CH_4 production. (b) and (d) zoom in to the 0-8% Faradaic efficiency range and highlight relative CO, HCOOH, and C_2H_4 production. All error bars are the standard deviations from at least 3 measurements within the interval. Half-shaded symbols represent average values from less than 3 measurements within the potential interval. 62

Figure 2-3 Concentration of Ag^+ in aqueous solution detected by ICP-MS after storing reference electrodes in pure water for 24 h. Error bars are standard deviations from at least 3 independent measurements. Note, the measurements for the double-junction reference electrode and water background are near the limit of quantification for the ICP-MS instrument (0.5 ppb). 65

Figure 2-4 (a) Concentration of Ag^+ in the electrolyte solution detected by ICP-MS after HER CPEs. The H_2SO_4 background is the Ag^+ concentration measured in an as-prepared 0.1 M H_2SO_4 solution. Note the measurements for the double-junction reference electrode and the H_2SO_4 background are near the limit of quantification for the ICP-MS instrument (0.5 ppb). (b) Amount of Ag^+ etched from HER post-CPE Ni electrodes using 1 M HNO_3. The Ni background is the amount of Ag^+ etched from as-polished Ni electrodes. Note that all etched Ag^+ amounts are near the limit of quantification for these electrodes (5 ng). All error bars are standard deviations from at least 3 independent measurements. 70

Figure 2-5 Amount of Ag^+ etched from CO_2RR Cu electrodes post-CPE using 1 M HNO_3. The Cu background is the amount of Ag^+ etched from as-polished Cu electrodes. Error bars are standard deviations from at least 3 independent measurements. Note that etched Ag^+ amounts from the Cu background and double-junction reference electrode experiments are near the limit of quantification for these electrodes (5 ng)..... 71

Figure 2-6 (a) Product distributions of CH_4 and CO for long-term (12 h) CO_2RR at a Cu electrodes at between -1.600 V to -1.630 V vs Ag/AgCl/KCl(sat.) with (a) single junction and (b) double junction reference electrodes. Faradaic efficiencies for the short-term experiments are from the data in our initial studies summarized in Figure 2-2 and Table 0-1 and Table 0-2. All error bars are the standard deviations from at least 3 measurements..... 74

Figure 2-7 Amount of Ag^+ etched from CO_2RR Cu electrodes after long-term (12 h) CPE measurements using 1 M HNO_3. The Cu background is the amount of Ag^+ etched from as-polished Cu electrodes. Error bars are standard deviations from at least 3 independent measurements. Note that etched Ag^+ amounts from the Cu background and double-junction reference electrode experiments are near the limit of quantification for these electrodes (5 ng). 75

Figure 2-8 (a) Product distributions for CO_2RR at Cu electrodes at a potential range of –1.570 V to –1.600 V vs Ag/AgCl/KCl(sat.)/$NaHCO_3$(0.1 M) double-junction reference electrodes at different concentrations of externally-added Ag^+. (b) Bar graph better illustrating the increase in Faradaic Efficiency for CO with increasing concentration of externally-added Ag^+. Error bars for the single products are standard deviations from at least 3 measurements within the interval. Error bars for the summed total Faradaic efficiency are the standard deviations calculated from the summed total of each experiment. 77

Figure 2-9 Amount of Ag^+ etched from Cu electrodes using 1 M HNO_3 after CO_2RR CPEs at –1.570 V to –1.600 V vs Ag/AgCl/KCl(sat.)/$NaHCO_3$(0.1 M) with various concentrations of Ag^+ added to the electrolyte solution in the working chamber. Error bars are standard deviations from at least 3 independent measurements. Note that the etched Ag^+ amounts from the Cu electrodes used in the CPEs in electrolyte solutions with 0 ppb and 1 ppb of added Ag^+ are near the limit of quantification for these electrodes (5 ng). 78

Figure 3-1 Amount of (a) Fe and (b) Sn etched from Nafion and Selemion AMV membranes. Error bars are standard deviations from at least 3 independent measurements. Limit of quantification is 5 ng..... 93

Figure 3-2 Metals etched out from auxiliary electrodes using 1 M HNO_3. Error bars are standard deviations from at least 3 independent measurements. Limit of quantification is 5 ng..... 94

Figure 3-3 Trace metals detected in 0.1 M H_2SO_4 electrolyte after Ni HER with (a) Nafion/carbon rod (b) Nafion/Pt (c) Selemion AMV/carbon rod and (d) Selemion AMV/Pt. Note that the axis scale of (d) is significantly different from others. Error bars are standard deviations from at least 3 independent measurements. Limit of quantification is 0.5 ppb. 97

Figure 3-4 Metals etched from Ni after HER using different membrane/auxiliary. Error bars are standard deviations from at least 3 independent measurements. Limit of quantification is 5 ng. 98

Figure 3-5 Product distribution of Cu CO_2RR with under standard conditions + different combinations of membrane/auxiliary. (a) Faradaic efficiencies of all measured products and (b) emphasis on the Faradaic efficiencies of H_2 and CH_4 for comparison. Potential between –1.55 V

and –1.61 V vs Ag/AgCl/KCl(sat.). Error bars are standard deviations from at least 3 independent measurements. 100

Figure 3-6 Faradaic efficiencies of H_2 and CH_4 of Cu CO_2RR under standard condition + different foil purities. Potential between –1.55 V and –1.61 V vs Ag/AgCl/KCl(sat.). Error bars are standard deviations from at least 3 independent measurements. 102

Figure 3-7 Faradaic efficiencies of H_2 and CH_4 from Cu CO_2RR under standard condition + resin-treated electrolyte, different starting grades. Potential between –1.55 V and –1.61 V vs Ag/AgCl/KCl(sat.). Error bars are standard deviations from at least 3 independent measurements. 105

Figure 3-8 Faradaic efficiencies of H_2 and CH_4 from Cu CO_2RR under standard condition + different starting purities and different electrolyte pre-treatments. Potential between –1.55 V and –1.61 V vs Ag/AgCl/KCl(sat.). Error bars are standard deviations from at least 3 independent measurements. 106

Figure 3-9 Change in current over time during Cu CO_2RR under standard condition + HPLC grade electrolyte with different pre-treatments. A representative sample of each condition is shown. Currents at each time point are normalized to the initial current. 109

Figure 3-10 Change in current over time during Cu CO_2RR under standard condition + resin-treated electrolyte with different starting purities. A representative sample of each condition is shown. Currents at each time point are normalized to the initial current. 110

Figure 3-11 Change in current over time during Cu CO_2RR under standard condition + untreated electrolyte with different starting purities. A representative sample of each condition is shown. Currents at each time point are normalized to the initial current. 111

Figure 3-12 Change in current over time during Cu CO_2RR under standard condition + 0 and 50 ppb of externally added Ag ions titrated into the resin-treated HPLC grade electrolyte with different pre-treatments. A representative sample of each condition is shown. Currents at each time point are normalized to the initial current. Inserted bar graph shows the product distribution when 0 an d50 ppb of Ag ions was added. 113

Figure 4-1 An example of overlayer-coated electrode.[111] Adapted with permission from ACS Catal. 2018, 8, 457−465. Copyright (2018) American Chemical Society. 124

Figure 4-2 Graphical representation of blend polymers. Blend polymer AB can be prepared by blending polymer A and B together before being deposited onto an electrode surface. 126

Figure 4-3 Pictures of (a) a polished glassy carbon disc electrode, (b) a glassy carbon disc electrode coated with 0.04% P4VP and 0.16% Au, before CO_2RR, (c) a glassy carbon disc electrode coated with 0.04% P4VP and 0.16% Au, after CO_2RR, (d) a solid state planar polycrystalline Au disc with 1% P4VP, before CO_2RR, (e) a solid state planar polycrystalline Au disc with 1% P4VP, after CO_2RR. 130

Figure 0-1 (a) Custom-made single-junction Ag/AgCl/KCl(sat.) reference electrode design. The AgCl-coated Ag wire is enclosed within a glass body filled with saturated KCl(*aq*) and separated from the electrolyte solution by a CoralPor® glass frit. (b) Glass frit which serves as the second junction. Custom-made glass body enclosed with a CoralPor® glass frit (c) Double-junction

Ag/AgCl/KCl(sat.)/$NaHCO_3$(0.1 M) reference electrode constructed by placing the single-junction Ag/AgCl/KCl(sat.) reference electrode into the glass body that serves as the second junction. The glass body is filled with electrolyte (resin-treated 0.1 M $NaHCO_3$(*aq*) or 0.1 M H_2SO_4) and separated from the electrolyte solution in the electrochemical cell by a CoralPor® glass frit. A stainless steel rod with an alligator clip is attached to the reference electrode during electrochemical measurements. 134

Figure 0-2 Design of glass electrochemical cell filled with electrolyte and stir bar. (1) single-junction Ag/AgCl/KCl(sat.) or double-junction Ag/AgCl/KCl(sat.)/$NaHCO_3$(0.1 M) reference electrode, (2) Nafion membrane, (3) carbon rod as auxiliary electrode, and (4) metal foil working electrode. Stainless steel rods and alligator clips were used for electrical contact for reference electrode and metal foil. Metal foil working electrode was submerged such that ~0.6 cm^2 was exposed to solution during each electrolysis. 135

Figure 0-3 (a) Ag (b) Fe (c) Mg (d) Pt (e) Sn and (f) Zn etched from different purities of Cu foils before and after CO_2RR under standard conditions. Error bars are standard deviations from at least 3 independent measurements. Limit of quantification is 5 ng. 149

Figure 0-4 (a) Ag (b) Fe (c) Mg (d) Pt (e) Sn and (f) Zn etched from Cu after CO_2RR under standard condition + different purity and pre-treatment of electrolytes. Error bars are standard deviations from at least 3 independent measurements. Limit of quantification is 5 ng. 155

List of Equations

CO_2 (g) ⇌ CO_2 (aq) 1-1 9

CO_2 (aq) + H_2O ⇌ H_2CO_3 1-2 9

H_2CO_3 ⇌ HCO_3^- + H^+ 1-3 9

HCO_3^{--} ⇌ CO_3^{2-} + H^+ 1-4 9

$kCO_2 + n(H^+ + e^-) \rightleftharpoons P + mH_2O$ 1-5 [13] 11

$FE = VHSVg \times G \times n \times FQ$ 2-1 57

$FE = M \times Vl \times n \times FQ$ 2-2 57

Abstract

Transforming carbon dioxide into a chemical feedstock or usable fuel has been one of the most widely studied topics in electrochemistry. Solid-state heterogeneous Cu surfaces and Cu-containing catalysts are among the most extensively studied electrochemical systems for the CO_2 reduction reaction (CO_2RR). However, reported electrocatalytic studies of the CO_2RR by Cu catalysts under putatively identical conditions show large variances in measured product distributions. In this dissertation, I share my efforts to quantify the effects of trace metal contamination on product distributions for the CO_2RR by Cu catalysts. Specifically, I show that Cu is *extremely* sensitive to trace metal impurities, and even sub-ppm levels of some impurities can measurably influence the product distributions. In this work, I identify the sources of trace metal contamination in typical electrochemical electrolysis experiments, quantify the amount of trace metal present under different electrolysis conditions, and demonstrate that seemingly trivial differences in experimental set up, purity of material, and material pre-treatment can have significant impacts on product distribution.

In **Chapter 1**, the background and motivation of my research is outlined. Although my initial dissertation research focused on studying the effect of controlled mass transport to Cu surfaces to control CO_2RR activity and product distribution, many of my initial attempts at reproducing experiments reported in the literature show very different product distributions than those reported. The discrepancies between my data and the literature reports became the motivation that led to my exploration of each step in the experimental procedure and material

preparation of Cu CO_2RR, and the associated changes in trace metal contamination as well as the effect in product distribution.

In **Chapter 2**, I present my work showing that the reference electrode can be a source of trace metal contamination that influences CO_2RR product distributions. One of the most common choices of reference electrodes, Ag/AgCl/KCl(sat.), was found to be a source of trace Ag^+ contamination, to which Cu surfaces were found to be extremely sensitive. Even ppb levels of Ag^+ in solution were shown to have dramatic effects on CO_2RR product distribution—for instance, decreasing Faradaic efficiency for CH_4 production and increasing Faradaic efficiency for CO production. We demonstrated that this problem can be mitigated by employing a different configuration of the reference electrode.

In **Chapter 3**, other materials used in CO_2RR experiments were explored as possible sources of trace metal contamination. It was observed that the ion exchange membrane and auxiliary electrode introduce trace metals into the electrochemical system. In addition, the starting purity of the foil and electrolyte and the pre-treatments of the electrolyte all influence the product distribution of CO_2RR. My results suggest that the Cu system is highly complex. The change in product distribution based on differences in experimental procedure cannot be easily predicted.

In **Chapter 4**, the major conclusions and future directions of Cu CO_2RR research are addressed. The use of a protective overlayer, such as a polymer coating, is critical for future research on the Cu system. Preliminary data as well as recommendations on future experiments are also included.

This dissertation work demonstrates the importance of understanding the true nature of the electrochemical system when performing CO_2RR, developing carefully designed control

experiments, and incorporating standardized experimental procedure across research groups for meaningful comparisons between CO_2RR studies.

Chapter 1: Research Motivation of CO_2 Reduction at Cu Electrodes: Factors Influencing Activity and Product Distribution

1.1 Introduction to problem: CO_2RR on Cu electrodes

The electrochemical conversion of CO_2 into value-added products and fuels in the CO_2 reduction reaction (CO_2RR) is one of the most important processes for the development of solar fuels technologies.[1-7] Different types of catalysts, including solid state catalysts and molecular catalysts, have been heavily investigated for their CO_2RR activity, and new catalysts are being synthesized. Among the most promising and most studied catalysts for the CO_2RR are solid-state Cu-based electrocatalysts in aqueous media because they can convert CO_2 to other C_1 and C_2 hydrocarbons at relatively high Faradaic efficiencies. However, a significant drawback of Cu electrocatalyst is that the conversion has poor selectivity. As many as 16 different products with various Faradaic efficiencies can be formed in the CO_2RR using polycrystalline Cu in aqueous electrolyte.[1,8-12] The large variety of products that can be generated using Cu catalysts suggests that the CO_2RR mechanism is rich and complex.[13] It is important to note that there are two different mechanistic criteria when considering the product distribution of the CO_2RR. The first is the reaction selectivity: whether the reaction will selectively perform CO_2RR over competitive hydrogen evolution reaction (HER). The second is the product selectivity: whether the reaction will selectively produce certain CO_2RR products over others.[14] Although the exact mechanism is still not completely understood, significant research has been conducted to shine light on the interplay of various factors such as applied potential, CO_2 concentration, bulk and local pH, buffer

capacity, cation of the electrolyte, and catalyst structure and their effects on product distributions in the CO_2RR on Cu electrocatalysts.[2,15-22]

The initial proposed research of this dissertation focused on understanding the CO_2RR mechanism by studying the role of mass transport of reactive species in controlling the product distribution. Specifically, the mass transport of CO_2, H^+, and intermediate species would be directly controlled using a forced convective electrochemical flow cell and the changes in product distribution would be analyzed. However, during the initial control experiments I was unable to reproduce literature results. Upon further exploration of the published literature, I found that the results of CO_2RR experiments were inconsistent between research groups. There were also seemingly minute discrepancies in sample and electrochemical cell preparation between different groups, and even within the same groups between different students. These discrepancies likely caused differences in the amount of trace metal contamination present in the electrochemical system, and led to further deviation in product distribution. The sources and differences in trace metal contamination due to the differences in sample preparation and experimental procedure, an area that is often overlooked by researchers of the CO_2RR, is extensively discussed in this original dissertation.

In this chapter, I will review and discuss the major factors that affects the product distribution of the Cu CO_2RR in **1.2** through **1.5**. Detailed explanation of the initial control experiments that deviated from the literature results and the resulting research motivation are discussed in **1.6**. Parts of sections **1.3**, **1.4**, and **1.5** are reprinted with permission from Yingshuo Liu, Kwan Yee Leung, Samuel E. Michaud, Taylor L. Soucy & Charles C. L. McCrory. *Comments on Inorganic Chemistry*, 2019.

1.2 Applied Potential

The two main types of CO_2RR catalysts are solid state and molecular catalysts. A primary advantage of solid state catalysts like heterogeneous Cu surfaces for theCO_2RR is the high activity and current density, but they suffer from low selectivity.[23] In general, high product selectivity can only be reached with very specific experimental conditions, such as operating within in narrow range of applied potentials in a specific electrolyte concentration, with a specific pH, and with a specific CO_2 concentration. Different applied potentials can drastically change the product distribution of Cu-catalyzed CO_2RR systems, as illustrated in Figure 1-1. The Faradaic efficiency of H_2 varies from 20% at –1.0 V to 80% at –0.65 V, and CH_4 from 0% at –1.1 V to about 30% at –0.9 V vs RHE. The origin and mechanism of the large differences in product distribution due to applied potential has been widely explored in literature.

When investigating the mechanism of the CO_2RR, Ag and Au are common model systems because of their relatively simple product distributions, which consist mainly of H_2 and CO. However, both Ag and Au suffer from low selectivity unless the reaction takes place within a narrow potential range. For example, as shown in Figure 1-2, Faradaic efficiency for CO of the Ag foil-catalyzed CO_2RR can reach over 90% within a narrow applied potential range between –1.0 to –1.1 V vs RHE. The selectivity for CO drops dramatically outside this range. A similar trend is observed for the Au foil-catalyzed CO_2RR as shown in Figure 1-3. The high product selectivity for CO only occurs within the potential range from –0.5 to –0.6 V vs RHE.

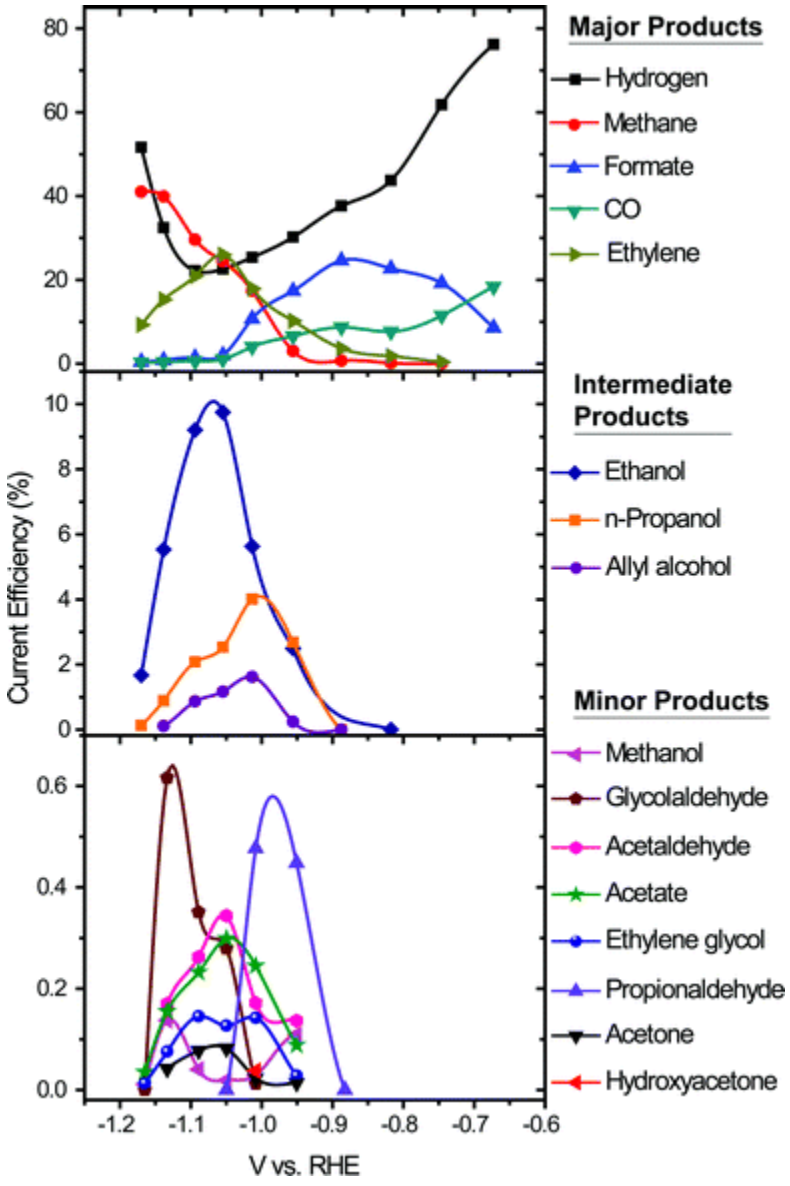

Figure 1-1 The product distribution of Cu catalyzed CO_2RR under different applied potentials.[11] Republished with permission of the Royal Society of Chemistry (Great Britain), from Energy Environ. Sci., 2012, 5, 7050–7059; permission conveyed through Copyright Clearance Center, Inc.

In the case of Ag as the model system, it is observed that as the applied potential becomes more negative, the current density of CO first increases then decreases, while the current density of H_2 remains relatively constant until it increases at a sufficiently negative potential, around –1.1 V vs RHE. The authors attributed this observation to a reaction switch from a kinetic limitation at more positive potentials to a mass transport limitation at more negative potentials.[24] Potentials more positive than –1.0 V show lower Faradaic efficiency for CO because the potential is not able to kinetically drive the CO_2RR to CO. At potentials more negative than –1.1 V, the rate of CO_2 consumption exceeds the rate at which CO_2 can be replenished at the electrode surface through mass transport. Therefore, the Faradaic efficiency for CO is highest in the narrow range of between –1.0 and –1.1 V, where the potential is sufficiently negative to kinetically drive the reaction, while the rate of CO_2 consumption is balanced by the rate of replenishment through mass transport. This mechanism can also be used to explain a similar phenomenon in Cu systems where the Faradaic efficiency for H_2 is lower at moderately negative potentials, but is much higher at potentials more negative than –1.1 V.

An interesting observation in Ag systems is that they catalyze the reduction of CO_2 to hydrocarbons such as CH_4 at very negative potentials. Computational studies show that the formation of hydrocarbons occurs via an adsorbed CO species on the electrode surface and is kinetically limited unless the system is polarized to very negative potentials (more negative than –1.2 V.[24] Computational studies have also helped to explain the unique capability of Cu systems to catalyze the reduction of CO_2 to various hydrocarbons. An optimal catalyst for hydrocarbon production from CO_2 should have an intermediate binding energy for adsorption of CO intermediate species on the catalyst surface. Cu has the appropriate CO adsorption energy: strong

enough to allow the CO intermediate to remain on the surface for further electrochemical reduction, but not so strong that the Cu electrode is poisoned by an inactive CO intermediate.[13]

Cu displays low product selectivity, and the product distribution is sensitive to the applied potential. Using Ag and Au as model systems, it is shown that the limitations in reaction kinetics and in mass transport are the underlying reasons for the effect of the applied potential. Furthermore, given the appropriate applied potential, Cu can form hydrocarbons at a relatively high Faradaic efficiency because of the appropriate binding energy for CO adsorption. In the cases of Ag and Cu shown here, the effect of the applied potential on the reaction selectivity is prominent, with the applied potential playing a significant role in determining whether the reaction will select the CO_2RR or HER path. However, it is only one of the many factors that affect the product distribution of Cu-catalyzed systems.

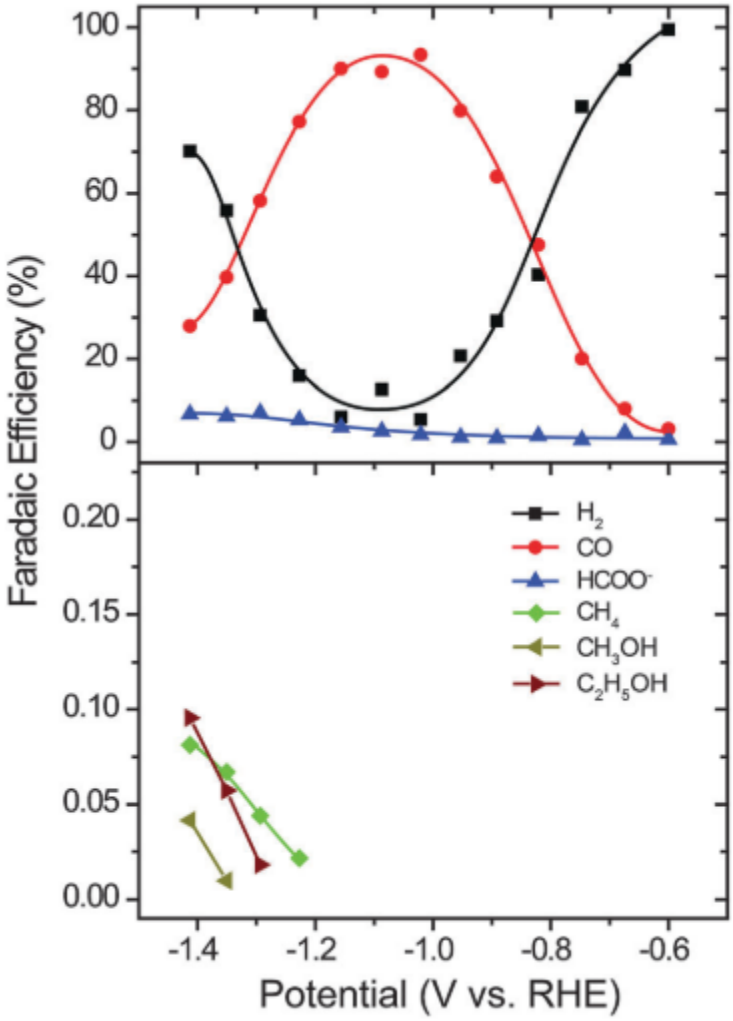

Figure 1-2 The product distribution of the Ag-catalyzed CO_2RR under different applied potentials.[24] Republished with permission of the Royal Society of Chemistry (Great Britain), from Phys. Chem. Chem. Phys., 2014,16, 13814-13819; permission conveyed through Copyright Clearance Center, Inc.

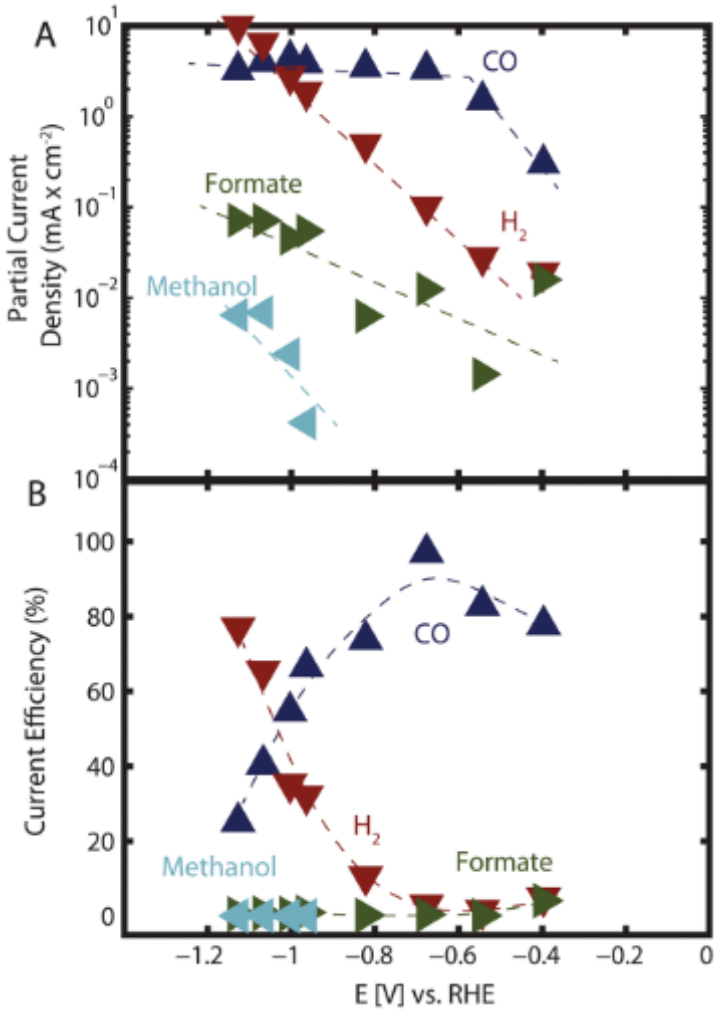

Figure 1-3 The product distribution of the Au-catalyzed CO_2RR under different applied potentials.[25] Republished with permission of the Royal Society of Chemistry (Great Britain), from Phys. Chem. Chem. Phys., 2017, 19, 15856; permission conveyed through Copyright Clearance Center, Inc.

1.3 CO_2 Concentration, Bulk and Local pH, and Buffer Capacity

The effects of CO_2 concentration, pH (both in the bulk electrolyte and the local electrolyte close to the electrode surface), and buffer capacity are considered the most complicated factor in product distribution of the CO_2RR because these elements are convoluted, and their individual effect cannot be easily separated and studied. The reaction selectivity and product selectivity of the CO_2RR heavily rely on the amount of CO_2 molecules available to be reduced at the surface.[2] One way to adjust the bulk concentration of CO_2 in the electrolyte is to perform CO_2RR experiments under different pressures of CO_2. Figure 1-4 illustrates the product distribution of gaseous hydrocarbons, H_2, HCOOH, and CO during Cu CO_2RR under different pressures of CO_2. The authors found that as the pressure increases, H_2 production decreases, suggesting the reaction selectivity towards CO_2RR increases with higher CO_2 concentration in the electrolyte. When the CO_2 pressure increases further, the product selectivity is also found to change from favoring gaseous hydrocarbons to favoring HCOOH. These observations illustrate the effect of bulk CO_2 concentration on product distribution, both on reaction selectivity and product selectivity.

The dissolution of CO_2 gas and the resulting CO_2 concentration in aqueous media during the CO_2RR is a complex process involving multiple equilibria as shown in equations 1-1 to 1-4.

$$CO_2\ (g) \rightleftharpoons CO_2\ (aq) \qquad 1\text{-}1$$

$$CO_2\ (aq) + H_2O \rightleftharpoons H_2CO_3 \qquad 1\text{-}2$$

$$H_2CO_3 \rightleftharpoons HCO_3^- + H^+ \qquad 1\text{-}3$$

$$HCO_3^{--} \rightleftharpoons CO_3^{2-} + H^+ \qquad 1\text{-}4$$

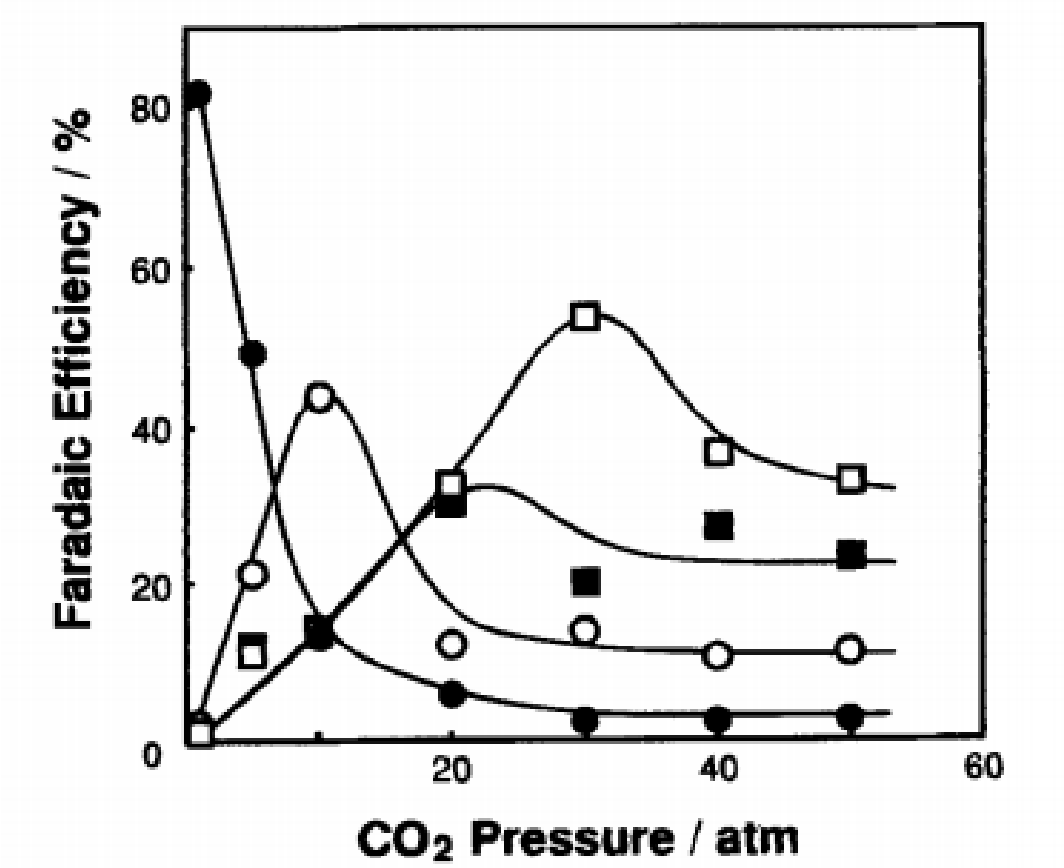

Fig. 2. Effect of CO_2 pressure on the electrochemical reduction of CO_2 on a Cu electrode with stirring of 0.1 mol dm^{-3} $KHCO_3$ at 25°C. Current density: 163 mA cm^{-2}. (○) Hydrocarbons, (●) H_2, (□) HCOOH, (■) CO.

Figure 1-4 Product distribution of the Cu CO_2RR under various CO_2 pressure.[26] Republished with permission of IOP Publishing, Ltd, from Electrochimica Acta, 2006, 51, 4880*;* permission conveyed through Copyright Clearance Center, Inc.

The CO_2/HCO_3^- equilibrium and the CO_2 solubility are dependent on the pH, with lower pH leading to more dissolved CO_2.[20,27] In addition to being affected by the bulk pH, the concentration of available molecular CO_2, especially at the local area near the electrode, is significantly affected by the reduction reaction itself.[28] Both the CO_2RR and HER consume H^+, as shown in equation 1-5, where P is the product of the reaction, and *k, n,* and *m* are integers to balance the chemical equation.

$$kCO_2 + n(H^+ + e^-) \rightleftharpoons P + mH_2O \qquad 1\text{-}5\ ^{13}$$

As the reduction reaction proceeds, bulk $[H^+]$ and bulk $[CO_2]$ decrease. Furthermore, because the electrochemical reaction occurs at the surface of the electrode, the local environment (the local pH and the local $[CO_2]$) plays an even more significant role in determining the reaction selectivity and product selectivity.[2] In electrochemical reactions, the local environment is often drastically different from the bulk. In the case of HER with an unbuffered electrolyte at bulk pH 4, the local pH at then electrode surface can increase to 10 at a current density of 1 mA cm^{-2}.[29] In most research done in aqueous media, a buffered electrolyte such as a phosphate or bicarbonate solution is commonly used to mitigate the change in bulk and local pH. Although the local pH can be mitigated to some extent, due to mass transport limitations, it is difficult to buffer the local pH at the electrode surface at a rate sufficient to prevent pH changes. This is true even with an electrolyte with high buffer capacity, defined as the buffer's ability to counteract a change in the pH.[20] The buffer capacity can be determined by the identity of the buffer as well as the concentration of the buffer. A phosphate buffer has higher buffer capacity than a bicarbonate buffer, and a more concentrated buffer solution has higher buffer capacity than a more dilute buffer solution. As shown in Figure 1-5, a more concentrated buffer (or in other words, one with a higher buffer capacity) can maintain the local pH closer to the value of the bulk than a more dilute buffer

(lower buffer capacity). The current density and the duration of the experiment will also affect the local environment of the electrode. At higher current densities, the local pH is higher than at lower current densities, further emphasizing the sensitivity of the local environment.

The increase of the local pH and the decrease in local [CO_2] are illustrated in Figure 1-6 as a function of reaction time. At higher current densities, the local pH increases more rapidly, with the difference being more prominent at longer reaction times. The local [CO_2] also decreases more drastically, especially at higher current densities. The concentration gradient of H^+ and CO_2 at the surface of the electrode is depicted in Figure 1-7. The depletion of local CO_2 at high current densities supports the suggested mechanism discussed earlier under **1.1 Applied Potential**. When the rate of CO_2 consumption is faster than the rate at which it can be replenished at the electrode surface through mass transport, the reaction selectivity will shift towards HER instead of the CO_2RR, affecting the product distribution. The increase in local pH, on the other hand, provides more complex mechanistic insights into the product selectivity and the process of the CO_2RR through the observed product distribution.

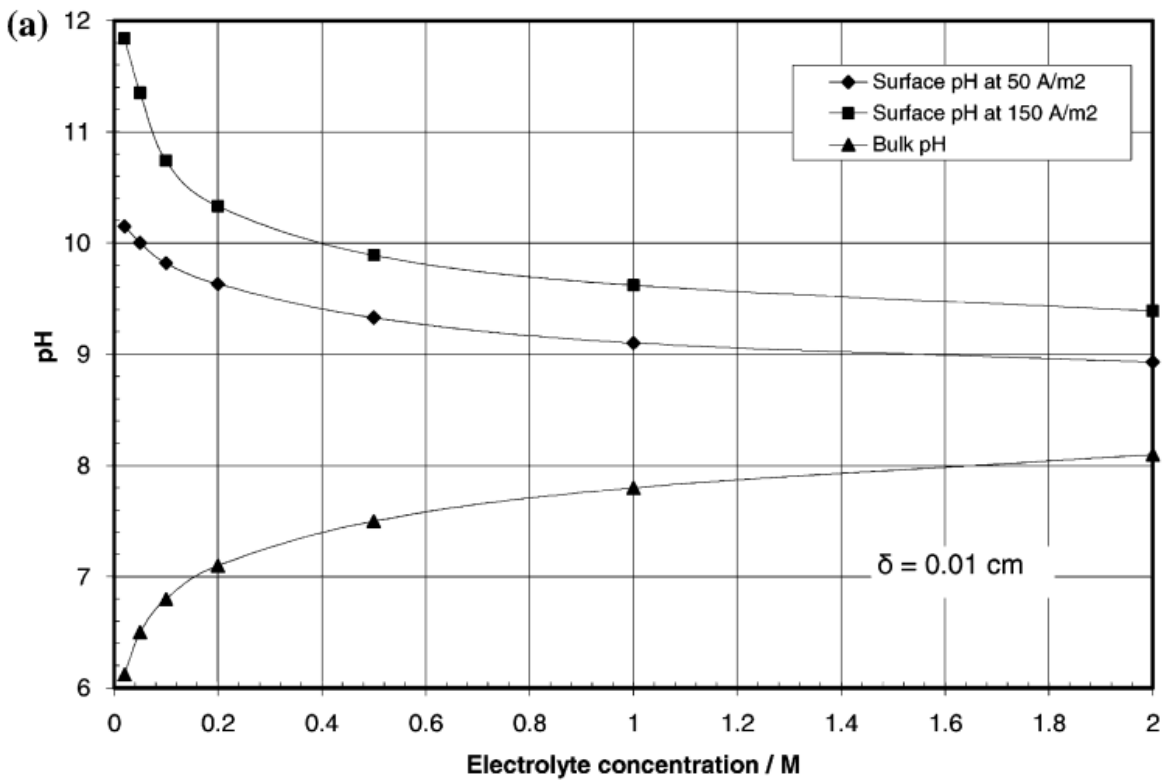

Figure 1-5 The calculated change in local pH in different electrolyte concentration with a $KHCO_3$ buffer solution at 50 A/m^2 and 150 A/m^2 current densities, assuming the boundary layer thickness of 0.01 cm.[27] Republished with permission of Springer Nature, from Journal of Applied Electrochemistry, 2006, 36, 161*;* permission conveyed through Copyright Clearance Center, Inc.

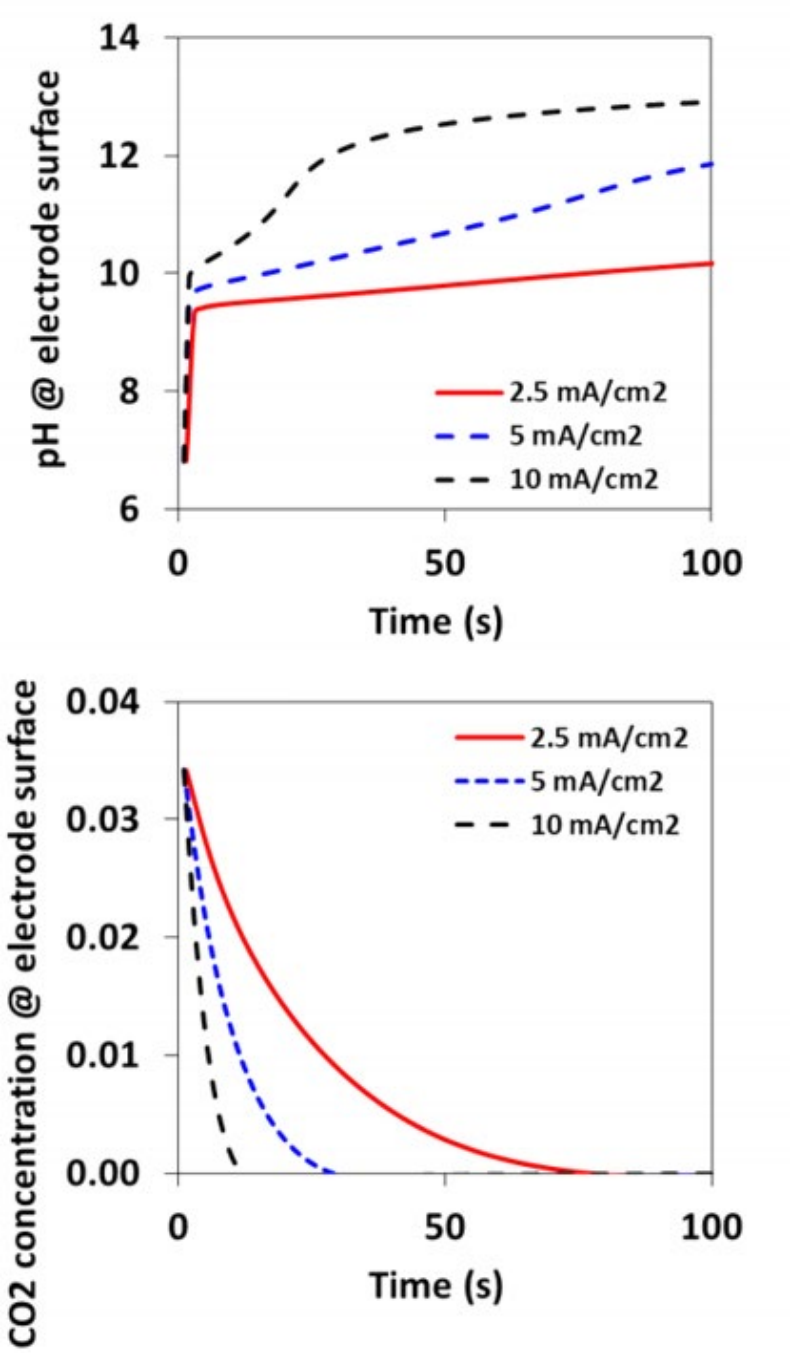

Figure 1-6 (top) Local pH at the electrode surface, and (bottom) local CO_2 concentration at the electrode surface as a function of time at 2.5, 5, and 10 mA/cm^2 current densities in a bicarbonate buffer.[20] Adapted with permission from *ACS Catal.* 2017, 7, 12, 8467-8479. Copyright 2017 American Chemical Society.

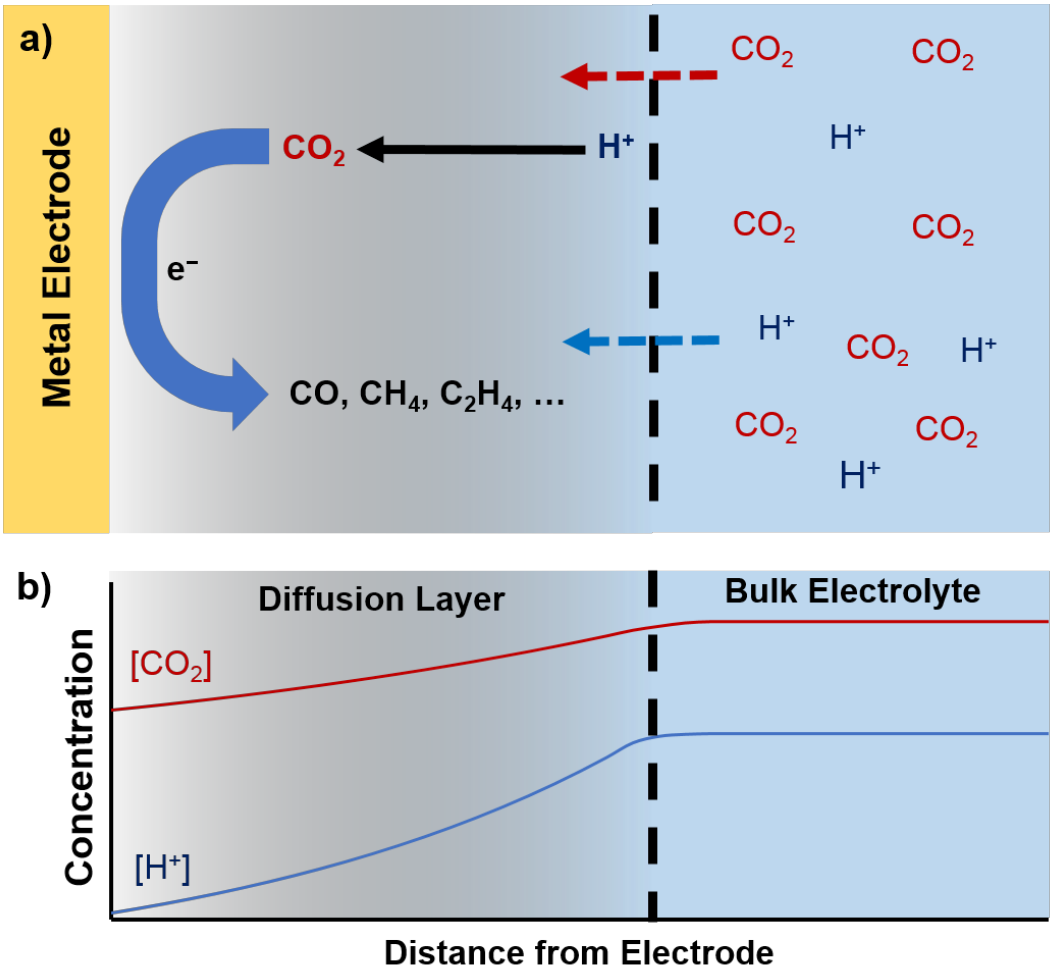

Figure 1-7 (a) Illustration of mass transport of CO_2 and H^+ species during CO_2RR at the surface of a metal electrode, and (b) the concentration gradient of CO_2 and H^+ near the electrode surface.[14] Reprinted with permission from Yingshuo Liu, Kwan Yee Leung, Samuel E. Michaud, Taylor L. Soucy & Charles C. L. McCrory. *Comments on Inorganic Chemistry*, 2019.

Within a small pH range between 6.5 to 7.15, the bulk pH is not crucial in determining the product distribution of the CO_2RR. Rather, it has been shown that the buffer capacity and local pH are the determining factors of product selectivity and the product distribution.[30] Hori *et. al.* showed that the product distribution of the Cu CO_2RR changes between electrolytes with different buffer capacities. When a higher buffer capacity electrolyte such as phosphate (compared to bicarbonate) is used, the Faradaic efficiencies of hydrocarbons decrease, while efficiency of H_2 increases.[31] Using bicarbonate buffers between 0.05 M (lower buffer capacity, bulk pH 6.5) and 0.2 M (higher buffer capacity, bulk pH 7.15), Faradaic efficiency for CH_4 production increases with higher buffer capacities while C_2H_4 production decreases.[30] Furthermore, when performing CO reduction reaction where CO is the major intermediate of the CO_2RR, as the concentration (and therefore the buffer capacity) of the bicarbonate buffer increases, the Faradaic efficiency of the more reduced C_2H_4 decreases while the less reduced CH_4 increases.[32] As the buffer capacity increases, H^+ can be replenished at a sufficient rate such that the local pH remains relatively consistent with that of the bulk. A sufficient supply of H^+ favors the reaction selectivity towards HER, but also product selectivity within the CO_2RR towards CH_4, the product that consumes more H^+ per CO_2 molecule during the reduction process. As the buffer capacity decreases, H^+ cannot be replenished at a sufficient rate and the local pH will be significantly higher than the bulk. With a lower supply of H^+, the reaction selectivity would favor the CO_2RR, and the product selectivity would favor C_2H_4, a product that consumes less H^+ per CO_2 during the reaction process. The bulk pH in these studies is not the determining factor of product distribution within this narrow pH range. The Faradaic efficiencies of C_2H_4 are lower and CH_4 are higher with a higher bulk pH where bulk concentration of H^+ is relatively low. These observations in reaction selectivity and product selectivity cannot be

explained by the change in bulk pH. Rather, the observations are consistent with a change in local pH, emphasizing the significance of the local environment during CO_2RR.

The extent of the change in local pH during the CO_2RR predominantly depends on the buffer capacity of the electrolyte. Buffer capacity has a significant effect on CO_2RR product distributions not only on planar Cu metals,[33,34] but also on other Cu-based catalysts. The change in production distribution using Cu nanoparticles was investigated with various concentrations, which dictate the buffer capacity, of bicarbonate buffers. It was shown that as the bicarbonate concentration is increased from 0.1 M (weaker buffer capacity) to 0.5 M (stronger buffer capacity), there is a corresponding increase in CH_4 production and decrease in C_2H_4 production.[19] These observations are consistent with the proposed mechanisms originating from planar Cu foil surfaces. The authors also showed that increasing CO_2 pressure increases the Faradaic efficiency for C_2H_4 from the CO_2RR (Figure 1-8).[19] This observation is consistent with a rate-limiting CO dimerization step for the CO_2RR to C_2H_4—as the bulk CO_2 concentration increases, the relative coverage of *CO adducts on the surface also increases, leading to an increased probability of CO dimerization. Another recent study has suggested there is a competition between formation of *CO and *H on Cu surfaces, and the increased Faradaic efficiency for C_2H_4 production at increased CO_2 pressures is due to suppression of CH_4 and H_2 production rather than increased rate of C_2H_4 production. This is because at higher CO_2 pressures, there is a larger surface concentration of *CO adsorbed to Cu active sites, resulting in a lower surface concentration of *H.[35] This leads to a decrease in CH_4 and H_2 production, since both require surface *H, but there was no corresponding increase in C_2H_4 production rate.[35] This competition for active sites between CO_2RR and HER is consistent with studies showing that HER is suppressed in the presence of CO_2, and that this suppression is enhanced with increased bulk and local concentration of CO_2. [36,37]

In another study, a rotating disk electrode assembly was used to control the transport of substrate to a Cu disk electrode in bicarbonate buffer solutions and to study the effects of rotation rate on CO_2RR product distributions.[38] As the rotation rate of the electrode increases, there is a corresponding decrease in the formation of CH_4 and an increase in the formation of CO and H_2.[38] The authors attribute this change in product distribution to changes in local pH and local CO_2 and CO concentrations. The increase in CO production with faster rotation rates is attributed to the weakly adsorbed *CO leaving the electrode surface before it is further reduced to other hydrocarbons. The increase in HER at faster rotation rates is attributed to the decrease in surface CO coverage, which increases the number of active sites for proton reduction.[38] Other studies using rotating disc voltammetry showed that HER is inhibited by surface adsorbed CO, which blocks active sites for water reduction. This inhibition becomes more pronounced as transport of CO_2 is improved.[37] These studies highlight the importance of controlling mass transport and local concentration of reactive species in CO_2RR to improve reaction selectivity and product distribution.

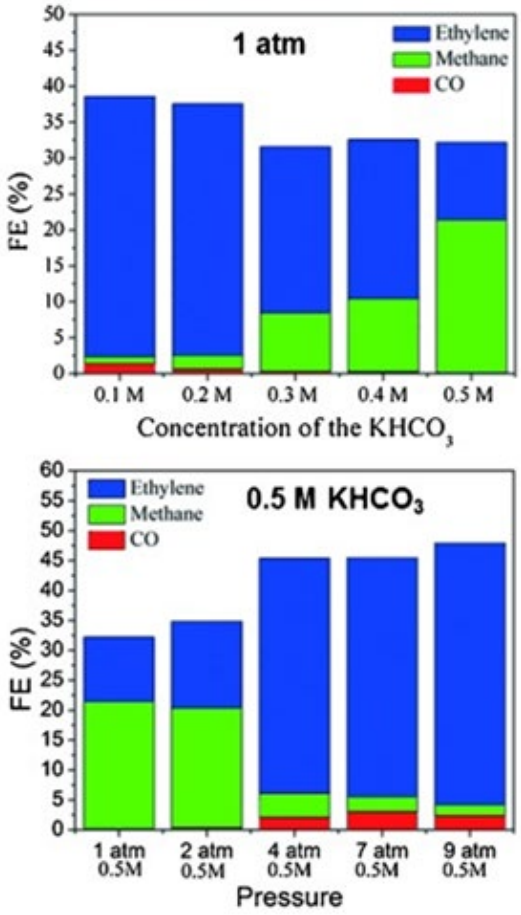

Figure 1-8 (top) The product distribution of Cu nanoparticle catalyzed CO_2RR using different concentration of bicarbonate buffers, and (bottom) under different CO_2 pressure.[19] Adapted with permission.

In addition to variations in product distribution, studies on bulk and local pH can also be used to investigate the reduction mechanism. Single crystal Cu surfaces are often used to study the mechanistic pathways of CO_2RR and to understand the role of both bulk and local pH. One such study investigated the effect of bulk pH on product distributions for the CO_2RR at Cu(111) and Cu(100) electrocatalysts in buffered and unbuffered solutions.[39] In particular, they showed that at intermediate bulk pH, the onset potential vs NHE of the 8 e^- reduction of CO_2 to CH_4 on Cu(100) and Cu(111) is pH dependent on both surfaces, whereas the onset potential vs NHE for the 12 e^- reduction of CO_2 to C_2H_4 on a Cu(100) surface is pH-independent.[39] This suggests that rate-limiting step for CO_2 reduction to CH_4 on Cu(100) and Cu(111) involves a proton transfer event (such as the formation of a CHO species), whereas CO_2 reduction to C_2H_4 on a Cu(100) surface operates via a pH-independent rate limiting step (such as the formation of a surface CO dimer) as shown in Figure 1-9.[39] CO_2 reduction to C_2H_4 on Cu(111) surfaces shows a pH dependence similar to that for CO_2 reduction to CH_4, suggesting there also exists a pH-dependent pathway for C_2H_4 formation on this crystal facet that shares a common intermediate with CH_4.[39] Other studies also found local pH dependence of certain products on polycrystalline Cu. As the local pH increases, the rate of HER and CH_4 formation plateau, showing local pH-dependence of these products. In contrast, the rate of C_2H_4 production was local pH-independent, agreeing with the results observed on Cu(100) surfaces.[30] The proposed mechanisms from these pH-dependent studies are consistent with other experimental[33,34,40,41] and computational[42,43] mechanistic investigations. It is important to note, however, that multiple pathways of the proposed mechanism can occur on the polycrystalline surfaces, and the crystal orientation of the surface is susceptible to change under experimental conditions.[44]

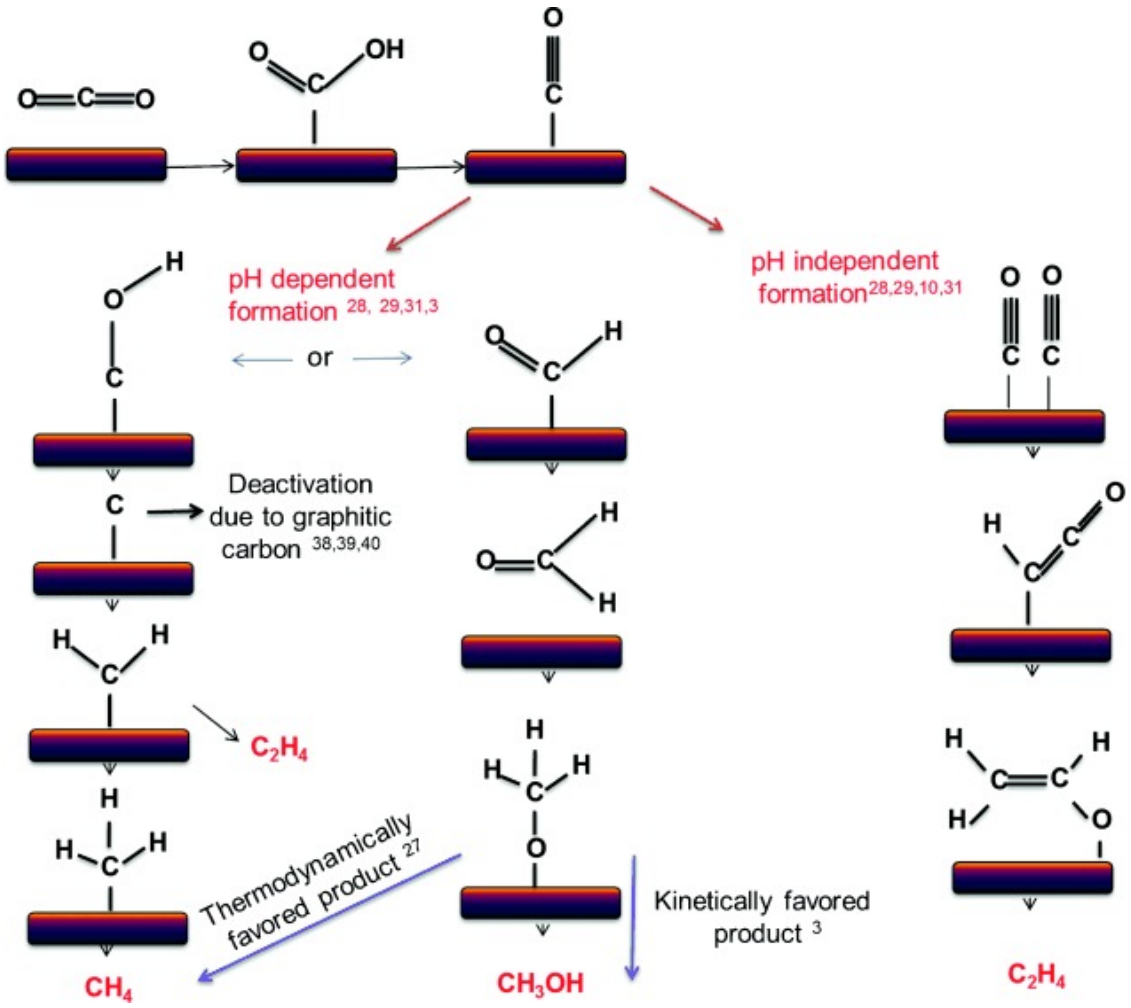

Figure 1-9 Possible mechanism for CO_2RR basic on the pH-dependence observed for the formation of products such as CH_4 and CH_3OH, and pH-independence observed for the formation of C_2H_4. Reprinted with permission.[19]

It should be noted that the commonly used bicarbonate buffer solution serves not only as the buffering agent, but also the main source of available CO_2 as the equilibrium shifts from HCO_3^- species to CO_2 species shown in equations 1-1 through 1-4. Using isotope studies, it had been experimentally observed that the bicarbonate is the source of the CO_2 in the reaction.[45] This observation can be explained by the much faster proton transfer equilibrium compared to the gas-liquid CO_2 mixing in the electrolyte. The replenishment of aqueous CO_2 from gaseous CO_2 dissolved in the solution is slow, which forces the system to replenish CO_2 from the bicarbonate instead. The observed result of the isotope study, however, contradicts the local pH argument established above. Higher local pH is observed to lead to higher reaction selectivity towards CO_2RR, but a higher local pH also makes it unfavorable for the HCO_3^- species to equilibrate to a CO_2 species, and therefore limits the amount of local CO_2 available for reduction. Whether a low or high local pH would lead to higher reaction selectivity and product selectivity is still a constant debate between researchers. A delicate balance of local $[H^+]$ and local $[CO_2]$ is necessary in CO_2RR, which depends on the rate of CO_2 consumption and rate of CO_2 hydration.

1.4 Effect of Electrolyte Cation on Product Distribution

The identity of the cation associated with the buffer system has also been observed to alter the product distribution during the CO_2RR on Cu surfaces,[22,46] and this may be partially due to local pH effects, although the exact mechanism is not clear. A recent study investigated the product distribution for CO_2RR on Ag and Cu surfaces in CO_2-saturated bicarbonate solutions as a function of cation size ($Li^+ \rightarrow Cs^+$).[47] An increase in CO production and decrease in competitive HER on Ag electrodes was observed when increasing the cation size from Li^+ to Cs^+. When exploring CO_2RR on Cu electrodes, the authors found that rate of production of highly-reduced C_2 products such as C_2H_4 and CH_3CH_2OH increase as cation size increases (Figure 1-10) although interestingly the rates of CO and H_2 production are unaffected.[47,48] One hypothesis provided by the authors to explain this observation is that larger cations have higher buffering capacity than smaller cations and are able to keep local pH sufficiently low to retain higher concentrations of CO_2 near the electrode and available for reduction.[47] Higher CO_2 concentrations near the electrode surface would account for increased CO production at Ag electrodes, and also for increased production of C_2 products at Cu electrodes. However, this argument disagrees with other mechanistic studies that suggest low local pH favors HER and CH_4 production because of a pH-dependent reaction mechanism.[33,34,39-43] An alternative explanation is that the interaction between solvated cations and adsorbed species on the electrode can stabilize intermediates such as $*CO_2$ and *CO, therefore increasing the product selectivity towards CO and hydrocarbons, and this is supported by DFT calculations.[48] Although the exact explanation is still unclear, cation identity had been experimentally shown to affect product distribution in CO_2RR.[47,48]

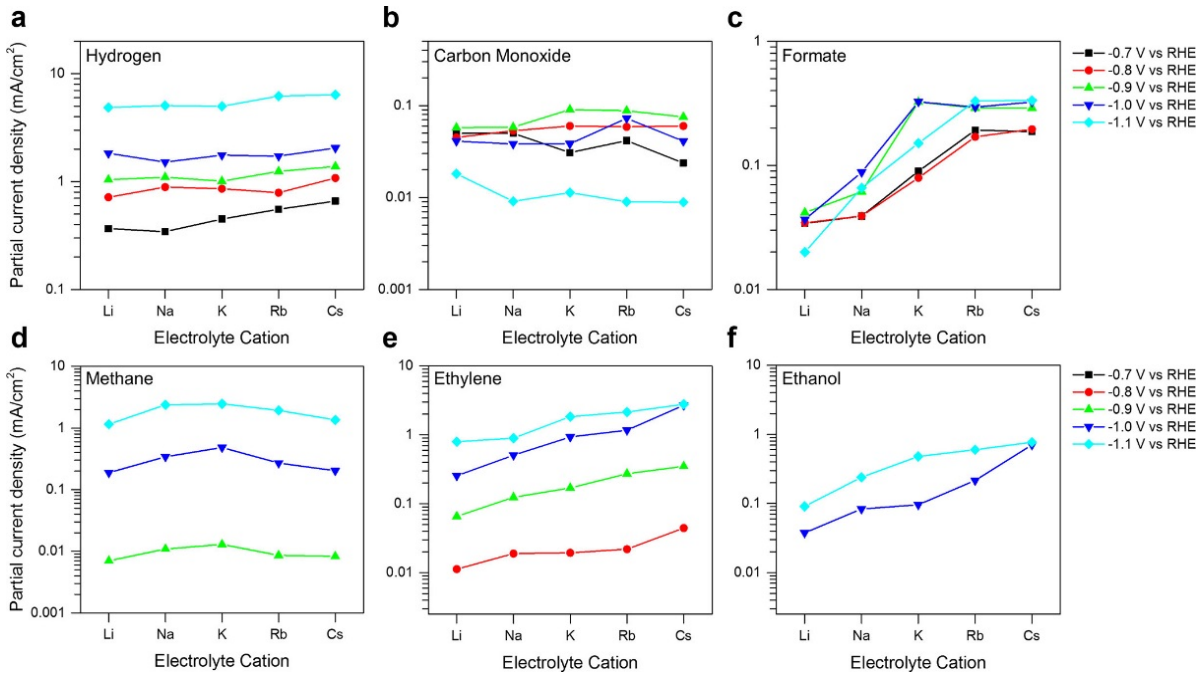

Figure 1-10 Partial current densities of CO_2RR products (H_2, CO, $COOH^-$, CH_4, C_2H_4, and EtOH) as a function of electrolyte cations.[49] As the size of the electrolyte cation increases, there is increased production of HCOOH and the C_2 products C_2H_4 and CH_3CH_2OH. Adapted with permission from J. Am. Chem. Soc. 2017, 139, 11277−11287. Copyright (2017) American Chemical Society.

1.5 Porous and Nanostructured Cu Catalysts

Researchers have designed nanostructured and porous catalyst systems to better control local pH to increase CO_2RR product selectivity. In one series of studies, mesoporous Ag and Au catalysts have shown high selectivity for CO_2RR to CO over the competitive HER.[50,51] For instance, in the case of mesostructured Ag films, as the roughness factor is increased by growing thicker porous films, there is a corresponding increase in CO production from the CO_2RR and a decrease in competitive HER (Figure 1-11).[51,52] This reaction selectivity is attributed to increased local pH within the porous catalyst that suppresses HER and promotes CO_2 adsorption on the metal surfaces.[50,51] When comparing electropolished, nanoparticles covered, and sputtered Cu surfaces in Figure 1-12, different product distributions were observed with the nanoparticles covered Cu surface showing the highest efficiency of C_2H_4. In another study, Cu nanoparticles deposited onto a high-surface area carbon paper support showed higher activity for C_2+ products than the same nanoparticles deposited at similar loadings onto a planar graphite plate.[10] The authors suggest the increased activity for C_2+ products for the Cu nanoparticles on the high-surface carbon paper may be due to increased local pH.[10] Likewise, studies of the effects of surface roughness on C_2H_4 production have shown a general increase in C_2+ products with increasing surface roughness, which has been attributed to an increase in local pH.[53,54] However, there was an optimal roughness beyond which the local pH was thought to increase too much, decreasing local CO_2 concentration, thus inhibiting CO_2RR.[54] It is important to note that other factors may contribute to increased activity for more highly-reduced products in porous and nanostructured materials including increasing numbers of defect sites, grain boundaries[15,55-58] the mobility of reaction intermediates[59], and the difference in dominant facets of the catalyst.

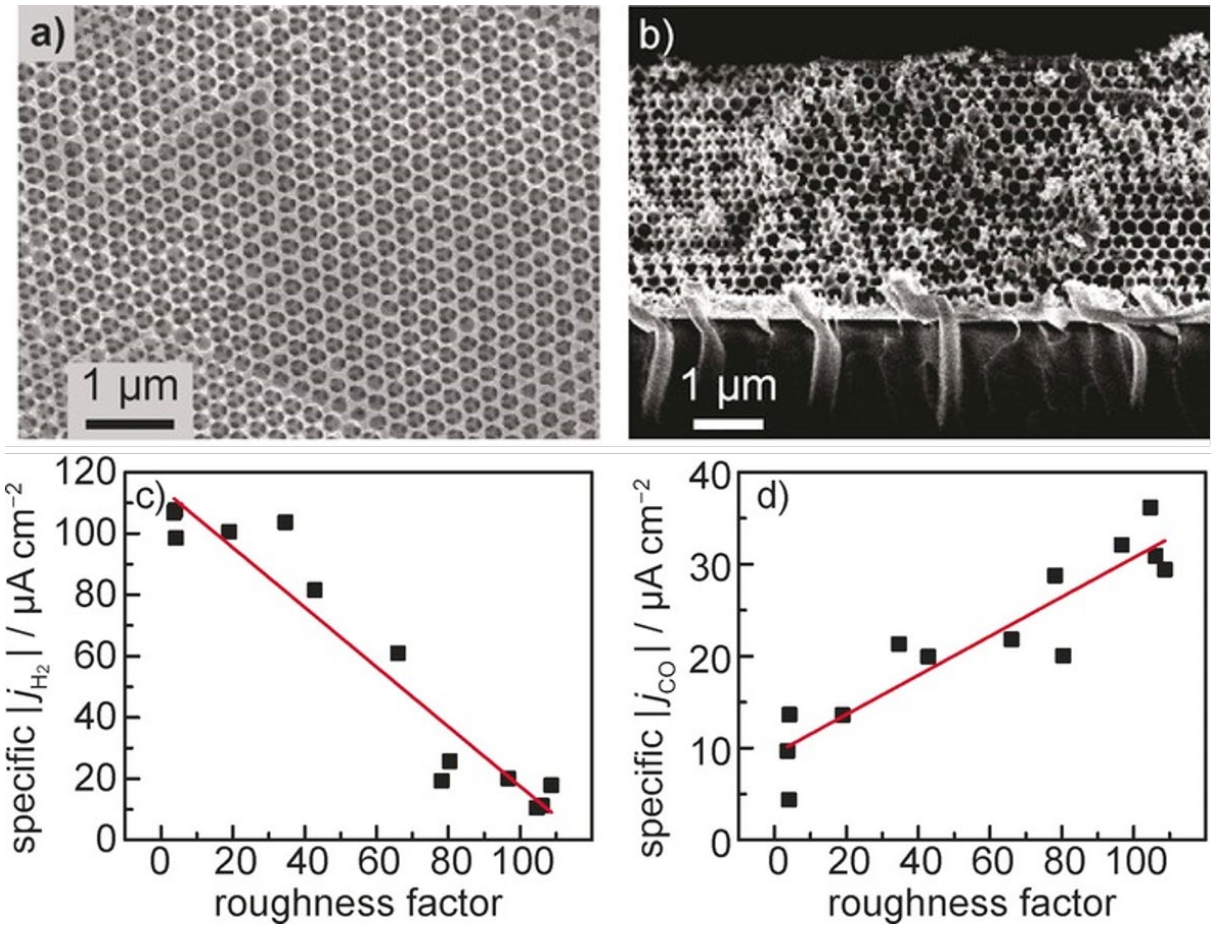

Figure 1-11 (a) Top down and (b) cross-sectional SEM images of a mesostructured Ag film with ~200 nm voids interconnected by ~50 nm diameter channels. (c) H_2 production shown here as a specific current density j_{H2}, decreases with increasing roughness factor, and (d) CO production increases with increasing roughness factor.[52] Adapted with permission.

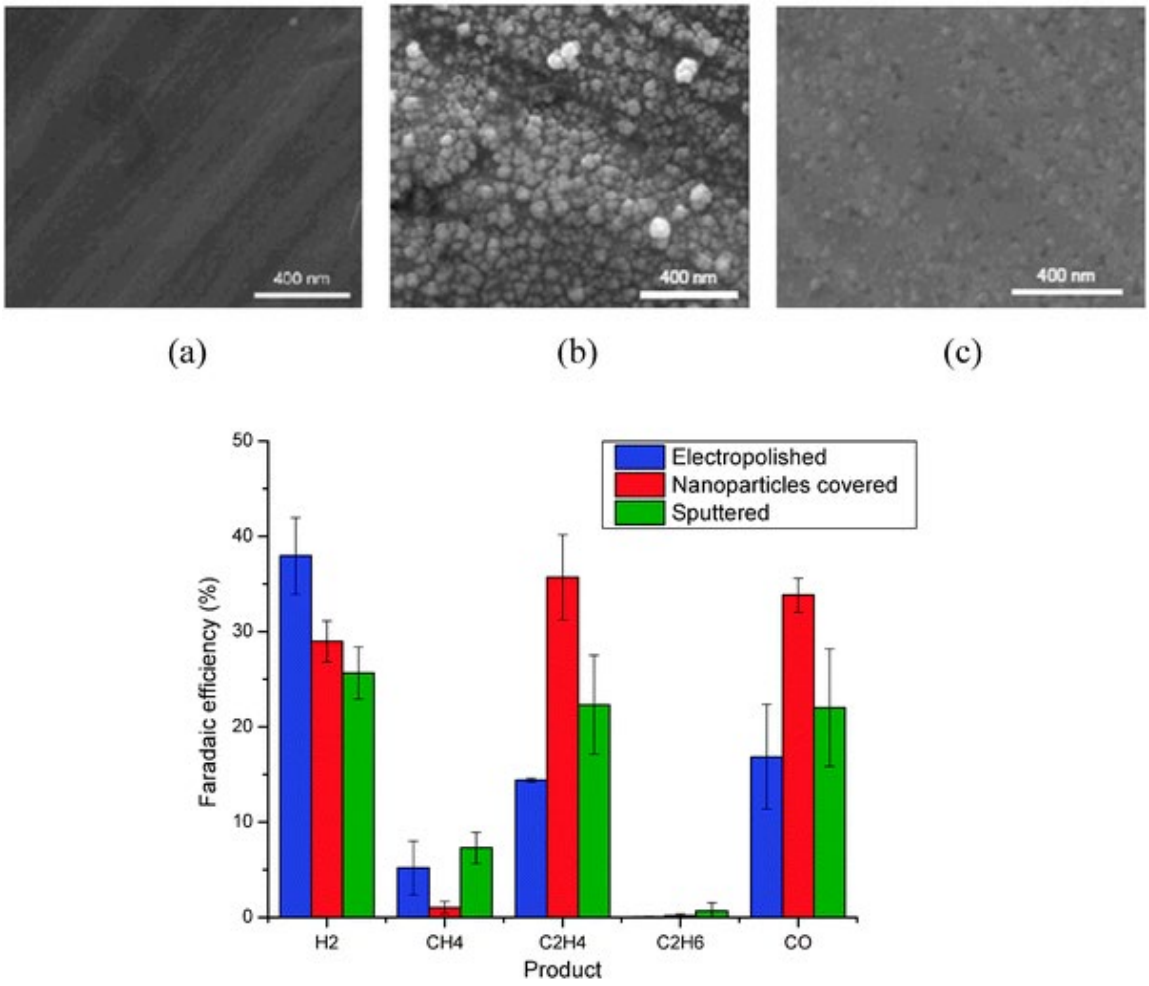

Figure 1-12 SEM images showing (a) electropolished Cu surface (b) nanoparticles covered Cu surface (c) sputtered Cu surface, and (bottom) the CO_2RR product distribution using these surfaces.[15] Adapted with permission of Royal Society of Chemistry (Great Britain), from Phys. Chem. Chem. Phys., 2012, 14, 76–81*;* permission conveyed through Copyright Clearance Center, Inc.

1.6 Research Motivation and Trace Metal Contamination

The importance of mass transport of the reactive species, especially CO_2 and H^+, had been emphasized in previous sections. The initial proposed research was to study the role of mass transport of reactants and intermediates in CO_2RR mechanism using a forced convective electrochemical flow cell. The design and photo of the prototype flow cell are shown in Figure 1-13. In particular, I was interested in understanding the role of mass transport of adsorbed CO, the major intermediate, during CO_2RR. I hypothesized that a slower mass transport of adsorbed CO would lead to higher local concentration of adsorbed CO, which would then lead to more CO dimerization to form C_2H_4, therefore altering the product distribution to be selective towards C_2H_4. A faster mass transport of adsorbed CO, on the contrary, would lead to lower local concentration of adsorbed CO and less CO dimerization, therefore resulting in lower selectivity towards C_2H_4. By controlling the flow rate of the bulk electrolyte, the mass transport and the local concentrations of CO_2, H^+, and adsorbed CO can be directly controlled. A lower flow rate would lead to lower local concentrations of CO_2 and H^+, and a higher local concentration of CO. A higher flow rate would lead to higher local concentrations of CO_2 and H^+, and a lower local concentration of CO. By adjusting flow rate, varying the identity and buffer capacity of electrolytes, and using gas mixtures with different partial pressures of CO_2, I would systematically modify the local concentration gradients of CO_2, and H^+, allowing me to analyze the role of mass transport and local concentration of CO.

As one of the first steps of collecting preliminary data, I performed control experiments and measured the product distribution using Cu foil under conditions described in literature[1]. However, as shown in Figure 1-14, there were problems with my preliminary control experiments. First, the major product I observed was H_2 at between 20 to 40% Faradaic efficiency. Second, I

did not observe similar Faradaic efficiencies for CH_4 and C_2H_4 to those previously reported in the literature[1]. Third, the total Faradaic efficiency was very low at consistently below 60%. The major differences between my results and those from literature became my motivation to carry out a vigorous analysis of the reported experimental procedures from literature.

By taking a close look at the control experiments in the existing literature, it is evident that there are discrepancies in the results of control experiments from different research groups. Despite the immense amount of research on Cu-catalyzed systems, factors that cannot be easily controlled have been empirically shown to alter the product distribution, posing challenges to catalyst development in Cu-based CO_2RR.[1,11,17,20,60-75] A significant challenge observed in the literature of the CO_2RR community is the lack of reproducibility of CO_2RR product distributions between research groups under similar reaction conditions.[11,59,73,76-80] For example, for control experiments of the Cu-catalyzed CO_2RR using Cu foil under as-claimed identical conditions, the Faradaic efficiency for CH_4 can differ drastically between different research groups, from 30% to 60%.[11,59] In addition, some research groups only report the product distributions for certain products of interest, making it difficult to compare the results with those from other researchers.[81] These differences in the measured product distributions in the literature suggests that the actual experimental conditions may vary significantly between different research groups, despite the assumption that the reaction conditions are similar.

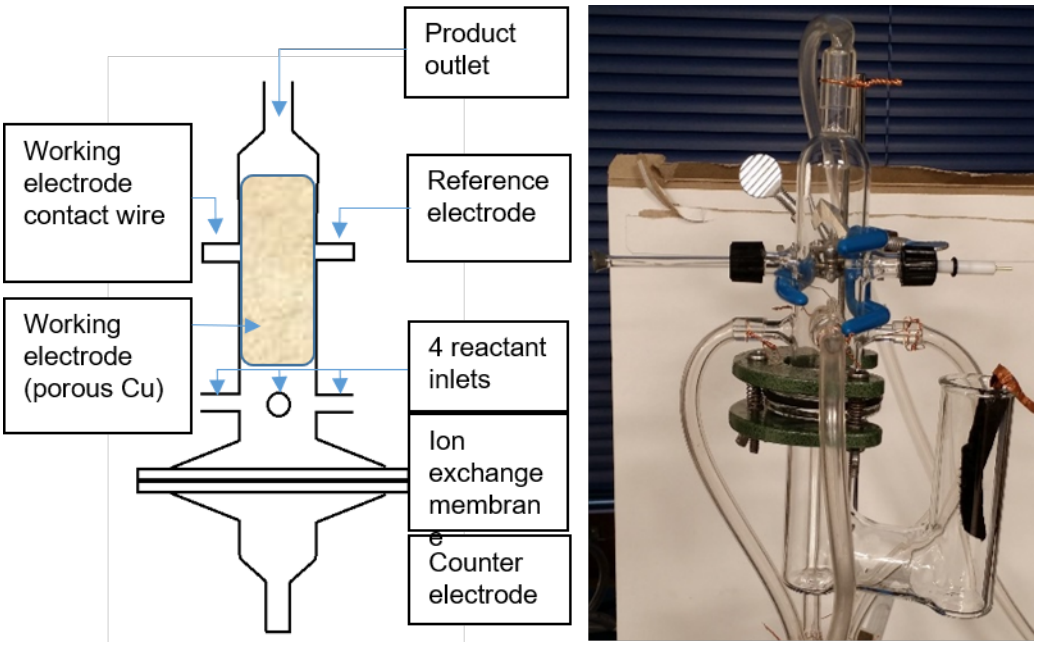

Figure 1-13 Design of the forced convective electrochemical flow cell, used in the initially proposed research.

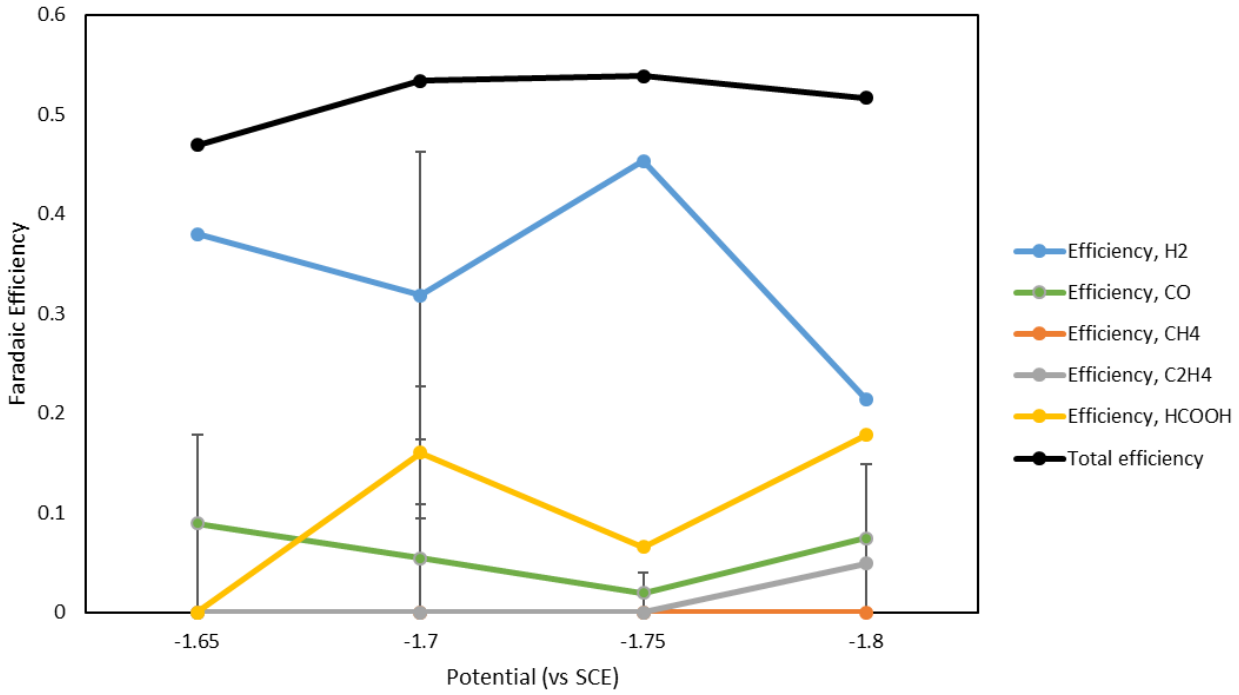

Figure 1-14 Product distribution of the initial preliminary data of Cu CO_2RR, with a saturated calomel electrode (SCE) as the reference electrode.

These inter-lab and intra-lab variations in CO_2RR product distributions have been generally ascribed to factors that are not easily controlled such as crystal orientation,[44,82] local pH,[19,27,32,79] and mass transport[20,38]. One factor that is particularly relevant to the Cu-based CO_2RR is contamination and impurities, as Cu electrodes are extremely sensitive to surface modification and deactivation by organic and inorganic contaminants.[1,60-66]Although some reports suggest that Cu poisoning is caused by adsorbed organic species[83] or oxide/hydroxide species[84], a particularly pervasive class of impurities in electrochemical measurements are trace metal contaminants, which can dramatically change the electrochemical properties of catalytic systems. For example, it has been shown that trace amounts of Fe (< 1 ppm) significantly enhance the catalytic activity of Ni-based catalysts for the oxygen evolution reaction (OER), and this trace Fe contamination is likely responsible for the inconsistency in OER activity measurements by Ni-based catalysts.[71,85,86] In the case of the CO_2RR, differences in electrolyte purities between experiments have been linked to differences in catalyst activity and product distributions, and this prior work has led to recommendations for purifying electrolytes and normalizing measurement conditions.[60,67,73,74] A recent report demonstrated that using a chelating resin to pre-treat the electrolyte can effectively remove the trace amount of metals present in the electrolyte and prevent the poisoning of the electrode, as shown in Figure 1-15. The product distribution of a resin-treated electrolyte showed stable product distribution over the course of the experiment, while untreated and EDTA-treated electrolytes both showed changes in product distribution over time. The result suggests surface poisoning occurred when the electrolyte was not pre-treated with a chelating resin.

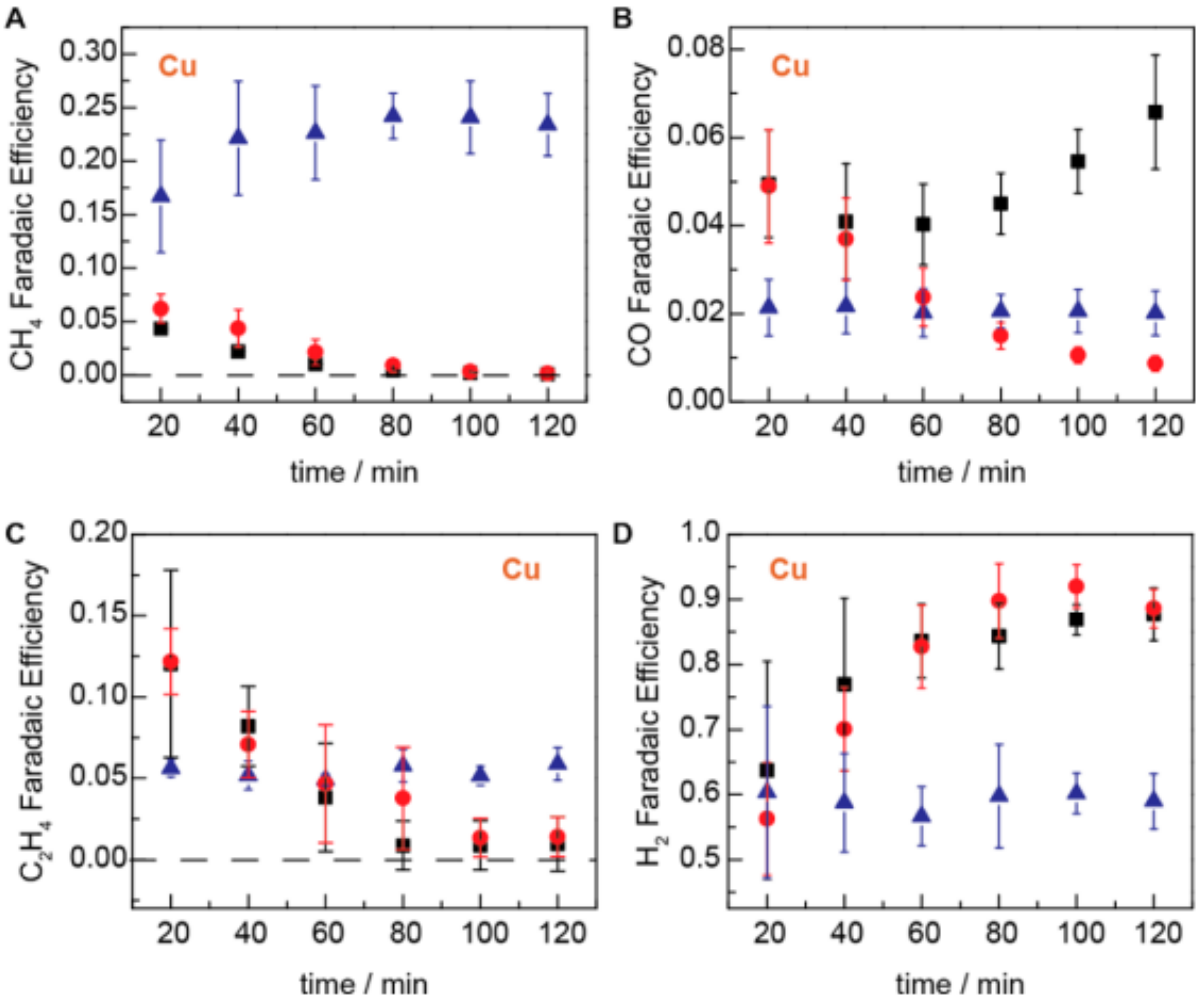

Figure 1-15 Faradaic efficiencies of (A) CH_4 (B) CO (C) C_2H_4 and (D) H_2 of the Cu CO_2RR over time when the bicarbonate electrolyte was untreated (black), pre-treated with EDTA (red), and pre-treated with chelating resin (blue).[73] Reprinted with permission from *ACS Catal.* 2015, 5, 7, 4479-4484. Copyright (2015) American Chemical Society.

Other CO_2RR studies have focused on mitigating the deactivating effects of electrolyte impurities by altering catalyst structure [87-89] or stripping impurities by holding the electrode at anodic potentials before CO_2RR experiments.[83] However, there are still missing pieces in our understanding of the sources and the effects of trace metal impurities on the CO_2RR. Upon close inspection of experimental procedure in the literature, there is no standard practice for pre-treatment of the Cu foil catalyst, of the electrolyte, or of the electrochemical cell. Furthermore, there is no standard for the purity of materials used or the choice of the ion exchange membrane or auxiliary electrode. The lack of a standard common practice of experimental condition is likely the source of the variations in trace metal contamination, and therefore variations in CO_2RR product distributions in control experiments, between literature.

Although the CO_2RR on Cu is among the most studied electrochemical systems, the factors that affect the catalytic activity and product distribution are still not well understood. This dissertation will fill in one of those gaps through an in-depth exploration on the sources of trace metal contamination and their effects on catalyst performance. Specifically, my work explains the effect of trace metal contaminations in the CO_2RR product distribution, and the effect of starting purity and pre-treatments of the materials. It is important to note that the research described in this dissertation does not aim for a specific product distribution or optimization of the experimental condition. Instead, the trends and changes of the CO_2RR product distribution due to the differences in experimental condition are the focus of this study. The sources of trace metal contamination and observed trends in product distribution are explained in the following chapters.

1.7 References

(1) Hori, Y. "Electrochemical CO2 Reduction on Metal Electrodes," *Mod Asp Electrochem* **2008**, 89-189. http://dx.doi.org/Book_Doi 10.1007/978-0-387-49489-0

(2) Gattrell, M.; Gupta, N.; Co, A. "A review of the aqueous electrochemical reduction of CO2 to hydrocarbons at copper," *Journal of Electroanalytical Chemistry* **2006**, *594*, 1-19. http://dx.doi.org/10.1016/j.jelechem.2006.05.013

(3) De Luna, P.; Hahn, C.; Higgins, D.; Jaffer, S. A.; Jaramillo, T. F.; Sargent, E. H. "What would it take for renewably powered electrosynthesis to displace petrochemical processes?," *Science* **2019**, *364*. http://dx.doi.org/10.1126/science.aav3506

(4) Majumdar, A.; Deutch, J. "Research Opportunities for CO2 Utilization and Negative Emissions at the Gigatonne Scale," *Joule* **2018**, *2*, 805-809. http://dx.doi.org/10.1016/j.joule.2018.04.018

(5) Graves, C.; Ebbesen, S. D.; Mogensen, M.; Lackner, K. S. "Sustainable hydrocarbon fuels by recycling CO 2 and H 2 O with renewable or nuclear energy," *Renewable and Sustainable Energy Reviews* **2011**, *15*, 1-23. http://dx.doi.org/10.1016/j.rser.2010.07.014

(6) Kondratenko, E. V.; Mul, G.; Baltrusaitis, J.; Larrazábal, G. O.; Pérez-Ramírez, J. "Status and perspectives of CO2 conversion into fuels and chemicals by catalytic, photocatalytic and electrocatalytic processes," *Energy & Environmental Science* **2013**, *6*. http://dx.doi.org/10.1039/c3ee41272e

(7) Montoya, J. H.; Seitz, L. C.; Chakthranont, P.; Vojvodic, A.; Jaramillo, T. F.; Norskov, J. K. "Materials for solar fuels and chemicals," *Nat Mater* **2016**, *16*, 70-81. http://dx.doi.org/10.1038/nmat4778

(8) Hori, Y.; Kikuchi, K.; Murata, A.; Suzuki, S. "Production of Methane and Ethylene in Electrochemical Reduction of Carbon-Dioxide at Copper Electrode in Aqueous Hydrogencarbonate Solution," *Chem Lett* **1986**, 897-898. http://dx.doi.org/DOI 10.1246/cl.1986.897

(9) Yang, K. D.; Ko, W. R.; Lee, J. H.; Kim, S. J.; Lee, H.; Lee, M. H.; Nam, K. T. "Morphology-Directed Selective Production of Ethylene or Ethane from CO2 on a Cu Mesopore Electrode," *Angew Chem Int Ed Engl* **2017**, *56*, 796-800. http://dx.doi.org/10.1002/anie.201610432

(10) Kim, D.; Kley, C. S.; Li, Y.; Yang, P. "Copper nanoparticle ensembles for selective electroreduction of CO₂ to C₂–C₃ products," *Proceedings of the National Academy of Sciences* **2017**, *114*, 10560. http://dx.doi.org/10.1073/pnas.1711493114

(11) Kuhl, K. P.; Cave, E. R.; Abram, D. N.; Jaramillo, T. F. "New insights into the electrochemical reduction of carbon dioxide on metallic copper surfaces," *Energy & Environmental Science* **2012**, *5*. http://dx.doi.org/10.1039/c2ee21234j

(12) Hori, Y.; Wakebe, H.; Tsukamoto, T.; Koga, O. "Electrocatalytic Process of Co Selectivity in Electrochemical Reduction of Co2 at Metal-Electrodes in Aqueous-Media," *Electrochimica Acta* **1994**, *39*, 1833-1839. http://dx.doi.org/Doi 10.1016/0013-4686(94)85172-7

(13) Kortlever, R.; Shen, J.; Schouten, K. J.; Calle-Vallejo, F.; Koper, M. T. "Catalysts and Reaction Pathways for the Electrochemical Reduction of Carbon Dioxide," *J Phys Chem Lett* **2015**, *6*, 4073-4082. http://dx.doi.org/10.1021/acs.jpclett.5b01559

(14) Liu, Y.; Leung, K. Y.; Michaud, S. E.; Soucy, T. L.; McCrory, C. C. L. "Controlled Substrate Transport to Electrocatalyst Active Sites for Enhanced Selectivity in the Carbon Dioxide Reduction Reaction," *Comments on Inorganic Chemistry* **2019**, 1-28. http://dx.doi.org/10.1080/02603594.2019.1628025

(15) Tang, W.; Peterson, A. A.; Varela, A. S.; Jovanov, Z. P.; Bech, L.; Durand, W. J.; Dahl, S.; Norskov, J. K.; Chorkendorff, I. "The importance of surface morphology in controlling the selectivity of polycrystalline copper for CO2 electroreduction," *Phys Chem Chem Phys* **2012**, *14*, 76-81. http://dx.doi.org/10.1039/c1cp22700a

(16) Liu, X.; Xiao, J.; Peng, H.; Hong, X.; Chan, K.; Norskov, J. K. "Understanding trends in electrochemical carbon dioxide reduction rates," *Nat Commun* **2017**, *8*, 15438. http://dx.doi.org/10.1038/ncomms15438

(17) Schouten, K. J. P.; Pérez Gallent, E.; Koper, M. T. M. "The influence of pH on the reduction of CO and CO_2 to hydrocarbons on copper electrodes," *Journal of Electroanalytical Chemistry* **2014**, *716*, 53-57. http://dx.doi.org/10.1016/j.jelechem.2013.08.033

(18) Hall, A. S.; Yoon, Y.; Wuttig, A.; Surendranath, Y. "Mesostructure-Induced Selectivity in CO2 Reduction Catalysis," *J Am Chem Soc* **2015**, *137*, 14834-14837. http://dx.doi.org/10.1021/jacs.5b08259

(19) Kas, R.; Kortlever, R.; Yılmaz, H.; Koper, M. T. M.; Mul, G. "Manipulating the Hydrocarbon Selectivity of Copper Nanoparticles in CO2 Electroreduction by Process Conditions," *ChemElectroChem* **2015**, *2*, 354-358. http://dx.doi.org/doi:10.1002/celc.201402373

(20) Billy, J. T.; Co, A. C. "Experimental Parameters Influencing Hydrocarbon Selectivity during the Electrochemical Conversion of CO2," *ACS Catalysis* **2017**, *7*, 8467-8479. http://dx.doi.org/10.1021/acscatal.7b02373

(21) Varela, A. S.; Kroschel, M.; Leonard, N. D.; Ju, W.; Steinberg, J.; Bagger, A.; Rossmeisl, J.; Strasser, P. "pH Effects on the Selectivity of the Electrocatalytic CO2 Reduction on Graphene-Embedded Fe–N–C Motifs: Bridging Concepts between Molecular Homogeneous and Solid-State Heterogeneous Catalysis," *ACS Energy Letters* **2018**, *3*, 812-817. http://dx.doi.org/10.1021/acsenergylett.8b00273

(22) Kyriacou, G. Z.; Anagnostopoulos, A. K. "Influence of Co2 Partial-Pressure and the Supporting Electrolyte Cation on the Product Distribution in Co2 Electroreduction," *Journal of Applied Electrochemistry* **1993**, *23*, 483-486.

(23) Windle, C. D.; Reisner, E. "Heterogenised Molecular Catalysts for the Reduction of CO2 to Fuels," *CHIMIA International Journal for Chemistry* **2015**, *69*, 435-441. http://dx.doi.org/10.2533/chimia.2015.435

(24) Hatsukade, T.; Kuhl, K. P.; Cave, E. R.; Abram, D. N.; Jaramillo, T. F. "Insights into the electrocatalytic reduction of CO(2) on metallic silver surfaces," *Phys Chem Chem Phys* **2014**, *16*, 13814-13819. http://dx.doi.org/10.1039/c4cp00692e

(25) Cave, E. R.; Montoya, J. H.; Kuhl, K. P.; Abram, D. N.; Hatsukade, T.; Shi, C.; Hahn, C.; Norskov, J. K.; Jaramillo, T. F. "Electrochemical CO2 reduction on Au surfaces: mechanistic aspects regarding the formation of major and minor products," *Phys Chem Chem Phys* **2017**, *19*, 15856-15863. http://dx.doi.org/10.1039/c7cp02855e

(26) Hara, K.; Tsuneta, A.; Kudo, A.; Sakata, T. "Electrochemical Reduction of C02 on a Cu Electrode under High Pressure Factors that Determine the Product Selectivity," *J. Electrochem. Soc.* **1994**, *141*, 2097-2103.

(27) Gupta, N.; Gattrell, M.; MacDougall, B. "Calculation for the cathode surface concentrations in the electrochemical reduction of CO2 in KHCO3 solutions," *Journal of Applied Electrochemistry* **2005**, *36*, 161-172. http://dx.doi.org/10.1007/s10800-005-9058-y

(28) Lee, S.; Hong, S.; Lee, J. "Bulk pH contribution to CO/HCOO− production from CO2 on oxygen-evacuated Cu2O electrocatalyst," *Catalysis Today* **2017**, *288*, 11-17. http://dx.doi.org/10.1016/j.cattod.2016.09.025

(29) Katsounaros, I.; Meier, J. C.; Klemm, S. O.; Topalov, A. A.; Biedermann, P. U.; Auinger, M.; Mayrhofer, K. J. J. "The effective surface pH during reactions at the solid–liquid interface," *Electrochemistry Communications* **2011**, *13*, 634-637. http://dx.doi.org/10.1016/j.elecom.2011.03.032

(30) Varela, A. S.; Kroschel, M.; Reier, T.; Strasser, P. "Controlling the selectivity of CO 2 electroreduction on copper: The effect of the electrolyte concentration and the importance of the local pH," *Catalysis Today* **2016**, *260*, 8-13. http://dx.doi.org/10.1016/j.cattod.2015.06.009

(31) Hori, Y.; Murata, A.; Takahashi, R. "Formation of Hydrocarbons in the Electrochemical Reduction of Carbon-Dioxide at a Copper Electrode in Aqueous-Solution," *J Chem Soc Farad T 1* **1989**, *85*, 2309-2326. http://dx.doi.org/DOI 10.1039/f19898502309

(32) Hori, Y.; Takahashi, R.; Yoshinami, Y.; Murata, A. "Electrochemical reduction of CO at a copper electrode," *J Phys Chem B* **1997**, *101*, 7075-7081. http://dx.doi.org/DOI 10.1021/jp970284i

(33) Hori, Y.; Takahashi, R.; Yoshinami, Y.; Murata, A. "Electrochemical Reduction of CO at a Copper Electrode," *J. Phys. Chem. B* **1997**, *101*, 7075-7081. http://dx.doi.org/10.1021/jp970284i

(34) Varela, A. S.; Kroschel, M.; Reier, T.; Strasser, P. "Controlling the selectivity of CO2 electroreduction on copper: The effect of the electrolyte concentration and the importance of the local pH," *Catal. Today* **2016**, *260*, 8-13. http://dx.doi.org/10.1016/j.cattod.2015.06.009

(35) Schreier, M.; Yoon, Y.; Jackson, M. N.; Surendranath, Y. "Competition between H and CO for Active Sites Governs Copper-Mediated Electrosynthesis of Hydrocarbon Fuels," *Angew. Chem. Int. Ed.* **2018**, *57*, 10221-10225. http://dx.doi.org/10.1002/anie.201806051

(36) Wuttig, A.; Yaguchi, M.; Motobayashi, K.; Osawa, M.; Surendranath, Y. "Inhibited proton transfer enhances Au-catalyzed CO_2-to-fuels selectivity," *Proc. Natl. Acad. Sci. U.S.A.* **2016**, 201602984. http://dx.doi.org/10.1073/pnas.1602984113

(37) Ooka, H.; Figueiredo, M. C.; Koper, M. T. M. "Competition between Hydrogen Evolution and Carbon Dioxide Reduction on Copper Electrodes in Mildly Acidic Media," *Langmuir* **2017**, *33*, 9307-9313. http://dx.doi.org/10.1021/acs.langmuir.7b00696

(38) Lim, C. F. C.; Harrington, D. A.; Marshall, A. T. "Effects of mass transfer on the electrocatalytic CO 2 reduction on Cu," *Electrochimica Acta* **2017**, *238*, 56-63. http://dx.doi.org/10.1016/j.electacta.2017.04.017

(39) Schouten, K. J. P.; Pérez Gallent, E.; Koper, M. T. M. "The influence of pH on the reduction of CO and to hydrocarbons on copper electrodes," *J. Electroanal. Chem.* **2014**, *716*, 53-57. http://dx.doi.org/10.1016/j.jelechem.2013.08.033

(40) Schouten, K. J. P.; Kwon, Y.; van der Ham, C. J. M.; Qin, Z.; Koper, M. T. M. "A new mechanism for the selectivity to C1 and C2 species in the electrochemical reduction of carbon

dioxide on copper electrodes," *Chem. Sci.* **2011**, *2*, 1902-1909. http://dx.doi.org/10.1039/c1sc00277e

(41) Schouten, K. J. P.; Pérez Gallent, E.; Koper, M. T. M. "Structure Sensitivity of the Electrochemical Reduction of Carbon Monoxide on Copper Single Crystals," *ACS Catalysis* **2013**, *3*, 1292-1295. http://dx.doi.org/10.1021/cs4002404

(42) Calle-Vallejo, F.; Koper, M. T. M. "Theoretical Considerations on the Electroreduction of CO to C2 Species on Cu(100) Electrodes," *Angew. Chem. Int. Ed.* **2013**, *52*, 7282-7285. http://dx.doi.org/10.1002/anie.201301470

(43) Montoya, J. H.; Peterson, A. A.; Nørskov, J. K. "Insights into C□C Coupling in CO2 Electroreduction on Copper Electrodes," *ChemCatChem* **2013**, *5*, 737-742. http://dx.doi.org/10.1002/cctc.201200564

(44) Kim, Y. G.; Baricuatro, J. H.; Javier, A.; Gregoire, J. M.; Soriaga, M. P. "The evolution of the polycrystalline copper surface, first to Cu(111) and then to Cu(100), at a fixed CO(2)RR potential: a study by operando EC-STM," *Langmuir* **2014**, *30*, 15053-15056. http://dx.doi.org/10.1021/la504445g

(45) Dunwell, M.; Lu, Q.; Heyes, J. M.; Rosen, J.; Chen, J. G.; Yan, Y.; Jiao, F.; Xu, B. "The Central Role of Bicarbonate in the Electrochemical Reduction of Carbon Dioxide on Gold," *J Am Chem Soc* **2017**, *139*, 3774-3783. http://dx.doi.org/10.1021/jacs.6b13287

(46) Hori, Y. "Electrochemical CO_2 Reduction on Metal Electrodes," In *Modern Aspects of Electrochemistry*; Vayemas, C. G., Ed.; Springer: New York, 2008; Vol. 42, p 89-189.

(47) Singh, M. R.; Kwon, Y.; Lum, Y.; Ager, J. W., 3rd; Bell, A. T. "Hydrolysis of Electrolyte Cations Enhances the Electrochemical Reduction of CO2 over Ag and Cu," *J Am Chem Soc* **2016**, *138*, 13006-13012. http://dx.doi.org/10.1021/jacs.6b07612

(48) Resasco, J.; Chen, L. D.; Clark, E.; Tsai, C.; Hahn, C.; Jaramillo, T. F.; Chan, K.; Bell, A. T. "Promoter Effects of Alkali Metal Cations on the Electrochemical Reduction of Carbon Dioxide," *J. Am. Chem. Soc.* **2017**, *139*, 11277-11287. http://dx.doi.org/10.1021/jacs.7b06765

(49) Resasco, J.; Chen, L. D.; Clark, E.; Tsai, C.; Hahn, C.; Jaramillo, T. F.; Chan, K.; Bell, A. T. "Promoter Effects of Alkali Metal Cations on the Electrochemical Reduction of Carbon Dioxide," *J Am Chem Soc* **2017**, *139*, 11277-11287. http://dx.doi.org/10.1021/jacs.7b06765

(50) Hall, A. S.; Yoon, Y.; Wuttig, A.; Surendranath, Y. "Mesostructure-Induced Selectivity in CO_2 Reduction Catalysis," *J. Am. Chem. Soc.* **2015**, *137*, 14834-14837. http://dx.doi.org/10.1021/jacs.5b08259

(51) Yoon, Y.; Hall, A. S.; Surendranath, Y. "Tuning of Silver Catalyst Mesostructure Promotes Selective Carbon Dioxide Conversion into Fuels," *Angew. Chem. Int. Ed.* **2016**, *55*, 15282-15286. http://dx.doi.org/10.1002/anie.201607942

(52) Yoon, Y.; Hall, A. S.; Surendranath, Y. "Tuning of Silver Catalyst Mesostructure Promotes Selective Carbon Dioxide Conversion into Fuels," *Angewandte Chemie-International Edition* **2016**, *55*, 15282-15286. http://dx.doi.org/10.1002/anie.201607942

(53) Kas, R.; Kortlever, R.; Milbrat, A.; Koper, M. T.; Mul, G.; Baltrusaitis, J. "Electrochemical CO2 reduction on Cu2O-derived copper nanoparticles: controlling the catalytic selectivity of hydrocarbons," *Phys Chem Chem Phys* **2014**, *16*, 12194-12201. http://dx.doi.org/10.1039/c4cp01520g

(54) Lum, Y.; Yue, B.; Lobaccaro, P.; Bell, A. T.; Ager, J. W. "Optimizing C–C Coupling on Oxide-Derived Copper Catalysts for Electrochemical CO2 Reduction," *The Journal of Physical Chemistry C* **2017**, *121*, 14191-14203. http://dx.doi.org/10.1021/acs.jpcc.7b03673

(55) Ren, D.; Deng, Y.; Handoko, A. D.; Chen, C. S.; Malkhandi, S.; Yeo, B. S. "Selective Electrochemical Reduction of Carbon Dioxide to Ethylene and Ethanol on Copper(I) Oxide Catalysts," *ACS Catalysis* **2015**, *5*, 2814-2821. http://dx.doi.org/10.1021/cs502128q

(56) Feng, X.; Jiang, K.; Fan, S.; Kanan, M. W. "A Direct Grain-Boundary-Activity Correlation for CO Electroreduction on Cu Nanoparticles," *ACS Cent Sci* **2016**, *2*, 169-174. http://dx.doi.org/10.1021/acscentsci.6b00022

(57) Mariano, R. G.; McKelvey, K.; White, H. S.; Kanan, M. W. "Selective increase in CO2 electroreduction activity at grain-boundary surface terminations," *Science* **2017**, *358*, 1187-1191. http://dx.doi.org/10.1126/science.aao3691

(58) Durand, W. J.; Peterson, A. A.; Studt, F.; Abild-Pedersen, F.; Nørskov, J. K. "Structure effects on the energetics of the electrochemical reduction of CO2 by copper surfaces," *Surface Science* **2011**, *605*, 1354-1359. http://dx.doi.org/https://doi.org/10.1016/j.susc.2011.04.028

(59) Reske, R.; Mistry, H.; Behafarid, F.; Roldan Cuenya, B.; Strasser, P. "Particle size effects in the catalytic electroreduction of CO(2) on Cu nanoparticles," *J Am Chem Soc* **2014**, *136*, 6978-6986. http://dx.doi.org/10.1021/ja500328k

(60) Hori, Y.; Konishi, H.; Futamura, T.; Murata, A.; Koga, O.; Sakurai, H.; Oguma, K. "“Deactivation of copper electrode” in electrochemical reduction of CO2," *Electrochimica Acta* **2005**, *50*, 5354-5369. http://dx.doi.org/10.1016/j.electacta.2005.03.015

(61) Dewulf, D. W.; Jin, T.; Bard, A. J. "Electrochemical and Surface Studies of Carbon-Dioxide Reduction to Methane and Ethylene at Copper Electrodes in Aqueous-Solutions," *Journal of the Electrochemical Society* **1989**, *136*, 1686-1691. http://dx.doi.org/Doi 10.1149/1.2096993

(62) Wasmus, S.; Cattaneo, E.; Vielstich, W. "Reduction of Carbon Dioxide to Methane and Ethene—an On-line MS Study with Rotating Electrodes," *Elecrrochimica Acta* **1990**, *35*, 771-775. http://dx.doi.org/10.1016/0013-4686(90)90014-Q

(63) Hori, Y.; Suzuki, S. "Cathodic Reduction of Carbon Dioxide for Energy Storage," *Journal of the Research InstItute for Catalysis Hokkaido University* **1983**, *30*, 81-88.

(64) Kyriacou, G.; Anagnostopoulos, A. "Electrochemical Reduction of Co2 at Cu+Au Electrodes," *Journal of Electroanalytical Chemistry* **1992**, *328*, 233-243. http://dx.doi.org/Doi 10.1016/0022-0728(92)80181-3

(65) Augustynski, J.; Kedzierzawski, P.; Jermann, B. "Electrochemical reduction of CO2 at metallic electrodes," *Stud Surf Sci Catal* **1998**, *114*, 107-116.

(66) Terunuma, Y.; Saitoh, A.; Momose, Y. "Relationship between hydrocarbon production in the electrochemical reduction of CO2 and the characteristics of the Cu electrode," *Journal of Electroanalytical Chemistry* **1997**, *434*, 69-75. http://dx.doi.org/Doi 10.1016/S0022-0728(97)00122-8

(67) He, J.; Huang, A.; Johnson, N. J. J.; Dettelbach, K. E.; Weekes, D. M.; Cao, Y.; Berlinguette, C. P. "Stabilizing Copper for CO2 Reduction in Low-Grade Electrolyte," *Inorg Chem* **2018**, *57*, 14624-14631. http://dx.doi.org/10.1021/acs.inorgchem.8b02311

(68) Mayrhofer, K. J. J.; Wiberg, G. K. H.; Arenz, M. "Impact of glass corrosion on the electrocatalysis on Pt electrodes in alkaline electrolyte," *Journal of the Electrochemical Society* **2008**, *155*, P1-P5. http://dx.doi.org/10.1149/1.2800752

(69) Mayrhofer, K. J. J.; Crampton, A. S.; Wiberg, G. K. H.; Arenz, M. "Analysis of the impact of individual glass constituents on electrocatalysis on pt electrodes in alkaline solution," *Journal of the Electrochemical Society* **2008**, *155*, P78-P81. http://dx.doi.org/10.1149/1.2904882

(70) Klaus, S.; Cai, Y.; Louie, M. W.; Trotochaud, L.; Bell, A. T. "Effects of Fe Electrolyte Impurities on Ni(OH)2/NiOOH Structure and Oxygen Evolution Activity," *The Journal of Physical Chemistry C* **2015**, *119*, 7243-7254. http://dx.doi.org/10.1021/acs.jpcc.5b00105

(71) Trotochaud, L.; Young, S. L.; Ranney, J. K.; Boettcher, S. W. "Nickel-iron oxyhydroxide oxygen-evolution electrocatalysts: the role of intentional and incidental iron incorporation," *J Am Chem Soc* **2014**, *136*, 6744-6753. http://dx.doi.org/10.1021/ja502379c

(72) Sawyer, D. T.; Sobkowiak, A.; Roberts, J. L.; Sawyer, D. T. *Electrochemistry for chemists*; Wiley-Interscience, 1995.

(73) Wuttig, A.; Surendranath, Y. "Impurity Ion Complexation Enhances Carbon Dioxide Reduction Catalysis," *ACS Catalysis* **2015**, *5*, 4479-4484. http://dx.doi.org/10.1021/acscatal.5b00808

(74) Clark, E. L.; Resasco, J.; Landers, A.; Lin, J.; Chung, L.-T.; Walton, A.; Hahn, C.; Jaramillo, T. F.; Bell, A. T. "Standards and Protocols for Data Acquisition and Reporting for Studies of the Electrochemical Reduction of Carbon Dioxide," *ACS Catalysis* **2018**, *8*, 6560-6570. http://dx.doi.org/10.1021/acscatal.8b01340

(75) Ren, D.; Fong, J.; Yeo, B. S. "The effects of currents and potentials on the selectivities of copper toward carbon dioxide electroreduction," *Nat Commun* **2018**, *9*, 925. http://dx.doi.org/10.1038/s41467-018-03286-w

(76) Hori, Y.; Murata, A.; Takahashi, R. "Formation of Hydrocarbons in the Electrochemical Reduction of Carbon-Dioxide at a Copper Electrode in Aqueous-Solution," *J. Chem. Soc., Faraday Trans. 1* **1989**, *85*, 2309-2326. http://dx.doi.org/10.1039/f19898502309

(77) Kim, J. J.; Summers, D. P.; Frese, K. W. "Reduction of Co2 and Co to Methane on Cu Foil Electrodes," *Journal of Electroanalytical Chemistry* **1988**, *245*, 223-244. http://dx.doi.org/Doi 10.1016/0022-0728(88)80071-8

(78) Zhang, L.; Zhao, Z. J.; Gong, J. "Nanostructured Materials for Heterogeneous Electrocatalytic CO2 Reduction and their Related Reaction Mechanisms," *Angew Chem Int Ed Engl* **2017**, *56*, 11326-11353. http://dx.doi.org/10.1002/anie.201612214

(79) Reske, R.; Duca, M.; Oezaslan, M.; Schouten, K. J. P.; Koper, M. T. M.; Strasser, P. "Controlling Catalytic Selectivities during CO2 Electroreduction on Thin Cu Metal Overlayers," *The Journal of Physical Chemistry Letters* **2013**, *4*, 2410-2413. http://dx.doi.org/10.1021/jz401087q

(80) Kimura, K. W.; Fritz, K. E.; Kim, J.; Suntivich, J.; Abruna, H. D.; Hanrath, T. "Controlled Selectivity of CO2 Reduction on Copper by Pulsing the Electrochemical Potential," *ChemSusChem* **2018**, *11*, 1781-1786. http://dx.doi.org/10.1002/cssc.201800318

(81) Li, C. W.; Kanan, M. W. "CO2 reduction at low overpotential on Cu electrodes resulting from the reduction of thick Cu2O films," *J Am Chem Soc* **2012**, *134*, 7231-7234. http://dx.doi.org/10.1021/ja3010978

(82) Hori, Y.; Takahashi, I.; Koga, O.; Hoshi, N. "Electrochemical reduction of carbon dioxide at various series of copper single crystal electrodes," *Journal of Molecular Catalysis A: Chemical* **2003**, *199*, 39-47. http://dx.doi.org/10.1016/s1381-1169(03)00016-5

(83) Jermann, B.; Augustynski, J. "Long-Term Activation of the Copper Cathode in the Course of Co2 Reduction," *Electrochimica Acta* **1994**, *39*, 1891-1896. http://dx.doi.org/Doi 10.1016/0013-4686(94)85181-6

(84) Smith, B. D.; Irish, D. E.; Kedzierzawski, P.; Augustynski, J. "A surface enhanced Raman scattering study of the intermediate and poisoning species formed during the electrochemical reduction of CO2 on copper," *Journal of the Electrochemical Society* **1997**, *144*, 4288-4296. http://dx.doi.org/Doi 10.1149/1.1838180

(85) Corrigan, D. A. "The Catalysis of the Oxygen Evolution Reaction by Iron Impurities in Thin-Film Nickel-Oxide Electrodes," *Journal of the Electrochemical Society* **1987**, *134*, 377-384. http://dx.doi.org/Doi 10.1149/1.2100463

(86) Stevens, M. B.; Enman, L. J.; Batchellor, A. S.; Cosby, M. R.; Vise, A. E.; Trang, C. D. M.; Boettcher, S. W. "Measurement Techniques for the Study of Thin Film Heterogeneous Water Oxidation Electrocatalysts," *Chemistry of Materials* **2016**, *29*, 120-140. http://dx.doi.org/10.1021/acs.chemmater.6b02796

(87) Chen, Y.; Li, C. W.; Kanan, M. W. "Aqueous CO2 reduction at very low overpotential on oxide-derived Au nanoparticles," *J Am Chem Soc* **2012**, *134*, 19969-19972. http://dx.doi.org/10.1021/ja309317u

(88) Lee, S. Y.; Jung, H.; Kim, N. K.; Oh, H. S.; Min, B. K.; Hwang, Y. J. "Mixed Copper States in Anodized Cu Electrocatalyst for Stable and Selective Ethylene Production from CO2 Reduction," *J Am Chem Soc* **2018**, *140*, 8681-8689. http://dx.doi.org/10.1021/jacs.8b02173

(89) Ma, M.; Liu, K.; Shen, J.; Kas, R.; Smith, W. A. "In Situ Fabrication and Reactivation of Highly Selective and Stable Ag Catalysts for Electrochemical CO2 Conversion," *ACS Energy Lett* **2018**, *3*, 1301-1306. http://dx.doi.org/10.1021/acsenergylett.8b00472

Chapter 2: Effect and Prevention of Trace Ag Contamination from Ag/AgCl Reference Electrodes on CO_2 Reduction Product Distributions at Polycrystalline Copper Electrodes

2.1 Preface

This chapter presents the study of the reference electrode as a possible source of trace metal contamination in the Cu-catalyzed CO_2RR. In particular, single junction Ag/AgCl/KCl(sat.), a common choice of reference electrode, is found to be a source of Ag^+ contamination. My experimental data suggests that the Ag^+ contamination can deposit onto the Cu surfaces, where ppb levels of Ag^+ contamination can measurably alter the product distribution of Cu systems. This type of contamination can be prevented for at least 12 h by adopting a double junction configuration of the reference electrode. This chapter is derived from a previously published manuscript where I was the primary author responsible for all electrochemical measurement, analysis, and preparation of the manuscript. Reprinted with permission from *ACS Appl. Energy Mater.* 2019, 2, 11, 8283-829. Copyright 2019 American Chemical Society.

2.2 Introduction

Single junction Ag/AgCl/KCl(sat.) reference electrodes are one of the most commonly used reference electrodes in CO_2RR studies.[11,53,56,73,87,90] However, these reference electrodes have been previously reported to leak Ag^+ into electrolyte solutions, and this leaked Ag^+ has been shown to modulate the activity of the hydrogen evolution reaction (HER) on carbon cathodes.[91] Herein, we report that Ag/AgCl/KCl(sat.) reference electrodes are a source of trace Ag^+ contamination which measurably alters the CO_2RR product distribution at planar polycrystalline Cu electrodes.

Specifically, we show that single junction Ag/AgCl/KCl(sat.) reference electrodes leak measurable amounts of Ag^+ into solution over time, and this Ag^+ migrates to the working electrode where it electrodeposits under CO_2RR conditions. These Ag deposits have a profound impact on the CO_2RR product distribution, leading to increased Faradaic efficiency of CO and decreased Faradaic efficiency of CH_4.

We confirm that even trace amounts of Ag^+ in the electrolyte solution (~10 ppb) have measurable effects on the CO_2RR product distribution. We also confirm that using a double junction Ag/AgCl/KCl(sat.)/0.1 M $NaHCO_3$ reference electrode successfully prevents Ag^+ leakage during the course of our controlled potential electrolysis (CPE) experiments. Based on our findings, we conclude that single junction Ag/AgCl/KCl(sat.) reference electrodes are a significant source of Ag^+ contamination that measurably alters product distribution of the CO_2RR at Cu working electrodes. This is an important finding given the prevalence of Ag/AgCl/KCl(sat.) reference electrodes use in CO_2RR studies. We propose that using double-junction Ag/AgCl/KCl(sat.)/$NaHCO_3$(0.1 M) reference electrodes is a simple way to mitigate Ag^+ leakage and recommend their use in future CO_2RR studies.

2.3 Experimental

Cu foil (Puratronic, 99.999% metals basis) and Ni foil (Puratronic, 99.994% metals basis) were purchased from Alfa Aesar and used as working electrodes. Carbon rods (99.999%) were purchased from Strem Chemicals, Inc., and used as auxiliary electrodes. Nafion-117 cation exchange membranes were purchased from the Fuel Cell Store and used as a separating membrane between the working and auxiliary chambers of the electrochemical cell. Ag wire (99.9% trace metal basis, Acros Organics) and 1/8" chunks CoralPor® frits with 1/2" Teflon heat shrink tubing (BASi) were used in the construction of the custom-made Ag/AgCl reference electrodes. Commercial Ag/AgCl/KCl(3.0 M) reference electrodes were purchased from CH Instruments and stored in sat. KCl solution for several days to exchange the interior electrolyte solution and convert to Ag/AgCl/KCl(sat.). HPLC-grade sodium bicarbonate ($NaHCO_3$, 99+%, for HPLC) was purchased from Acros Organics. Resin-treatment of the sodium bicarbonate electrolyte was done using Chelex 100 resin (sodium form, Sigma-Aldrich). Phosphoric acid (H_3PO_4, 99.99% trace metal basis, Sigma-Aldrich), nitric acid (HNO_3, trace metal grade, Fisher), hydrochloric acid (HCl, trace metal grade, Fisher), hydrochloric acid (ACS grade, Acros Organics) used for cleaning Cu surfaces, sodium hydroxide (NaOH, 99.99% semiconductor grade, Sigma-Aldrich), sulfuric acid (H_2SO_4, OPTIMA grade, Fisher), and ferrocenecarboxylic acid (FcCOOH, 97%, Sigma-Aldrich) were used as received unless noted otherwise. Ag ICP-MS standards were purchased from Ricca Chemical. PTFE sealing tape (Poly-Temp MD, Anti-Seize Technology) was used for sealing edges and connection areas of electrochemical cells. All solutions were prepared with ultrapure water (18.2 MΩ·cm resistivity) purified with a Thermo Scientific GenPure UV-TOC/UF xCAD-plus water purification system. The same water was used for all water rinse steps.

Resin Treatment of Electrolyte

Electrolyte solutions were treated with a Chelex-100 ion-exchange resin to remove trace metal impurities based on a previously-reported procedure.[73] Before use, the Chelex-100 resin was regenerated using a procedure based on previously-published regeneration procedures with modification as follows: 20 g resin was stirred in 100 mL of 1 M trace metal grade HCl for 12 h. The resulting slurry was filtered and rinsed with 500 mL of water and dried with vacuum filtration, then immediately stirred for 24 h in 100 mL of 1 M semiconductor grade NaOH at 60 °C, followed by filtering and rinsing with 500 mL of water with vacuum filtration. The regenerated Chelex-100 resin was dried by vacuum filtration before use. The resin was completely submerged in solution when stirred.

To treat the electrolyte, dried regenerated resin was placed in the electrolyte (0.1 M $NaHCO_3$, or 0.05M Na_2CO_3 when sodium carbonate decahydrate was used) and stirred for at least 12 h before use. Resin was filtered out from electrolyte before experiment. 10 g of resin is used per 100mL 0.1 M $NaHCO_3$. All stir bars used were kept in 1 M trace metal grade HNO_3 overnight prior to use. High density polyethylene bottles (Nalgene, Thermo Scientific) were used for resin regeneration in HCl and NaOH as well as for electrolyte treatment to avoid trace metal contribution from glass containers during the process of NaOH bath.

Preparation of Electrodes

Cu foil was first rinsed in 3 M ACS grade HCl for 30 sec and rinsed with water, then electrochemically polished in 85% trace metal grade phosphoric acid at 2.1 V vs commercial Ag/AgCl/KCl(sat.) (CH instruments) for 5 min, followed by water rinse. Carbon rods were used as auxiliary electrodes in electrochemical polishing. For all electropolishing procedures, a three-electrode set up was used with no membrane separator. This was to prevent possible complications

arising from placing membranes under extremely acidic conditions (85% phosphoric acid). It is important to note that since the foils were always kept under positive potentials, we do not expect the electrochemical polishing setup led to trace Ag^+ contamination from reference or auxiliary electrodes during the process. Ni foil was mechanically polished using MetaDi diamond suspension with sequential grit size (9, 6, 3, 1, 0.1 μm, Buehler) followed by sonication in water. The area polished was at least twice as large as the area submerged in electrolytes in later experiments. The foils were then dried with N_2 before experiments.

Storage of Electrochemical Cell and Tools

To remove any lingering metal contaminants, all electrochemical cells and stir bars used in controlled potential electrolysis (CPE) experiments were stored in 1 M trace metal grade HNO_3 when not in used. This is to remove any metal contaminant that does not naturally occur. The cells and stir bars were rinsed with water prior to use. To avoid metal contamination from tools, only tools made of Teflon or glass materials were used. Metal tools were never in contact with the resin, electrodes, membrane separators, stir bars, or electrolyte with the exception of the stainless steel rods and alligator clips used for electrical contact of electrodes during electrochemical experiments (see Figure S1 and under Electrochemical measurements).

Electrochemical Measurements

Reference electrodes in controlled potential electrolysis (CPE) experiments were custom-made single-junction Ag/AgCl/KCl(sat.) or double-junction Ag/AgCl/KCl(sat.)/$NaHCO_3$(0.1 M) electrodes sealed with commercially available frit (1/8" chunks CoralPor® with 1/2" tubes Teflon heat shrink, BASi) and externally referenced to ferrocenecarboxylic acid in 0.2 M phosphate buffer at pH 7 (0.329 V vs. Ag/AgCl/KCl(sat.)). See Figure 0-1 for single-junction and double-junction reference electrode designs. To avoid trace Ag^+ accumulation in the external frit for the double-

junction reference electrode, the external frit was periodically cleaned by soaking in trace-metal grade 0.1 M HNO_3 for 1 h followed by soaking in water for storage. Note that 1 M HNO_3 was not used on reference electrodes for cleaning because the frits were unstable under these conditions.

Electrochemical measurements were performed using a Bio-Logic SP200 potentiostat/galvanostat. Data were recorded using the Bio-Logic EC-Lab V10.44 software package. Reported values are averages from at least three repetitions with separately prepared electrodes and electrochemical setups, and all reported errors are standard deviations. All electrochemical cells and stir bars were stored in trace metal grade 1 M HNO_3 between experiments to prevent leaching of trace metal contaminants during electrochemical measurements. In addition, the Nafion membrane was analyzed with ICP-MS prior to measurements to ensure no presence of Ag contamination.

CPE experiments were conducted at room temperature in a custom-made, gas-tight two-chamber H-cell (Figure 0-2). The working chamber contained the working electrode, the reference electrode, and ~30 mL of electrolyte. The working and reference electrodes were connected to the potentiostat using stainless steel rods soldered with stainless steel alligator clips. The exposed metal portions of the rods and clips were never submerged in solution, and they were covered with PTFE tape at all times to mitigate possible contact with electrolyte solution. The working electrode was submerged in the solution such that ~0.6 cm^2 of foil was exposed to solution for each measurement. The auxiliary chamber held a carbon rod as the auxiliary electrode and ~30 mL of electrolyte. The two chambers were separated with an ion exchange membrane (Nafion-117).

The headspace in the working chamber was individually measured after experiment as follows: after each CPE experiment, the working chamber containing the working and reference electrodes, stir bars, stainless steel rods and alligator clips, etc., was completely filled with water

such that no headspace remained, and the mass of the water needed to fill the working chamber was measured. The total volume of the working chamber was then calculated from the mass of water assuming a density of 1 g/mL for water. The headspace was then calculated by subtracting the amount of electrolyte in the CPE measurement from the total volume of the working chamber. A typical headspace volume measurement was ~160 mL. After experiment, the electrochemical cell and stir bar were soaked in 1 M HNO_3 to eliminate contamination from exposure to the stainless steel rods and alligator clips.

Prior to each experiment, the working chamber was sparged with the appropriate gas using a section of Tygon tubing for 60 min and was sealed under 1 atm atmosphere of the appropriate gas**.** In the case of hydrogen evolution reactions (HER) experiments with Ni electrodes, the working chamber containing 0.1 M trace metal grade H_2SO_4 was sparged and then sealed under 1 atm N_2 gas. Ni HER CPEs were then conducted for 1 h (constant time) and ~70 C was passed during each CPE measurement. In the case of CO_2RR experiments at Cu electrodes, the working chamber was sparged and then sealed under CO_2 gas. The pH of the CO_2 saturated electrolyte (0.1 M $NaHCO_3$) was measured to be pH = 6.8 using a Fisher Scientific Accumet AB200 pH meter with an Accumet pH/ATC Epoxy Body Combination Electrode calibrated at three points with pH = 4.01, 7.00, and 10.01 calibration solutions. In Cu CO_2RR experiments, CPE measurements were typically run until ~50 C of charge was passed (constant charge)—the time of the electrolyses varied with potential from ~1 h at the most negative –1.65 V vs Ag/AgCl/KCl(sat.) to ~1.5 h at the most positive –1.50 V vs Ag/AgCl/KCl(sat.). For long-term Cu CO_2RR experiments, CPE measurements were run for 12 h (constant time) in the potential range –1.60 to –1.63 V vs Ag/AgCl/KCl(sat.). For Cu CO_2RR with Ag^+ titration experiments, 0.1 M $NaHCO_3$ solutions

containing 1, 5, 10, 50, 100, and 1000 ppb Ag^+ were prepared by externally adding an appropriate amount of Ag ICP-MS standard (Ricca).

Before each CPE experiment, the uncompensated resistance of the cell was measured with a single-point high-frequency impedance measurement, and the applied potential was iR-compensated automatically at 85% through positive feedback using the Bio-Logic EC-Lab software. The remaining 15% was corrected manually after the experiment using the average current during each CPE measurement. This correction protocol was adapted from a literature procedure.[11] All working electrode potentials reported are iR-compensated and referenced vs Ag/AgCl/KCl(sat.).

Product detection and quantification

Gas chromatography (GC) and high-performance liquid chromatography (HPLC) were used to analyze gaseous and liquid products from CPE experiments. Gaseous samples were analyzed using a Thermo Scientific Trace 1310 GC system. Two analyzer channels were used to separately detect H_2 and carbon products. A Pressure-Lok gas-tight syringe (10 mL, Valco VICI Precision Sampling, Inc.) was used to collect a 10 mL aliquot from the headspace of the working chamber. The aliquot was then injected into the 3 mL GC sample loop. Thermo Scientific provided the valve system, configurations, and method for gas separation and detection. H_2 was detected on the first channel using Ar carrier gas. All other gases were detected on the second channel using He carrier gas. A thermal conductivity detector was used. The GC system was calibrated using calibration gas mixtures (SCOTTY Specialty Gas). Chromatographs were analyzed using the Chromeleon Console WorkStation software.

For liquid samples, 2 mL aliquots of post-CPE solutions were analyzed for formic acid using a Thermo Scientific UltiMate 3000 high-performance liquid chromatography (HPLC)

system equipped with a refractive index detector (RFD). The column configuration was a 5 cm Thermo Scientific™ HyperREZ™ XP Carbohydrate H^+ LC guard column and a 30 cm Thermo Scientific™ HyperREZ™ XP Carbohydrate H^+ LC analytical column in series at constant temperature of 50°C. An aqueous solution of 0.005 M H_2SO_4 was the mobile phase. Calibration of formic acid was done by analyzing calibration standards of formic acid from 0.1 μM to 27 μM. The detection limit of the HPLC for formic acid was determined to be 0.1 μM. Only formic acid was measured and analyzed in the liquid samples, though we are aware that other liquid products such as methanol and ethanol have also been reported previously for Cu-catalyzed CO_2RR.

Faradaic efficiencies of gaseous products were calculated using eq 2-1:

$$\mathrm{FE} = \frac{\frac{V_{HS}}{V_g} \times G \times n \times F}{Q} \qquad 2\text{-}1$$

where V_{HS} is the headspace volume in mL of the working chamber, V_g is the molar volume of gas at 25 °C and 1.0 atm (24500 mL/mol), G is the volume percent of gaseous product determined by GC (%), n is the number of electrons required for each product (n = 2 for H_2 and CO, 8 for CH_4, and 12 for C_2H_4), F is Faraday constant (C/mol), and Q is the charge passed during the CPE measurement (C).

Faradaic efficiencies of liquid products were calculated using eq 2-2:

$$\mathrm{FE} = \frac{M \times V_l \times n \times F}{Q} \qquad 2\text{-}2$$

where M is the molar concentration (mol/L) of formic acid determined by HPLC, V_l is the volume of electrolyte in the working chamber, n is the number of electrons required (n = 2 for formic acid), F is Faraday constant (C/mol), and Q is the charge passed during the CPE measurement (C).

Trace Ag^+ determination

Inductively coupled plasma- mass spectrometry (ICP-MS) was used to analyze trace metal contents using a Perkin-Elmer Nexion 2000 ICP-MS. Calibration standards were prepared at concentrations of 0.1, 0.3, 0.5, 1, 5, 10 ppb Ag^+. Measurements of Ag^+ in H_2O, HNO_3, and H_2SO_4 solutions were made by directly injecting the solution into the ICP-MS instrument. Solid samples analyzed for deposited Ag content were etched in 10 mL of 1 M trace metal grade HNO_3 for 1 h, and the HNO_3 solution was then analyzed. The limit of quantification for our measurements was determined to be 0.5 ppb, or 5 ng for a 10 mL liquid sample. Conversion from ppb to mass is shown in the following:

$$X\ ppb\ \times \frac{\frac{1\ \mu g}{L}}{1\ ppb}\ \times 0.010\ L\ \times \frac{1000\ ng}{1\ \mu g} = mass\ in\ ng$$

where X is the concentration of Ag^+ in the liquid sample in ppb. Ag^+ concentration in 0.1 M $NaHCO_3$ electrolyte solutions could not be directly measured because the high Na^+ content from the electrolyte could deposit on the skimmer cones, nebulizer, and spray chamber, and therefore damage the instrument.

2.4 Result and Discussion

Initial Studies and Key Hypotheses Regarding the Effect of Ag/AgCl Reference Electrodes on CO_2RR Product Distribution

Our first set of experiments highlights the difference in CO_2RR product distributions obtained at planar polycrystalline Cu working electrodes depending on whether a single-junction Ag/AgCl/KCl(sat.) or double-junction Ag/AgCl/KCl(sat.)/$NaHCO_3$(0.1 M) reference electrode was used. The results of these experiments informed our primary hypothesis—that Ag^+ contamination leaking from the reference electrodes appreciably changes the product distribution of the CO_2RR at Cu electrodes. Product distributions were measured by evaluating the headspace and electrolyte solution following ~1 to 1.5 h controlled potential electrolyses (CPEs) in a sealed two-chamber H-cell. The first chamber held the Cu working electrode and reference electrode, the second chamber held the carbon-rod auxiliary electrode, and the two chambers were separated by a Nafion 117 membrane. All electrolyte solutions were pre-treated with Chelex® resin prior to use as described in the experimental section and according to suggested best practices.[73]

To investigate the effect of the reference electrode on the potential-dependent product distributions at Cu electrodes, we conducted CPEs at 10 applied potentials: –1.555 V, –1.580 V, –1.596 V, –1.600 V, –1.630 V, –1.650 V, –1.670 V, –1.690 V, –1.700 V, and –1.710 V vs Ag/AgCl/KCl(sat.). However, because of the manual component in our iR-correction protocol, slight variations in the measured uncompensated resistance and differences in the measured operating currents between experiments led to a broader spread of iR-compensated potentials at the working electrode. For that reason, we report the results of our potential-dependent CPE measurements using single-junction and double-junction reference electrodes in two different ways. First, in Figure 2-1 we show the combined product distributions from all of the CPE

conducted for each study. This highlights the true potential-dependent nature of the product distribution and illustrates the relative qualitative variance in the product distribution data for the single-junction and double-junction reference electrodes. Second, to better illustrate potential-dependent trends in the product distributions, we averaged the product distribution data from our CPEs in 20 mV intervals from –1.51 V to –1.65 V vs Ag/AgCl/KCl(sat.). The resulting average Faradaic efficiencies in each 20 mV interval are reported as a function of the average iR-corrected working electrode potential in Figure 2-2 and summarized in Table 0-1 and Table 0-2.

A few key observations regarding the relative product distributions collected using the single-junction and double-junction reference electrodes can be seen from Figure 2-1 and Figure 2-2. First, in all CPEs regardless of reference electrode, we see ~91% total Faradaic efficiency. This suggests that conversion of CO_2 to the five products we report accounts for most of the charge passed in the CPEs. Conversion to other minor products (e.g. ethanol, n-propanol, allyl alcohol, etc.) produced in quantities below our detection limits are likely responsible for the additional unaccounted-for charge.[11] Second, the product distributions collected using the single-junction reference electrodes show increased Faradaic efficiency for CO and H_2 and decreased Faradaic efficiency for CH_4 and C_2H_4 at nearly every potential compared to those collected using the double-junction reference electrode. Third, there is a much larger variance in the Faradaic efficiencies for CO in the single-junction reference electrode experiments, especially at more negative potentials as evidenced by the large scatter in CO data in Figure 2-1b and the large standard deviations for the CO measurements in Figure 2-2b.

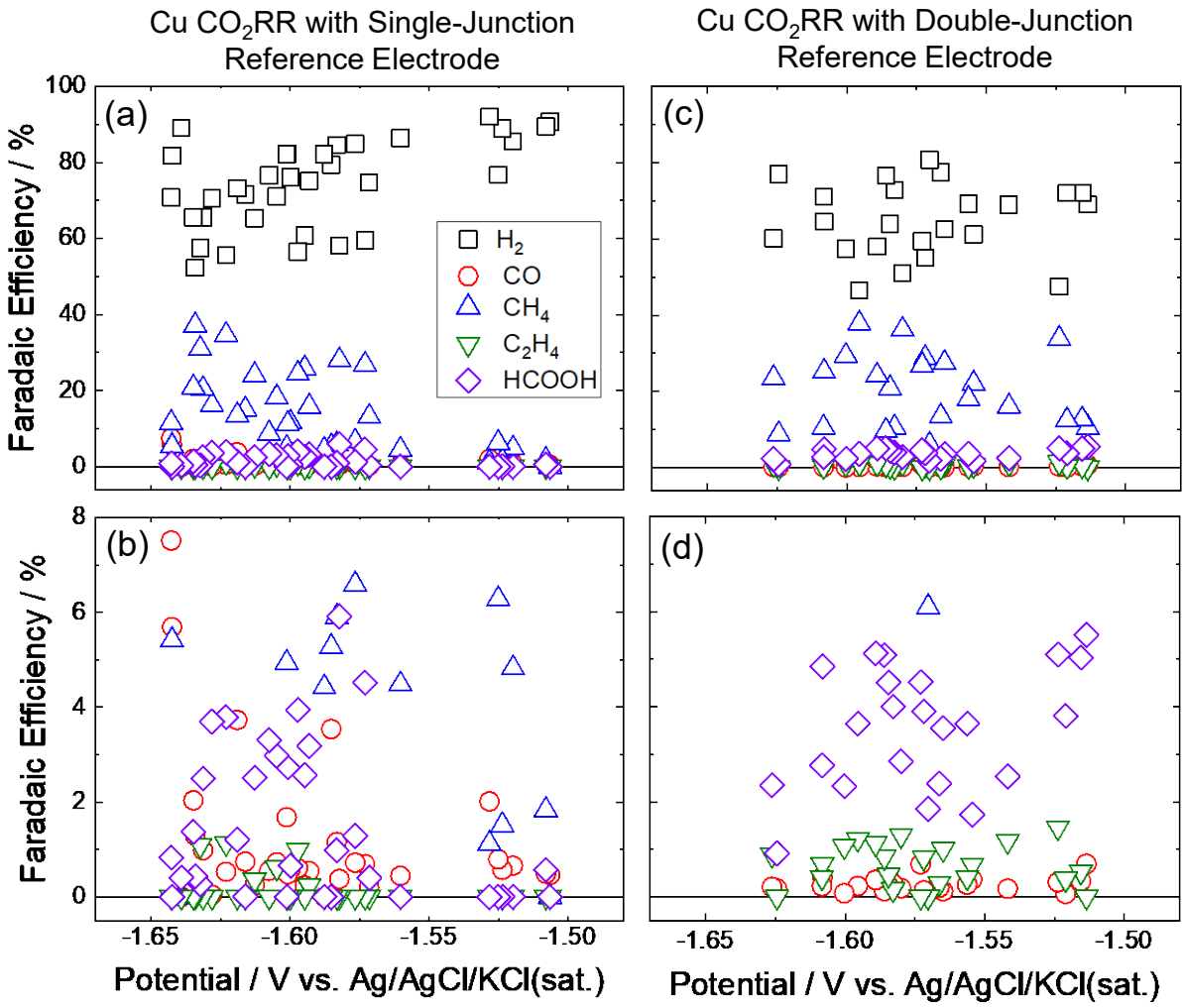

Figure 2-1 Product distributions for CO_2RR at Cu electrodes using (a-b) single junction Ag/AgCl/KCl(sat.) reference electrodes and (c-d) double junction Ag/AgCl/KCl(sat.)/$NaHCO_3$(0.1 M) reference electrodes. (a) and (c) show the full product distribution range (0-100% Faradaic efficiency) and highlight relative H_2 and CH_4 production. (b) and (d) zoom in to the 0-8% Faradaic efficiency range and highlight relative CO, HCOOH, and C_2H_4 production.

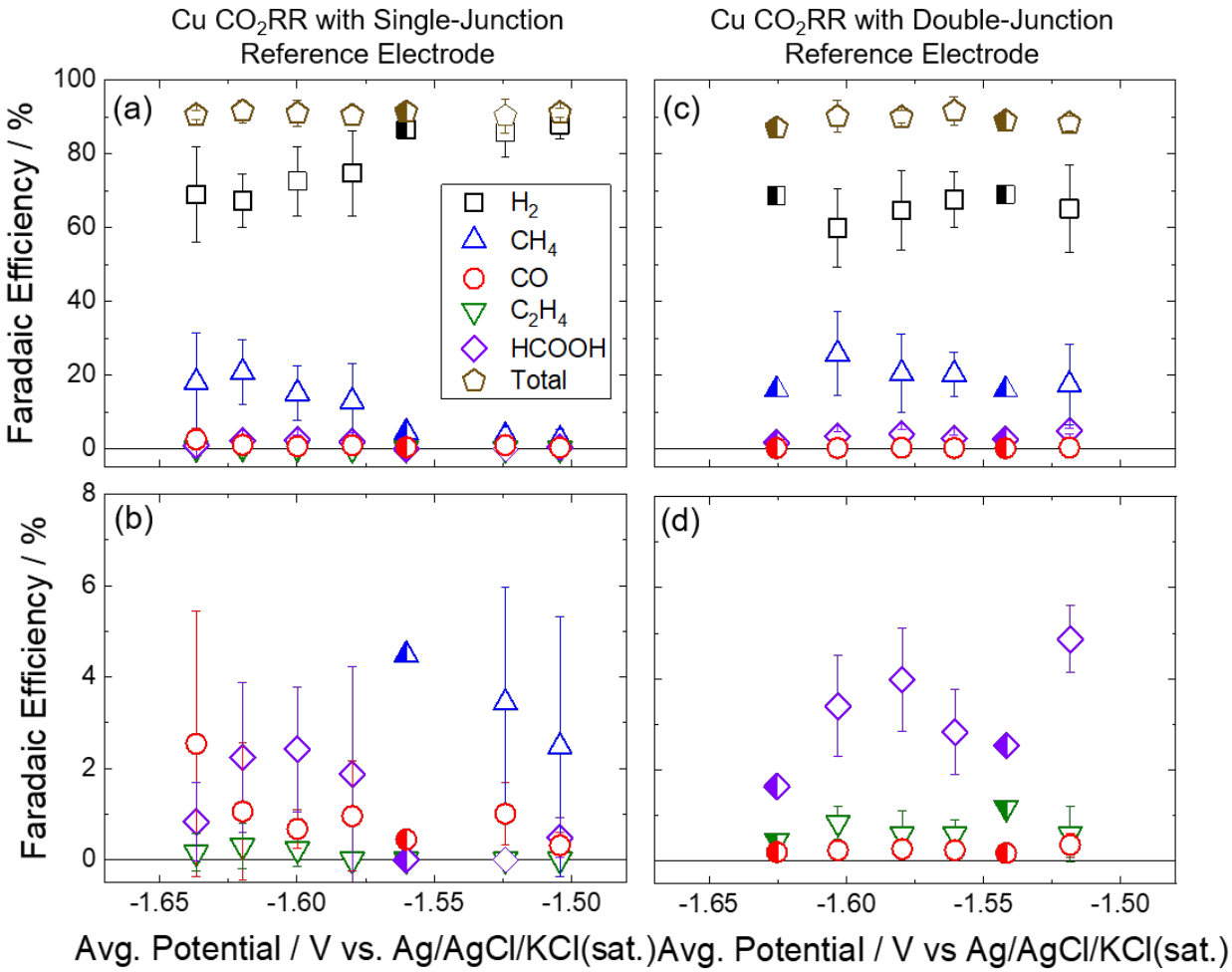

Figure 2-2 Average values of the product distributions for CO_2RR at Cu electrodes in 20 mV intervals using (a-b) single junction Ag/AgCl/KCl(sat.) reference electrodes and (c-d) double junction Ag/AgCl/KCl(sat.)/$NaHCO_3$(0.1 M) reference electrodes. (a) and (c) show the full product distribution range (0-100% Faradaic efficiency) and highlight relative H_2 and CH_4 production. (b) and (d) zoom in to the 0-8% Faradaic efficiency range and highlight relative CO, HCOOH, and C_2H_4 production. All error bars are the standard deviations from at least 3 measurements within the interval. Half-shaded symbols represent average values from less than 3 measurements within the potential interval.

Based on the results summarized in Figure 2-1 and Figure 2-2, we form the following 5 hypotheses consistent with our observations:

Hypothesis 1. Ag^+ is leaking from the Ag/AgCl/KCl(sat.) electrode and contaminating the electrolyte.

Hypothesis 2. The rate of leakage from the single-junction Ag/AgCl/KCl(sat.) reference electrode is faster than that from the double-junction Ag/AgCl/KCl(sat.)/$NaHCO_3$(0.1 M) reference electrode because the single-junction reference electrode has only one diffusion barrier to Ag^+ leakage (a CoralPor® glass frit), whereas the double-junction reference electrode has three diffusion barriers to Ag^+ leakage (two CoralPor® glass frits and the $NaHCO_3$ electrolyte solution between the frits).

Hypothesis 3. The leaked Ag^+ deposits onto the Cu working electrode during the CO_2RR experiment, and the quantity of deposited Ag is related to the amount of Ag^+ contamination in the electrolyte solution.

Hypothesis 4. Because Ag is known to selectively reduce CO_2 to CO with increased HER at more positive potentials,[1,24] the deposited Ag on Cu results in increased Faradaic efficiencies for CO and H_2. This is seen in the CPEs conducted with single-junction reference electrodes, but not in the CPEs conducted with double-junction reference electrodes where less Ag^+ leaks into the electrolyte.

Hypothesis 5. The large variance in the Faradaic efficiencies for CO from the CPEs using single-junction reference electrodes is due to inconsistent rates of Ag^+ leakage from the reference electrodes.

To further test these five hypotheses, we conducted a series of studies as follows. First, to test hypotheses 1, 2, and 5, we measured the amount of Ag^+ leakage from single-junction and

double-junction reference electrodes in pure water with no electrochemical polarization. Next, to test hypotheses 1, 2, 3, and 4, we measured the amount of Ag^+ leakage in an electrochemical cell under applied bias and quantified the amount of Ag deposited onto the working electrode during these experiments. Finally, to test hypotheses 3 and 4, we conducted CO_2RR measurements at Cu electrodes with specific amounts of Ag^+ added to the solution. The results of these studies are found in the sections below.

Study 1: Ag^+ Leakage from Reference Electrodes with No Applied Bias

We first investigated the amount of Ag^+ leaked from a single-junction Ag/AgCl/KCl(sat.) reference electrode and a double-junction Ag/AgCl/KCl(sat.)/$NaHCO_3$(0.1 M) reference electrode after soaking in scintillation vials filled with 10 mL of pure water for 24 h. For comparison, we also include the Ag^+ leakage data for a commercial Ag/AgCl/KCl(sat.) soaked in water under identical conditions. The results of these experiments as summarized in Figure 2-3 and Table 0-3.

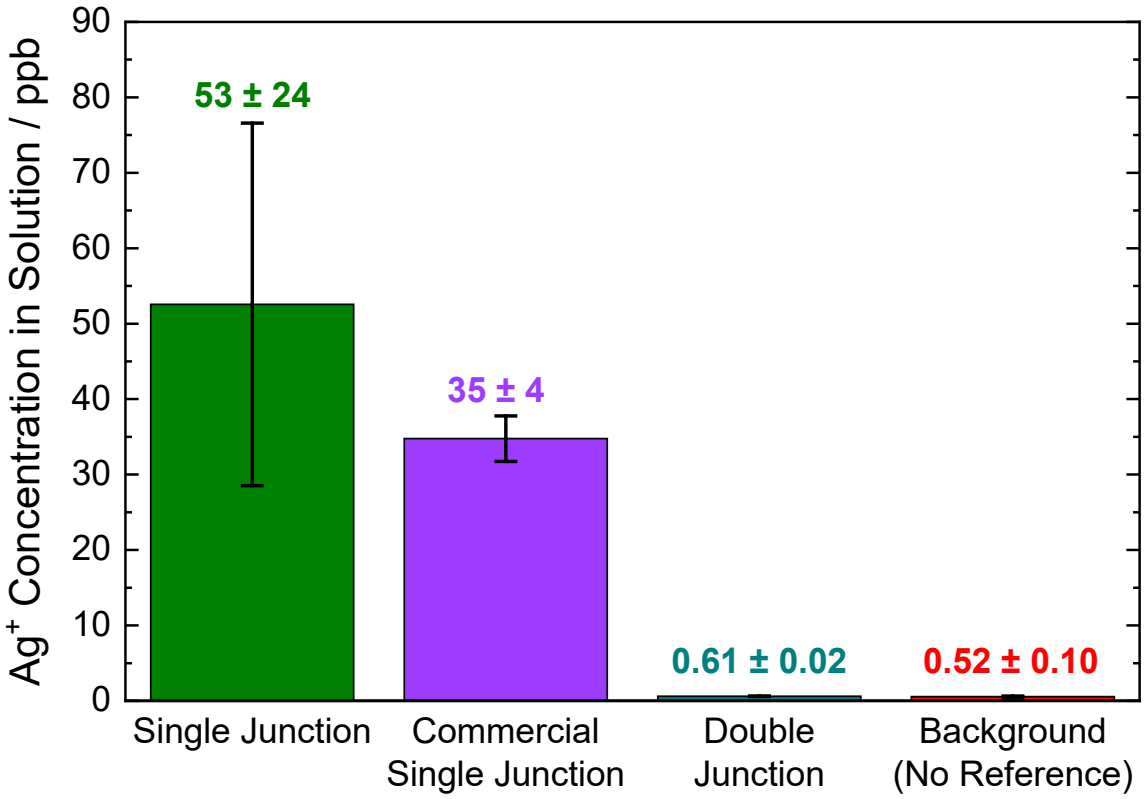

Figure 2-3 Concentration of Ag^+ in aqueous solution detected by ICP-MS after storing reference electrodes in pure water for 24 h. Error bars are standard deviations from at least 3 independent measurements. Note, the measurements for the double-junction reference electrode and water background are near the limit of quantification for the ICP-MS instrument (0.5 ppb).

The single-junction custom-made Ag/AgCl/KCl(sat.) leaked an appreciable amount of Ag^+ over the course of 24 h, leading to a total Ag^+ concentration of ~50 ppb in 10 mL of water. This is equivalent to 500 ng of Ag^+ leaking from the Ag/AgCl/KCl(sat.). In comparison, the double-junction custom-made Ag/AgCl/KCl(sat.)/$NaHCO_3$(0.1 M) reference electrode did not leak an appreciable amount of Ag^+ over 24 h—the measured concentration in water after the 24 h soak was only ~0.6 ppb which is equivalent to that of the water background and near the limit of quantification for the ICP-MS instrument. The commercial single-junction Ag/AgCl/KCl(sat.) reference electrodes leaked ~35 ppb of Ag^+ compared to the custom-made single-junction reference. Note that the commercial single-junction reference electrode does show a smaller standard deviation in Ag^+ leaked compared to the custom-made single-junction reference electrode, suggesting the rate of leakage for the commercial single-junction electrode was more reproducible from experiment to experiment.

The results of this study support hypotheses 1, 2, and 5. The single-junction Ag/AgCl/KCl(sat.) reference electrodes leak a measurable amount of Ag^+ when soaked in water without polarization for 24 h. However, the double-junction Ag/AgCl/KCl(sat.)/$NaHCO_3$(0.1 M) reference electrodes substantially decrease the rate of Ag^+ leakage and show essentially no Ag^+ in solution after 24 h. Moreover, the large variance in the amount of Ag^+ leaking from our custom-made single-junction reference electrode suggests experiment-to-experiment inconsistency in leakage rate. This result is consistent with our experiment-to-experiment variance in measured Faradaic efficiency for CO from CPEs under CO_2 on polycrystalline Cu electrodes using single-junction Ag/AgCl/KCl(sat.) electrodes shown in Figure 2-1 and Figure 2-2, assuming that the CO production is related to Ag^+ contamination. Note that the commercial single-junction reference electrodes show similar Ag^+ leakage compared to the custom-made

single-junction reference, suggesting that the Ag^+ leakage is not an artifact of the construction of our custom-made reference electrode. It remains a concern even when using commercial reference electrodes.

Study 2: Ag^+ Leakage from Reference Electrodes in Electrochemical Experiments

Before measuring possible Ag^+ contamination from the reference electrodes during electrochemical experiments, we determined baseline amounts of Ag^+ contamination from each of the electrochemical cell components present in the working electrode chamber. To do this, we independently soaked the electrochemical cell, the Nafion 117 membrane, Ni foil, Cu foil, and the Tygon sparging tube in 10 mL of 1 M HNO_3 for 1 h to etch any surface metals into solution. The resulting solutions were then investigated by ICP-MS to determine the extent of baseline Ag^+ contamination. For all components, a negligible amount of Ag^+ (near limit of quantification) was detected after the 1 h soak in HNO_3 as shown in Table 0-4 and Table 0-5. We also measured the Ag^+ etched from the carbon rod auxiliary electrodes after 1 h soaking in 1 M HNO_3, and in this case we see a very small concentration of Ag^+ slightly above the limit of quantification as summarized in Table 0-5.

Ag^+ Leakage from the Reference Electrode under HER conditions. We first measured the amount of Ag^+ leakage from the single-junction Ag/AgCl/KCl(sat.) and double-junction Ag/AgCl/KCl(sat.)/$NaHCO_3$(0.1 M) reference electrodes during the hydrogen evolution reaction (HER) at Ni electrodes in 0.1 M H_2SO_4. We chose the Ni-HER system for our initial tests of Ag^+ leakage under electrochemical polarization because we are unable to detect trace metal concentrations in Na^+-containing electrolyte solutions as Na^+ cations can damage the ICP-MS instrument when injected in the concentrations typically found in the electrolyte solutions (> 0.01 M). This means we are unable to quantify trace Ag^+ directly in the 0.1 M $NaHCO_3$ electrolyte

used in our CO_2RR studies without further dilution, which would hinder the detection of the small amounts of Ag^+ we expect (on the order of 1-10 ppb). Therefore, HER experiments measured at Ni electrodes in 0.1 M H_2SO_4, which can be directly injected into the ICP-MS instrument, are an ideal proxy for studying the extent of Ag^+ leaking from the reference electrodes during electrochemical measurements.

HER measurements in 0.1 M H_2SO_4 at Ni electrodes were conducted by holding the Ni electrode at an applied potential of –1.0 V vs Ag/AgCl/KCl(sat.) for 1 h under an N_2 atm. After each CPE, 10 mL of the solution in the working chamber was sampled and evaluated for Ag^+ via ICP-MS, the results of which are shown in Figure 2-4a and Table 0-6. The Ni electrode was then removed from the solution post-CPE and soaked in 10 mL of 1 M HNO_3 for 1 h to etch any deposited Ag from the surface. The etching solution was then evaluated for Ag^+ via ICP-MS, and the results are shown in Figure 2-4b and Table 0-7.

The concentration of Ag^+ measured in the electrolyte post-CPE conducted with the double-junction Ag/AgCl/KCl(sat.)/$NaHCO_3$(0.1 M) reference electrode is essentially equivalent to background Ag^+ concentration in the 0.1 M H_2SO_4 solutions and below the limit of quantification for the ICP-MS instrument. In contrast, the concentration of Ag^+ in the electrolyte post-CPE for HER studies conducted with a single-junction Ag/AgCl/KCl(sat.) electrode was ~7 ppb, significantly higher than the background Ag^+ concentration in the 0.1 M H_2SO_4 solutions. These studies are consistent with hypotheses 1 and 2. Moreover, there is significant standard deviation in the Ag^+ concentration for the single-junction reference electrodes studies which is consistent with hypothesis 5. However, in all cases the Ni surfaces show no appreciable Ag^+ contamination above background, suggesting that the increased Ag^+ concentration in the post-CPE electrolyte for the single-junction reference electrode study does not lead to significant Ag deposition onto Ni

electrode surfaces. Note that any small amount of possible Ag^+ contamination from the auxiliary electrode does not seem to cross over the Nafion separating membrane into the working electrode chamber in appreciable quantities on the timescale of our measurements as evidenced by the lack of Ag^+ contamination of the electrolyte solution in the double-junction reference electrode studies.

Ag^+ Leakage from the Reference Electrode under Cu CO_2RR conditions. We cannot directly measure Ag^+ concentrations in $NaHCO_3$ electrolytes used in CO_2RR studies due to limitations of the ICP-MS instrument as discussed above. However, we can measure the amount of Ag^+ deposited onto the Cu electrodes under CO_2RR conditions post-CPE. After each CPE, the Cu electrode was removed from the electrolyte solution and soaked in 10 mL of 1 M HNO_3 for 1 h to etch any deposited Ag from the surface. The etching solution was then investigated for Ag^+ via ICP-MS, and the results are summarized in Figure 2-5 and Table 0-8 and compared to the as-polished Cu electrode backgrounds, which show deposited Ag^+ amounts near our limit of quantification. For the CO_2RR experiments conducted using double-junction Ag/AgCl/KCl(sat.)/$NaHCO_3$(0.1 M) reference electrodes, the Cu electrodes post-CPE show no appreciable Ag^+ deposition, similar to the Cu backgrounds. However, the post-CPE Cu electrodes for the CO_2RR experiments conducted using single-junction Ag/AgCl/KCl(sat.) reference electrodes show increased Ag^+ deposition on the Cu surfaces. These results are consistent with hypothesis 2—single-junction reference electrodes leak Ag^+ at a faster rate than double-junction reference electrodes—and hypothesis 3—leaked Ag^+ deposits onto Cu electrode surfaces.

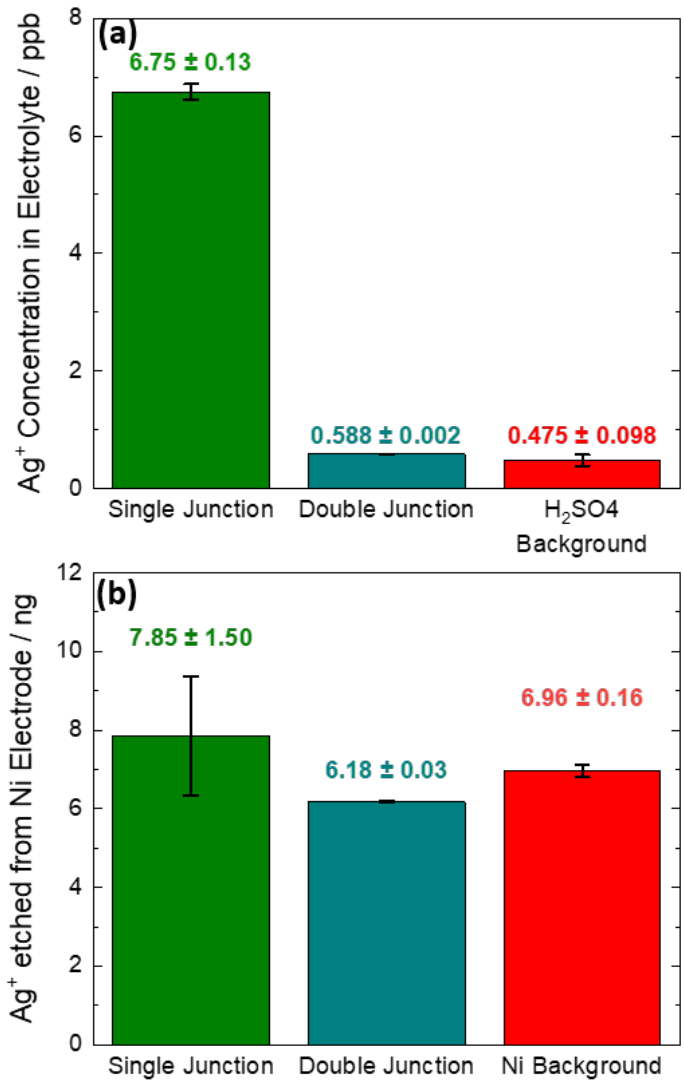

Figure 2-4 (a) Concentration of Ag^+ in the electrolyte solution detected by ICP-MS after HER CPEs. The H_2SO_4 background is the Ag^+ concentration measured in an as-prepared 0.1 M H_2SO_4 solution. Note the measurements for the double-junction reference electrode and the H_2SO_4 background are near the limit of quantification for the ICP-MS instrument (0.5 ppb). (b) Amount of Ag^+ etched from HER post-CPE Ni electrodes using 1 M HNO_3. The Ni background is the amount of Ag^+ etched from as-polished Ni electrodes. Note that all etched Ag^+ amounts are near the limit of quantification for these electrodes (5 ng). All error bars are standard deviations from at least 3 independent measurements.

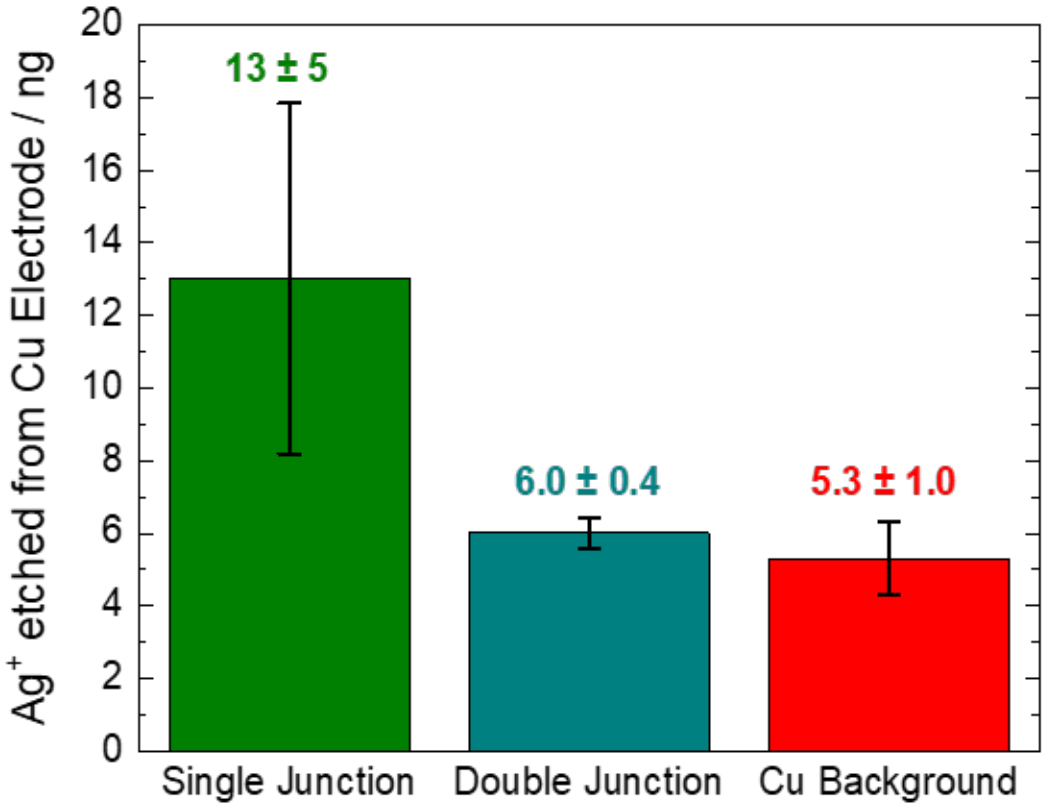

Figure 2-5 Amount of Ag^+ etched from CO_2RR Cu electrodes post-CPE using 1 M HNO_3. The Cu background is the amount of Ag^+ etched from as-polished Cu electrodes. Error bars are standard deviations from at least 3 independent measurements. Note that etched Ag^+ amounts from the Cu background and double-junction reference electrode experiments are near the limit of quantification for these electrodes (5 ng).

Study 3: Long-Term Cu CO_2RR Studies

Based on hypothesis 1-4, we would expect to see an increase in Ag^+ contamination as a function of increasing electrolysis time. In the case of Cu CO_2RR, as the electrolysis time is increased, the increasing Ag^+ contamination should manifest itself as an increase in Ag deposition on the Cu electrode, increased CO production, and decreased CH_4 production. Moreover, these changes should be significantly greater when using a single-junction Ag/AgCl/KCl(sat.) reference electrode compared to a double-junction Ag/AgCl/KCl(sat.)/$NaHCO_3$(0.1 M) reference electrode. To investigate the effect of Ag^+ contamination from reference electrodes on Cu CO_2RR product distributions as a function of time, we performed long-term (12 h) CPE experiments in the –1.60 V to –1.63 V potential range using both single-junction Ag/AgCl/KCl(sat.) reference electrodes and double-junction Ag/AgCl/KCl(sat.)/$NaHCO_3$(0.1 M) reference electrodes. The product distributions from CO_2RR of the long-term CPE measurements are summarized in Table 0-9. When using a single-junction reference electrode, we observed a significant increase in the Faradaic efficiency for CO production and a significant decrease in the Faradaic efficiency for CH_4 production after the long-term 12 h CPE compared to short-term < 2 h CPE, as illustrated in Figure 2-6a. Post CPE, the Cu surfaces were etched with 1 M HNO_3, and the etching solutions were analyzed with ICP-MS for Ag^+. We observed an increased amount of Ag deposited on the Cu surfaces after the long-term 12 h CPEs using the single-junction reference electrodes (Figure 2-7, Table 0-10) compared to the < 2 h CPEs under otherwise analogous conditions (Figure 2-5). These results are consistent with hypotheses 1, 3, and 4—because the single junction reference electrode is leaking Ag^+ at some rate, the amount of Ag^+ contamination in the electrolyte increases over time, leading to increased Ag deposition onto the Cu surface and increased Faradaic efficiency for CO.

In contrast, long-term 12 h CPEs conducted with double-junction Ag/AgCl/KCl(sat.)/$NaHCO_3$(0.1 M) reference electrodes showed no appreciable change in product distribution (Figure 2-6b) or amount of Ag deposited onto the Cu surface (Figure 2-7) compared to the short-term < 2 h CPE experiments. This finding is consistent with hypothesis 2—the rate of Ag^+ leakage from the double-junction reference electrodes is sufficiently lower than the single-junction that there is no appreciable Ag^+ contamination even after 12 h of electrolysis.

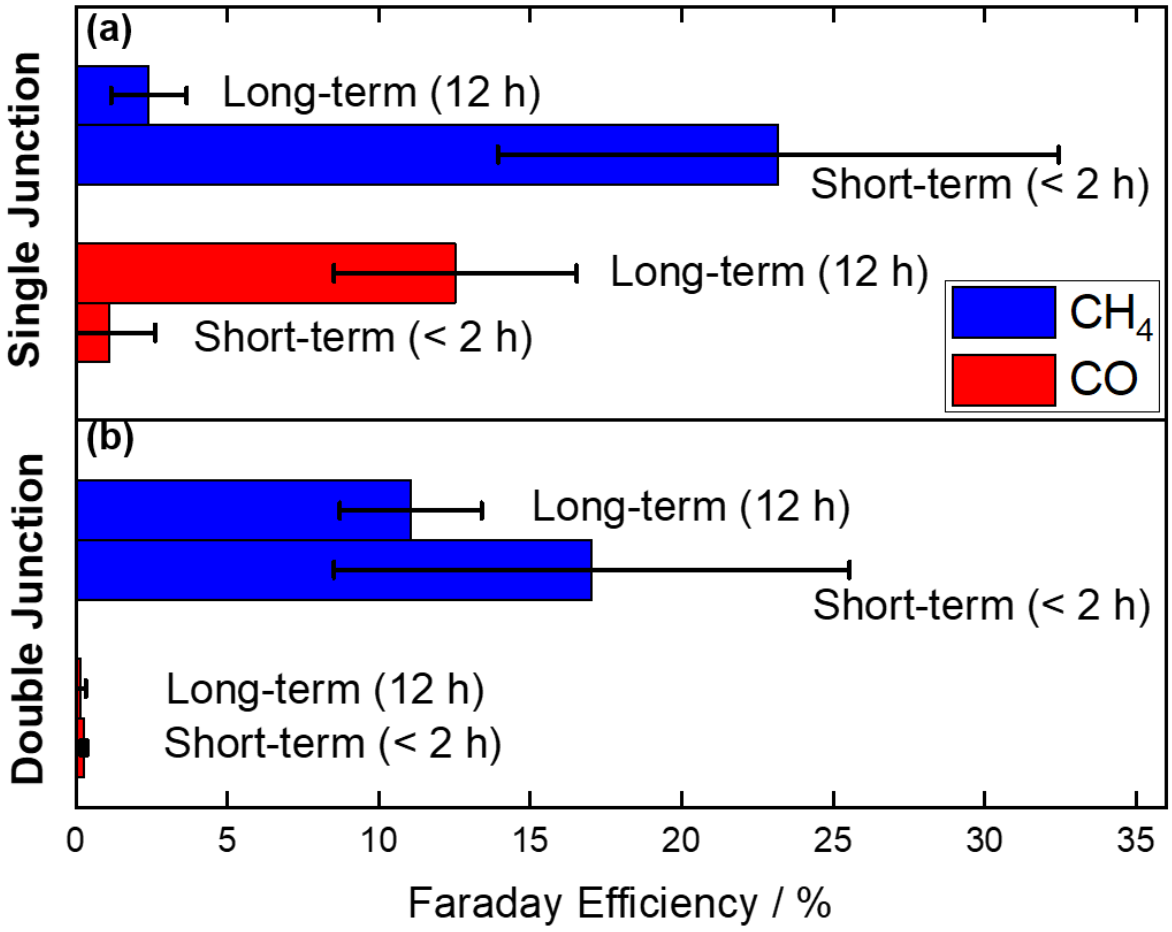

Figure 2-6 (a) Product distributions of CH_4 and CO for long-term (12 h) CO_2RR at a Cu electrodes at between -1.600 V to -1.630 V vs Ag/AgCl/KCl(sat.) with (a) single junction and (b) double junction reference electrodes. Faradaic efficiencies for the short-term experiments are from the data in our initial studies summarized in Figure 2-2 and Table 0-1 and Table 0-2. All error bars are the standard deviations from at least 3 measurements.

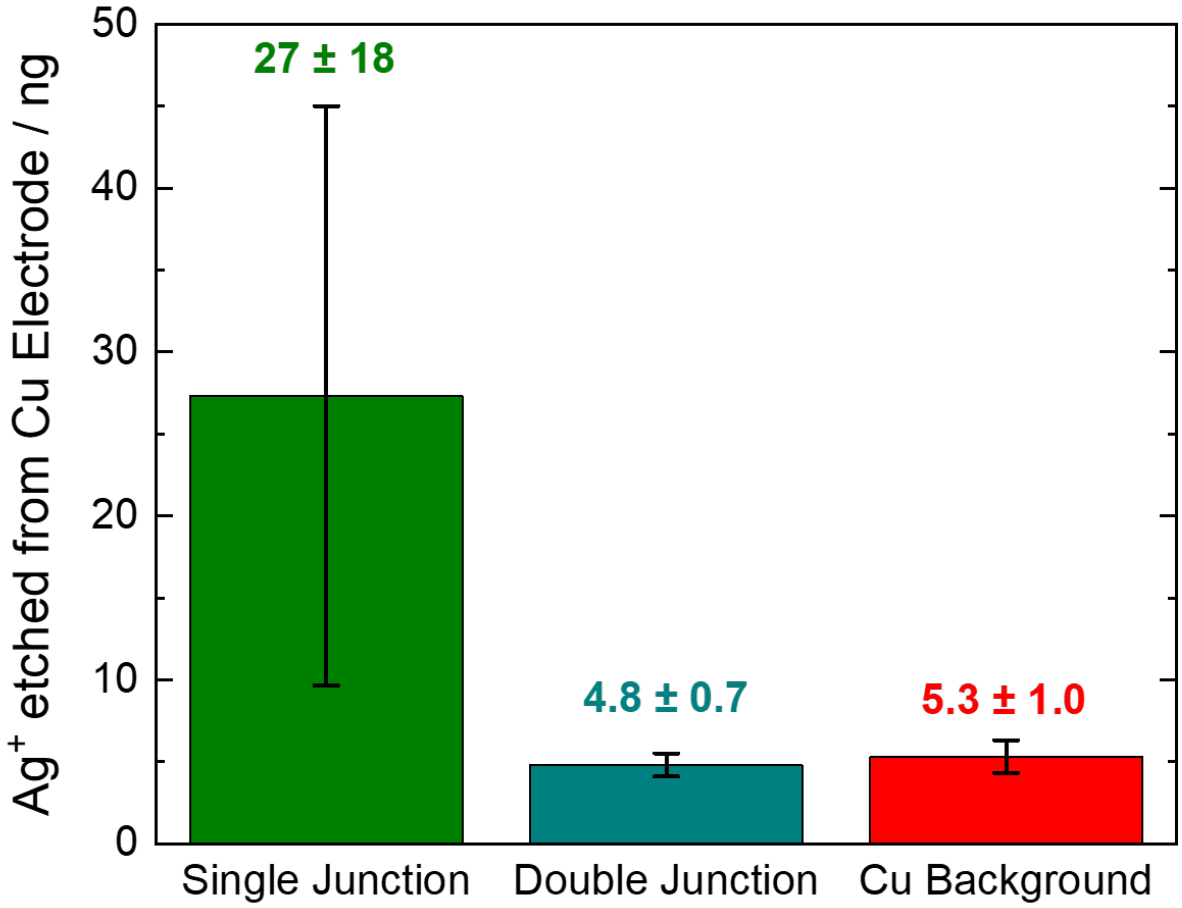

Figure 2-7 Amount of Ag^+ etched from CO_2RR Cu electrodes after long-term (12 h) CPE measurements using 1 M HNO_3. The Cu background is the amount of Ag^+ etched from as-polished Cu electrodes. Error bars are standard deviations from at least 3 independent measurements. Note that etched Ag^+ amounts from the Cu background and double-junction reference electrode experiments are near the limit of quantification for these electrodes (5 ng).

Study 4: Quantifying the Effect of Ag^+ on CO_2RR Product Distributions

To better quantify the effect of Ag^+ contamination on CO_2RR product distributions at Cu electrodes, we conducted a series of CO_2RR CPEs in 0.1 M $NaHCO_3$ electrolyte solutions at Cu electrodes held at between –1.570 and –1.600 V vs. Ag/AgCl/KCl(sat.)/$NaHCO_3$(0.1 M) double-junction reference electrodes in which external concentrations of Ag^+ ranging from 1 ppb (9.27 nM) to 1000 ppb (9271 nM) were added to the electrolyte solution in the working chamber. We then measured the product distribution from the CO_2RR experiments as summarized in Figure 2-8 and Table 0-11. We also etched any deposited Ag^+ from the Cu electrodes post-CPE by exposing the Cu electrodes to 10 mL of 1 M HNO_3 for 1 h and then quantifying the amount of Ag^+ in the etching solutions using ICP-MS. The measured quantities of Ag^+ etched from the Cu electrodes post-CPE are shown in Figure 2-9 and Table 0-12.

At very low (< 5 ppb) concentrations of added Ag^+, there is only a minor effect of added Ag^+ on CO_2RR product distributions, and little Ag is deposited on the electrode. However, as the concentration of added Ag^+ in the electrolyte solution is increased up to 100 ppb, we observe a corresponding increase in the amount of Ag deposited onto the Cu electrode, consistent with hypothesis 3. Moreover, in this range we observe a general increase in the Faradaic efficiency for CO (from ~0.2% in 1 ppb Ag^+ to ~17% in 100 ppb Ag^+) and a general decrease in the Faradaic efficiency for CH_4 (from ~18% in 1 ppb Ag^+ to ~1% in 100 ppb Ag^+) as a function of increasing added Ag^+, consistent with hypothesis 4. Even at the relatively low concentration of 10 ppb Ag^+ there is a measurable increase in the Faradaic efficiency for CO production (to ~2.5%), and by 50 ppb Ag^+ there is a dramatic increase in the Faradaic efficiency for CO (to ~11%) and a dramatic decrease in the Faradaic efficiency for CH_4 (to 2%).

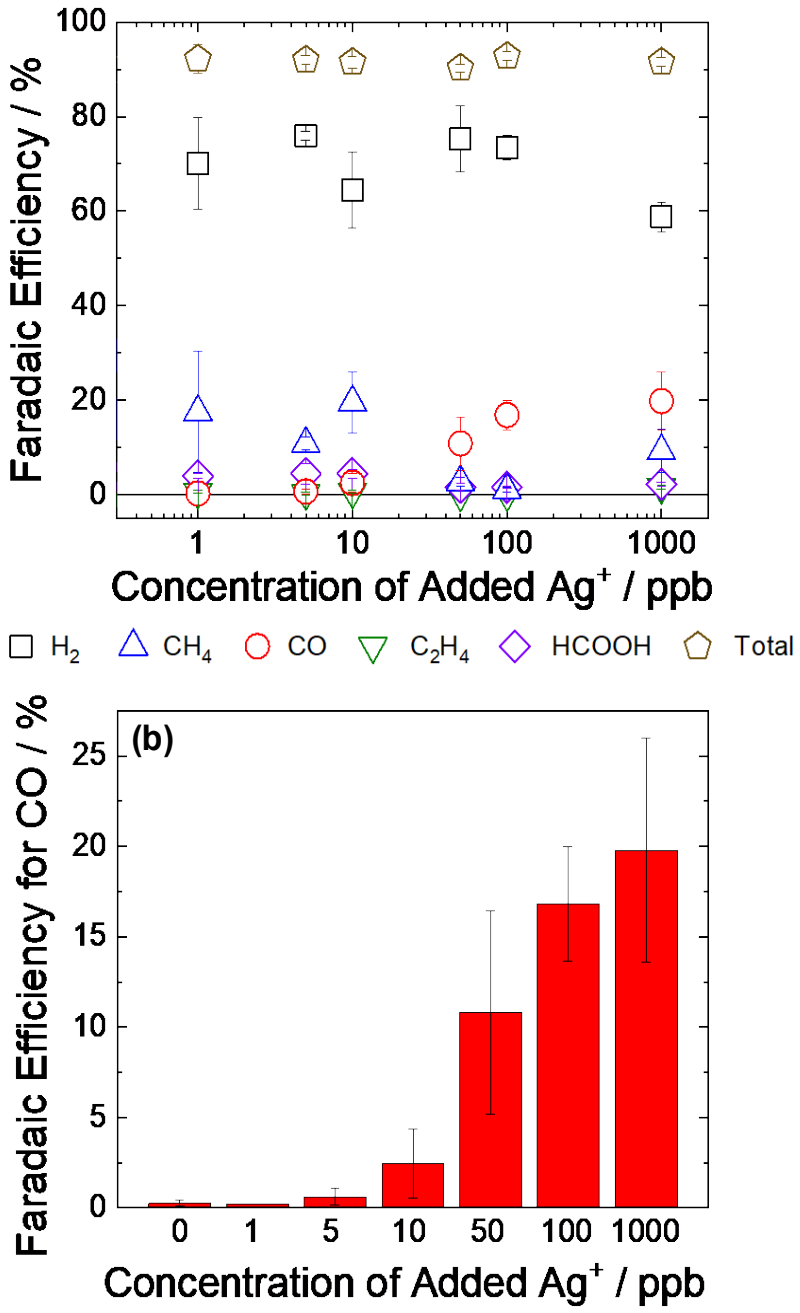

Figure 2-8 (a) Product distributions for CO_2RR at Cu electrodes at a potential range of –1.570 V to –1.600 V vs Ag/AgCl/KCl(sat.)/$NaHCO_3$(0.1 M) double-junction reference electrodes at different concentrations of externally-added Ag^+. (b) Bar graph better illustrating the increase in Faradaic Efficiency for CO with increasing concentration of externally-added Ag^+. Error bars for the single products are standard deviations from at least 3 measurements within the interval. Error bars for the summed total Faradaic efficiency are the standard deviations calculated from the summed total of each experiment.

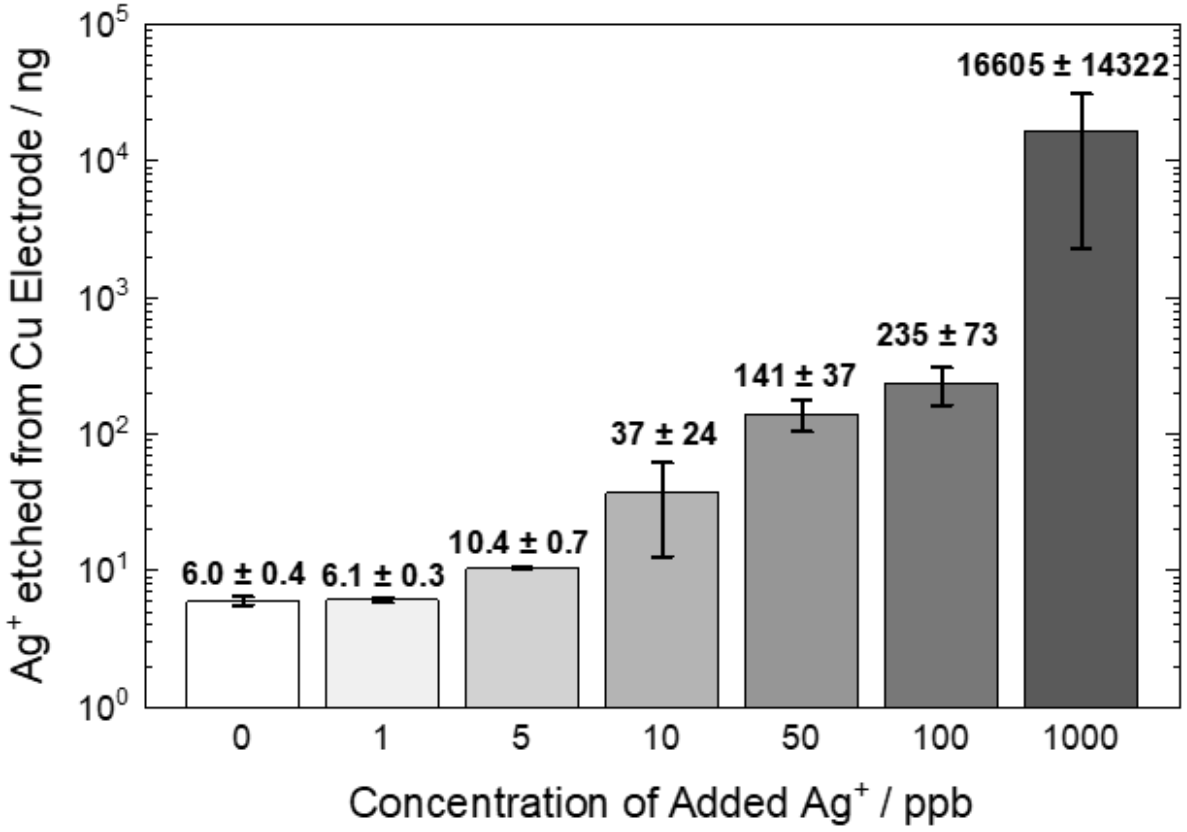

Figure 2-9 Amount of Ag^+ etched from Cu electrodes using 1 M HNO_3 after CO_2RR CPEs at –1.570 V to –1.600 V vs Ag/AgCl/KCl(sat.)/$NaHCO_3$(0.1 M) with various concentrations of Ag^+ added to the electrolyte solution in the working chamber. Error bars are standard deviations from at least 3 independent measurements. Note that the etched Ag^+ amounts from the Cu electrodes used in the CPEs in electrolyte solutions with 0 ppb and 1 ppb of added Ag^+ are near the limit of quantification for these electrodes (5 ng).

Note that at 1000 ppb of added Ag^+, the Faradaic efficiency for CO increases as expected compared to 100 ppb (to ~20%), but there is an additional increase in CH_4 (to ~9 %) compared to that measured in electrolyte with 50 and 100 ppb Ag^+. These results, along with the nearly μg quantities of Ag deposited on the Cu surface, may suggest the formation of bimetallic Cu-Ag active sites when 1000 ppb Ag^+ is added to the electrolyte,[90,92-97] although confirming the formation of such active sites would require additional studies beyond the scope of the present manuscript.

2.5 Conclusion

We have shown that single-junction Ag/AgCl/KCl(sat.) electrodes are a risk for trace Ag^+ contamination in electrochemical experiments and measurably change the product distribution in CO_2RRat planar polycrystalline Cu electrodes. In particular, our studies have demonstrated that single-junction Ag/AgCl/KCl(sat.) electrodes, both commercial and custom-made, leak Ag^+ into electrolyte solutions at an appreciable rate. We also demonstrated that minute concentrations of Ag^+ contamination in electrolyte solutions—as low as 10 ppb (or 92.7 nM)—leads to measurable deposition of Ag onto Cu electrodes and influences the CO_2RR product distribution, increasing the Faradaic efficiency for CO. At slightly higher concentrations of Ag^+ contamination (50-100 ppb), there is a dramatic increase of CO product fraction and a corresponding decrease in CH_4. A double-junction Ag/AgCl/KCl(sat.)/$NaHCO_3$(0.1 M) reference electrode design significantly decreases the rate of Ag^+ leakage and prevents significant Ag^+ contamination on the timescale (up to 12 h) of our measurements. Based on these findings and the prevalence of Ag/AgCl/KCl(sat.) reference electrodes in the CO_2RR community, we propose that an effective strategy for preventing Ag^+ contamination is the adoption of a double-junction reference electrode design. This should be coupled with periodic testing for trace Ag^+ contamination under CO_2RR conditions to ensure measured product distributions, especially unexpectedly large CO and small CH_4 Faradaic efficiencies, are not artifacts of trace metal contamination.

2.6 References

(1) Hori, Y. "Electrochemical CO2 Reduction on Metal Electrodes," *Mod Asp Electrochem* **2008**, 89-189. http://dx.doi.org/Book_Doi 10.1007/978-0-387-49489-0

(11) Kuhl, K. P.; Cave, E. R.; Abram, D. N.; Jaramillo, T. F. "New insights into the electrochemical reduction of carbon dioxide on metallic copper surfaces," *Energy & Environmental Science* **2012**, *5*. http://dx.doi.org/10.1039/c2ee21234j

(24) Hatsukade, T.; Kuhl, K. P.; Cave, E. R.; Abram, D. N.; Jaramillo, T. F. "Insights into the electrocatalytic reduction of CO(2) on metallic silver surfaces," *Phys Chem Chem Phys* **2014**, *16*, 13814-13819. http://dx.doi.org/10.1039/c4cp00692e

(53) Kas, R.; Kortlever, R.; Milbrat, A.; Koper, M. T.; Mul, G.; Baltrusaitis, J. "Electrochemical CO2 reduction on Cu2O-derived copper nanoparticles: controlling the catalytic selectivity of hydrocarbons," *Phys Chem Chem Phys* **2014**, *16*, 12194-12201. http://dx.doi.org/10.1039/c4cp01520g

(56) Feng, X.; Jiang, K.; Fan, S.; Kanan, M. W. "A Direct Grain-Boundary-Activity Correlation for CO Electroreduction on Cu Nanoparticles," *ACS Cent Sci* **2016**, *2*, 169-174. http://dx.doi.org/10.1021/acscentsci.6b00022

(73) Wuttig, A.; Surendranath, Y. "Impurity Ion Complexation Enhances Carbon Dioxide Reduction Catalysis," *ACS Catalysis* **2015**, *5*, 4479-4484. http://dx.doi.org/10.1021/acscatal.5b00808

(87) Chen, Y.; Li, C. W.; Kanan, M. W. "Aqueous CO2 reduction at very low overpotential on oxide-derived Au nanoparticles," *J Am Chem Soc* **2012**, *134*, 19969-19972. http://dx.doi.org/10.1021/ja309317u

(90) Clark, E. L.; Hahn, C.; Jaramillo, T. F.; Bell, A. T. "Electrochemical CO2 Reduction over Compressively Strained CuAg Surface Alloys with Enhanced Multi-Carbon Oxygenate Selectivity," *J Am Chem Soc* **2017**, *139*, 15848-15857. http://dx.doi.org/10.1021/jacs.7b08607

(91) Roger, I.; Symes, M. D. "Silver Leakage from Ag/AgCl Reference Electrodes as a Potential Cause of Interference in the Electrocatalytic Hydrogen Evolution Reaction," *ACS Appl Mater Interfaces* **2017**, *9*, 472-478. http://dx.doi.org/10.1021/acsami.6b13438

(92) Kottakkat, T.; Klingan, K.; Jiang, S.; Jovanov, Z. P.; Davies, V. H.; El-Nagar, G. A. M.; Dau, H.; Roth, C. "Electrodeposited AgCu Foam Catalysts for Enhanced Reduction of CO2 to CO," *ACS Appl Mater Interfaces* **2019**, *11*, 14734-14744. http://dx.doi.org/10.1021/acsami.8b22071

(93) Choi, J.; Kim, M. J.; Ahn, S. H.; Choi, I.; Jang, J. H.; Ham, Y. S.; Kim, J. J.; Kim, S.-K. "Electrochemical CO 2 reduction to CO on dendritic Ag–Cu electrocatalysts prepared by electrodeposition," *Chemical Engineering Journal* **2016**, *299*, 37-44. http://dx.doi.org/10.1016/j.cej.2016.04.037

(94) Chang, Z.; Huo, S.; Zhang, W.; Fang, J.; Wang, H. "The Tunable and Highly Selective Reduction Products on Ag@Cu Bimetallic Catalysts Toward CO2 Electrochemical Reduction Reaction," *The Journal of Physical Chemistry C* **2017**, *121*, 11368-11379. http://dx.doi.org/10.1021/acs.jpcc.7b01586

(95) Higgins, D.; Landers, A. T.; Ji, Y.; Nitopi, S.; Morales-Guio, C. G.; Wang, L.; Chan, K.; Hahn, C.; Jaramillo, T. F. "Guiding Electrochemical Carbon Dioxide Reduction toward Carbonyls Using Copper Silver Thin Films with Interphase Miscibility," *ACS Energy Letters* **2018**, *3*, 2947-2955. http://dx.doi.org/10.1021/acsenergylett.8b01736

(96) Hoang, T. T. H.; Verma, S.; Ma, S.; Fister, T. T.; Timoshenko, J.; Frenkel, A. I.; Kenis, P. J. A.; Gewirth, A. A. "Nanoporous Copper-Silver Alloys by Additive-Controlled Electrodeposition for the Selective Electroreduction of CO2 to Ethylene and Ethanol," *J Am Chem Soc* **2018**, *140*, 5791-5797. http://dx.doi.org/10.1021/jacs.8b01868

(97) Huang, J.; Mensi, M.; Oveisi, E.; Mantella, V.; Buonsanti, R. "Structural Sensitivities in Bimetallic Catalysts for Electrochemical CO2 Reduction Revealed by Ag-Cu Nanodimers," *J Am Chem Soc* **2019**, *141*, 2490-2499. http://dx.doi.org/10.1021/jacs.8b12381

Chapter 3: Effect of Trace Metal Contaminants and Material Pre-treatments on Product Distribution of CO_2 Reduction by Heterogeneous Copper Catalyst

3.1 Preface

This chapter presents the study of the presence of trace metals in all electrochemical components used in a Cu CO_2RR electrolysis experiment and the effect of differences in material purity and pre-treatment on the product distribution. The components and materials discussed are the ion exchange membrane, the counter electrode, the working electrode, and the electrolyte. My data show strong evidence that trace metals, especially Sn and Fe ions, leach out during electrochemical experiments and may contaminate the system. The difference in the starting purity and pre-treatments of the materials can have a significantly impact on the product distribution. For example, lower purity Cu foils will lead to lower production of CH_4. A complex trend in product distribution is observed when using electrolytes from different starting purity and pre-treatment, highlighting the difficulty in controlling all the factors within the Cu system. This chapter is derived from a manuscript in preparation for submission. I am the first author responsible for conducting the electrochemical measurements, analysis, and preparation of the manuscript.

3.2 Introduction

The sensitivity of metal electrocatalysts to metal contamination and deactivation is well established in the scientific literature. For example, trace metal contaminants can lead to catalyst deactivation or changes in measured product distributions for Cu-catalyzed electrocatalytic reactions, such as the CO_2RR. A common source of trace metal contamination is the electrolyte.

For example, in the oxygen evolution reaction (OER) literature, it has been observed that Fe impurities from the electrolyte can significantly impact the activity of a catalyst for the OER, and purification of the electrolyte is necessary to prevent such contamination.[70,71,85,86] The CO_2RR at Cu electrodes is particularly susceptible to trace metal contamination, which can lead to enhancement of the competing hydrogen evolution reaction (HER) over the CO_2RR. Hori *et. al.* reported that deactivation of the Cu surface is strongly dependent on the reagents used to prepare the electrolytes, and the main contaminants thought to deactivate the Cu electrodes were Fe^{2+} and Zn^{2+}.[60] Up to 0.05 ppm Fe contamination was found in a 0.1 M $KHCO_3$ electrolyte that was prepared using ACS grade $KHCO_3$ and ultrapure Milli Q water. Pre-treatments of electrolyte such as pre-electrolysis are shown to effectively remove these major contaminants and prevented catalyst deactivation.[60] In addition to the electrolyte salt, the water used to prepare the electrolyte can also contain contaminants that cause catalyst deactivation in the Cu CO_2RR. Electrolytes prepared using tap water show much faster Cu deactivation compared to ultrapure water.[67] These important studies have led to the development of methods to pre-treat and purify electrolyte including pre-electrolysis[60] or using chelating agents[73] to remove the trace metals contaminants.

Although there are several studies focused on the effect of electrolyte purity on electrocatalytic activity and product distributions, there are significantly fewer studies focused on other materials involved in the CO_2RR that may also contain trace metal contaminants and affect the product distribution. In this chapter, I demonstrate that the seemingly trivial differences in membrane, auxiliary electrodes, starting purity of materials (including the Cu electrode and electrolyte), and their pre-treatment can influence CO_2RR product distribution. Different types of membranes and auxiliary electrodes, different starting purity of Cu foils, and different starting purity of electrolytes with and without pre-treatment are analyzed in the study.

Different trace amounts of metals are found to leach into the electrolyte after electrochemical experiments when different types of membranes and auxiliary electrodes are used, possibly contaminating the electrochemical system. Although only small differences in the CO_2RR product distribution are observed using different membranes and auxiliary electrodes during the course of our experiments, the presence of trace metals may affect the extremely sensitive Cu systems over time. Both the starting purity of Cu foils and of electrolytes are found to lead to different product distributions (especially CH_4 production), even after identical cleaning processes and pre-treatment. Interestingly, an "intermediate" purity electrolyte shows the highest Faradaic efficiency for CH_4 after electrolyte pre-treatment. The electrolyte pre-treatment is found to affect each starting grade of electrolyte differently. Comparing electrolytes before and after pre-treatment, the higher purity electrolyte shows lower Faradaic efficiency for CH_4 after the pre-treatment. Lower purity electrolyte shows similar Faradaic efficiency for CH_4 in both cases during the duration of our experiments. However, decreased current is observed over time when the lower purity electrolyte is untreated, suggesting deactivation of the electrode when an untreated electrolyte is used. It is crucial to note that the change in current over time should not be used as the sole indicator of catalyst poisoning, as we also demonstrate in our results.

Although there are countless examples of catalyst deactivation caused by trace metal contamination, in some cases the contamination can lead to increased catalytic activity.[73,98-100] For example, in the OER, trace amounts of Fe[71,85] and Co^{2+} [101]impurities have been found to enhance OER activities. Fe impurities in an N-doped carbon catalyst were also found to activate the CO_2RR.[100] In our previous studies, we also showed that as little as 10 ppb of Ag^+ ion contamination can alter the product distribution of the CO_2RR to be more selective towards CO production.[102] These metal impurities can change the catalytic activity and product selectivity by altering the

reaction mechanism. Our results illustrate that it is crucial for researchers to be mindful about the true nature of their electrochemical systems, as well as the need for a carefully designed control experiments to rule out the effects of unintentional contaminations.

3.3 Experimental

Most experimental procedures are identical to those outlined in **Chapter 2**, with specific addition and modification explained in the following sections.

Materials and Supplies for Chapter 3

Metal foils and gauze including Ni foil (99.994% Puratronic™ metals basis), Pt foil (99.99% Premion®), Pt gauze (99.9% metals basis), and Cu foil of three different purities (99.999% Puratronic™ metals basis, 99.95% metals basis, and 99.8% metals basis) were purchased from Alfa Aesar. Auxiliary electrodes used were Pt foil and carbon rods (99.999%, Strem Chemicals Inc.). Membranes used were Nafion-117 cation exchange membranes (Fuel Cell Store©) and Selemion™ AMV anion exchange membranes (AGC Engineering). Carbon paper was purchased from Fuel Cell Store©. All solutions were prepared with ultrapure water (18.2 MΩ·cm resistivity) purified with a Thermo Scientific GenPure UV-TOC/UF xCAD-plus water purification system. Ultrapure water was used for all water rinse steps. Sodium bicarbonate of three different grades (ACS reagent, Sigma-Aldrich; 99+%, for HPLC, Acros Organics; BioXtra, Sigma-Aldrich) and sodium carbonate decahydrate (99.999% trace metal basis, Sigma-Aldrich) were used. Sodium carbonate decahydrate (99.999%, trace metal basis) was purchased from Sigma-Aldrich. Resin-treatment of electrolyte was done using Chelex® 100 resin (sodium form, Sigma-Aldrich). Phosphoric acid (99.99% trace metal basis, Sigma-Aldrich), nitric acid (trace metal grade, Fisher), hydrochloric acid (reagent ACS, Acros; trace metal grade, Fisher), sodium hydroxide (99.99%, semiconductor grade, Sigma-Aldrich), sulfuric acid (OPTIMA grade, Fisher), ICP-MS standard (RICCA), and ferrocenecarboxylic acid (97%, Sigma-Aldrich) were used as received unless noted otherwise. PTFE sealing tape (Poly-Temp® MD, Anti-Seize Technology) was used for sealing edges and connection areas of electrochemical cells.

Preparation of Membranes

Two membranes (Nafion and Selemion^{TM} AMV) were used in the study. The membranes were rinsed with water for 15 sec before being used in the trace metal measurements and different membrane/auxiliary electrode combination studies. In all other experiments including pre-electrolysis pre-treatments, Selemion AMV was cleaned by soaking in 1 M trace metal grade HNO_3 for 5 min, followed by rinsing and soaking in water for 15 min prior to use. Nafion was used after rinsing with water for 15 sec in all studies, since no significant difference in trace metal content was found before and after cleaning Nafion with HNO_3.

Pre-electrolysis Treatment of Electrolyte

Pre-electrolysis of the HPLC grade 0.1 M $NaHCO_3$ electrolyte (untreated) was conducted in an H-style electrochemical cell (Figure 0-2) where one chamber contained a Pt gauze working electrode and a custom made double-junction Ag/AgCl/KCl(sat) reference electrode, and the other chamber contained a carbon rod as the counter electrode. The two chambers were separated by a Selemion^{TM} AMV anion exchange membrane. The membrane was cleaned by soaking in 1 M trace metal grade HNO_3 for 5 min, followed by rinsing and soaking in water for 15 min prior to use. The untreated electrolyte in both the working and auxiliary chambers was sparged with N_2 for 1 h before pre-electrolysis. Both chambers were then blanketed under N_2 atmosphere during the entirety of pre-electrolysis. To minimize solvent evaporation, N_2 gas was first bubbled through a bubbler filled with water. -36 mA constant current was applied to the working electrode for 20 h. Stir bars were used in both chambers for constant stirring during the electrolyses. The working electrode was removed while it was still under the applied potential to prevent re-dissolution of trace metals into the electrolyte. The electrolyte from the working chamber was used for later electrolysis experiments.

Other Trace Metal Determination

Calibration standards were prepared at concentrations of 1, 5, 10 ppb for most metals, and 10, 50, 100 ppb for Fe.

3.4 Results and Discussion

Standard Conditions for CO_2RR

The presented results are from a series of systematic modifications of a set of standard conditions. It is necessary to establish these standard condition in order to compare observed changes or trends resulting from these modifications. The standard condition does not represent optimal CO_2RR conditions. Rather, it serves as a baseline condition that can be systematically modified. The standard condition is previously reported in **Chapter 2** (Figure 2-2c and d) as follows: a custom-made double junction Ag/AgCl/KCl(sat.) reference electrode, Nafion-117 membrane with a carbon rod auxiliary electrode, a 99.999% Cu planar foil working electrode, and 0.1 M HPLC grade $NaHCO_3$ electrolyte (Acros Organics) that was pre-treated using Chelex® 100 resin. Figure 2-2c and d and Table 0-1 shows the product distribution of CO_2RR under standard conditions.

The rest of the data in this chapter will be compared to those under standard condition. Because the main changes we observed are primarily on the product distributions of H_2 and CH_4, these two products will be the focus of comparison and analysis. The different conditions will be labeled as **Cu CO_2RR under standard condition + [changed variable]** in figures and summary tables.

Membrane/auxiliary electrodes at open circuit

The first factor we investigated was the choice of membrane and auxiliary electrodes. Common choices of membrane in CO_2RR research are Nafion[30,60] and Selemion AMV[11,31,57,81,103]. Common auxiliary electrodes are composed of either carbon (graphite or glassy carbon)[14,29,45,104] or Pt[8,11,30,57,59,73,81,105]. To test the effect of the choice of membrane and auxiliary electrode on trace

metal contamination and product distributions for the CO_2RR, we first measured the trace metal content of these components at open circuit by etching them in 1 M HNO_3 and analyzed the etching solution with ICP-MS.

Based on the ICP-MS measurements of the etching solutions collected at open circuit, we found that Selemion AMV has a significant amount of Sn ions present, while Nafion has a large amount of Fe ions and the carbon rod auxiliary electrode had a considerable amount of Cu ions. The Sn contamination from Selemion AMV is of particular interest because Sn is active in CO_2RR with high selectivity towards HCOOH. Conversely, since Fe is present in most other electrochemical components including the glass body of the electrochemical cell and the Cu foil itself as shown in Table 0-14 and Table 0-21 Fe is not known to be active in the CO_2RR[46], we do not expect the Fe contamination to impact the CO_2RR process. Similarly, because the catalyst used in the studies was Cu foil, we do not expect the Cu contamination from the carbon rods would contribute to a difference in product distribution, assuming it would be able to cross the membrane over time during electrochemical reaction. The most prominent metals present in the membranes and in the auxiliary electrodes prior to electrolysis are plotted in Figure 3-1 and Figure 3-2, respectively. The complete list of trace metal analyzed can be found in Table 0-15 in the Appendix. Contributions from the background (e.g. the acid solutions used and the glass body of the electrochemical cell), can be found in Table 0-13 and Table 0-14.

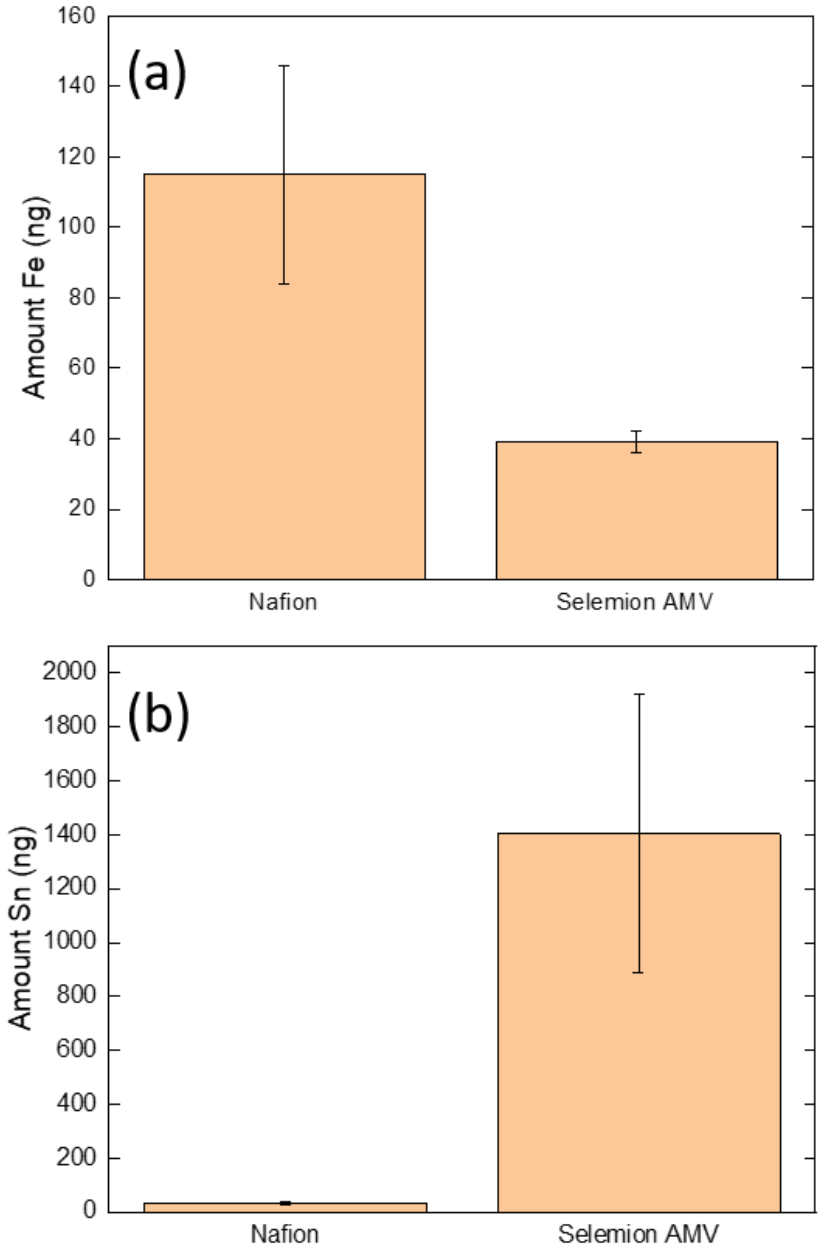

Figure 3-1 Amount of (a) Fe and (b) Sn etched from Nafion and Selemion AMV membranes. Error bars are standard deviations from at least 3 independent measurements. Limit of quantification is 5 ng.

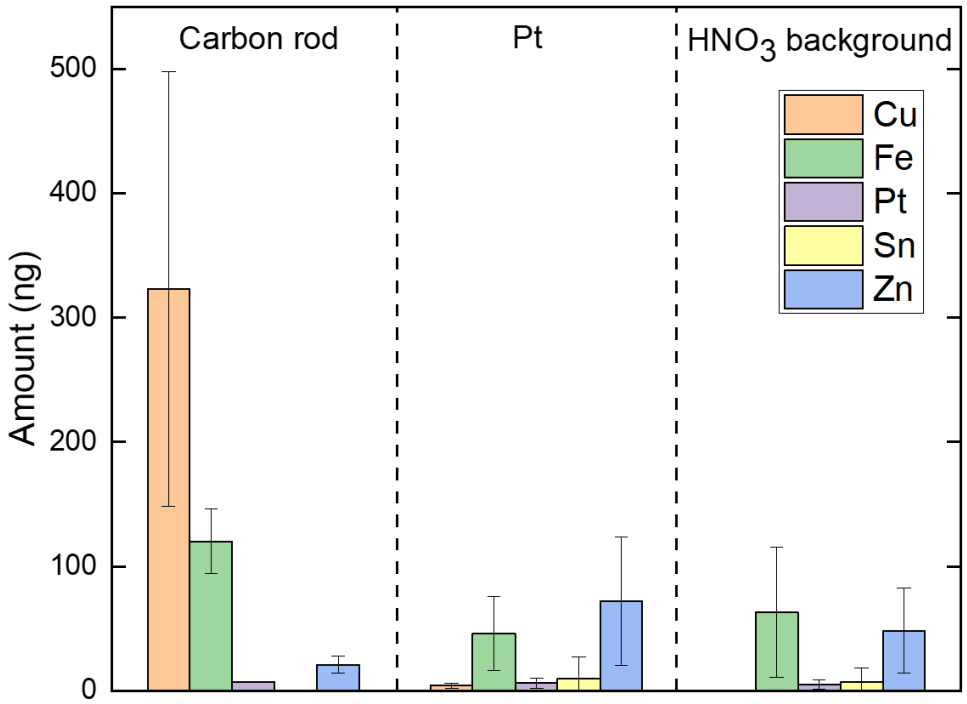

Figure 3-2 Metals etched out from auxiliary electrodes using 1 M HNO_3. Error bars are standard deviations from at least 3 independent measurements. Limit of quantification is 5 ng.

Membrane/auxiliary electrodes during electrochemical polarization

The Nafion membrane, Selemion AMV membrane, carbon rod auxiliary electrode, and Pt auxiliary electrode were assembled in an electrochemical cell to analyze the amount of trace metal leached from the membranes and auxiliary electrodes during electrochemical polarization. A total of four combinations of membranes and auxiliary electrodes were studied under electrochemical reaction conditions: Nafion/carbon rod, Nafion/Pt, Selemion AMV/carbon rod, and Selemion AMV/Pt. Because of the high Na^+ concentration in the 0.1 M $NaHCO_3$ electrolyte, we were not able to directly measure the amount of metal leached into the electrolyte under the standard CO_2RR conditions using ICP-MS. Instead, a proxy system of Ni-catalyzed hydrogen evolution reaction (HER) under 0.1 M H_2SO_4 for 1 h was used. We have previously used this proxy system to detect Ag^+ contamination.[102] Finally, the product distributions of the Cu CO_2RR using different combinations of these membranes/auxiliary electrodes were collected and analyzed.

After conducting Ni HER experiments, electrolytes (0.1 M H_2SO_4) in the working and auxiliary chambers were analyzed with ICP-MS for the concentration of trace metals. The most prominent metals are summarized in Figure 3-3, and data of all metals are summarized in Table 0-17. The amount of trace metals deposited on Ni surfaces after HER was analyzed and is summarized in Figure 3-4 and Table 0-18. There are a few key observations that should be noted. When Pt was used as the auxiliary electrode, we observed the presence of Pt ions in the auxiliary chamber. This suggests that the Pt oxidizes during electrochemical experiments to form Pt ions in solution. However, we did not observe Pt ions leaching into the working chamber over the course of our 1 h experiment, suggesting that the Nafion membrane is sufficient to prevent Pt ion crossover at least for a 1 h duration. When a graphite carbon rod was used as the auxiliary electrode, we observed a much higher concentration of Cu in the auxiliary chamber. However, as

mentioned above, because the catalyst used in the CO_2RR studies was a Cu foil, we do not expect that the Cu contamination from the carbon rod would affect the Cu CO_2RR process. When Selemion AMV was used in Ni HER, a large concentrations of Sn ions were found in the electrolytes, consistent with our observations from our trace metal measurements at open circuit. Additionally, we found a much higher average amount of Sn deposited on Ni surfaces.

When comparing the Fe concentration in the electrolyte using Nafion and Selemion AMV, we noticed an interesting pattern. We found that when Nafion was used during the electrochemical reaction, Fe ion concentration in the working chamber was consistently higher than in the auxiliary chamber. In contrast, when Selemion AMV was used, the Fe ion concentration in the working chamber was consistently lower than in the auxiliary chamber. Although a larger amount of Fe ions was observed with Nafion than with Selemion AMV prior to the electrochemical reaction, the difference in the original amount of Fe content alone does not explain the pattern of the difference in Fe ion concentration between the working and auxiliary chambers. We speculate that since the working electrode and working chamber were held at a negative potential, the positive Fe ion would be attracted and migrate to the working chamber. With Nafion, Fe cations may be small enough to cross over, while Selemion AMV (an anion exchange membrane) prevents the crossover of positive Fe ions. However, it is also possible that Fe ions were generated mostly in the working chamber during the HER study when Nafion was used, although the process by which this would occur is unclear.

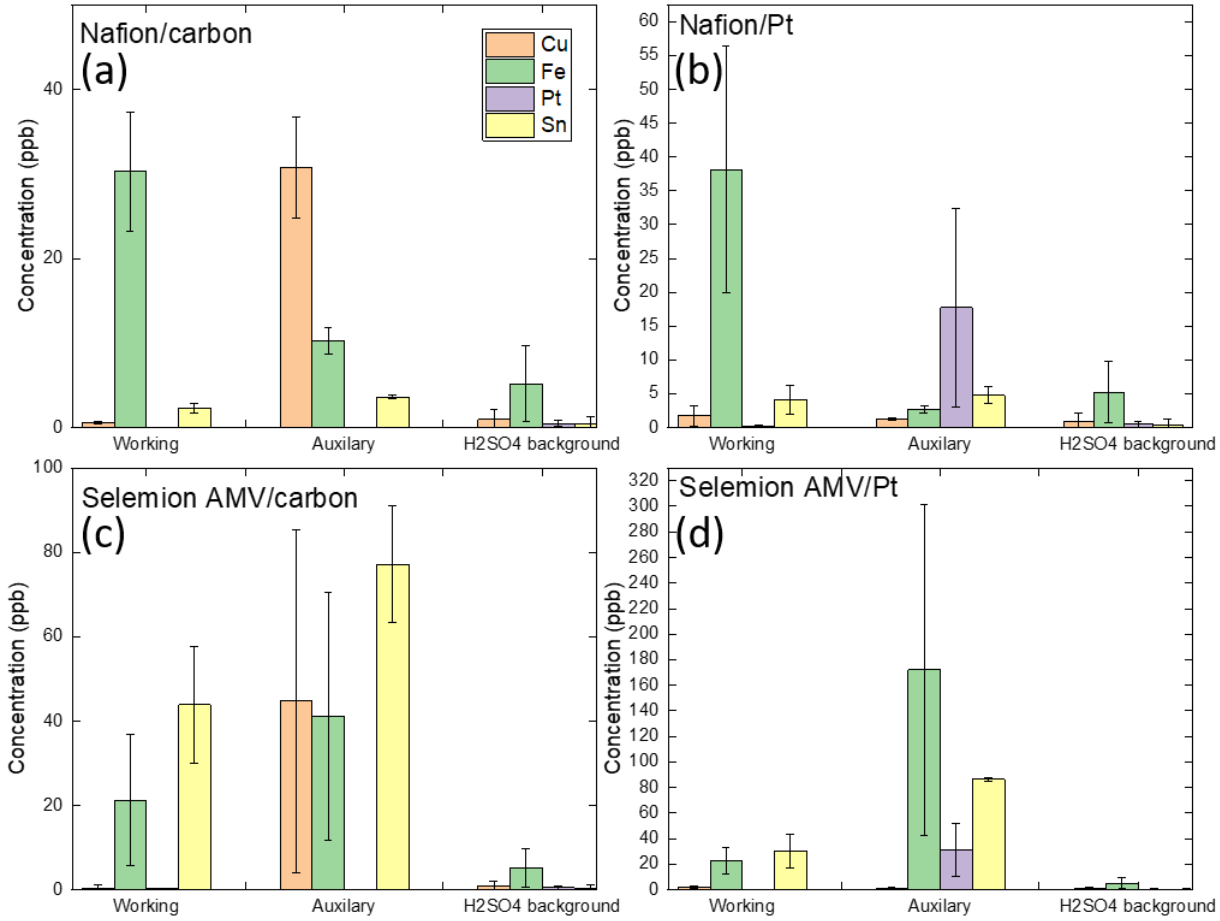

Figure 3-3 Trace metals detected in 0.1 M H_2SO_4 electrolyte after Ni HER with (a) Nafion/carbon rod (b) Nafion/Pt (c) Selemion AMV/carbon rod and (d) Selemion AMV/Pt. Note that the axis scale of (d) is significantly different from others. Error bars are standard deviations from at least 3 independent measurements. Limit of quantification is 0.5 ppb.

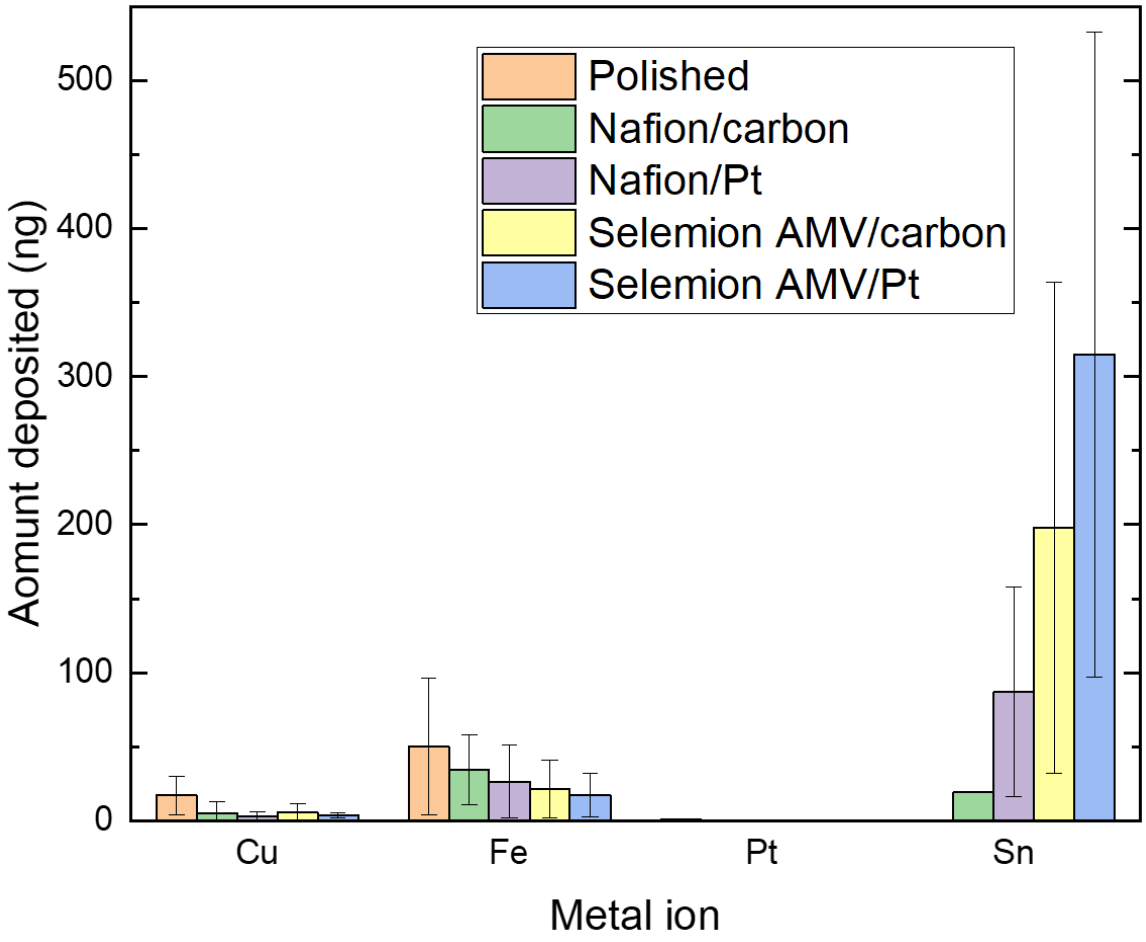

Figure 3-4 Metals etched from Ni after HER using different membrane/auxiliary. Error bars are standard deviations from at least 3 independent measurements. Limit of quantification is 5 ng.

After measuring the trace metal content present in the membranes and auxiliary electrodes under open circuit and during electrochemical polarization, we then examined if the product distribution of the Cu CO_2RR changes depending on the combination of membrane/auxiliary electrode used. The product distribution is summarized in Figure 3-5 and Table 0-16. Although the reasoning is unclear to us, the choice of membrane/auxiliary electrode combination did not result in significant differences in the product distributions, though electrolyses with carbon rod auxiliary electrodes showed lower Faradaic efficiencies for CH_4 overall than using Pt. Since there is a possibility of Sn contamination from using Selemion AMV as well as the possibility of Pt contamination from using Nafion/Pt combination, we expect to see a change in the product distribution especially if long term electrolysis experiments are conducted. We chose to use Nafion/carbon rod as the standard condition for the Cu CO_2RR in this manuscript to avoid possible contaminations from Selemion AMV membranes and Pt auxiliary electrodes.

We would like to point out that in many of the ICP-MS measurements, there are large standard deviations, which suggest large sample-to-sample variation. This may be due to a batch-to-batch differences in the electrochemical components, or possibly a slight unnoted difference in our experimental procedure. Although we are not sure the exact cause of the large variations, it is an indication of how difficult it is to control the presence of trace metal contaminants at the ppb level within an electrochemical system. Despite using the identical materials and preparation processes, the large variation in the amount of trace metals showed the complexity of maintaining a controlled experimental environment.

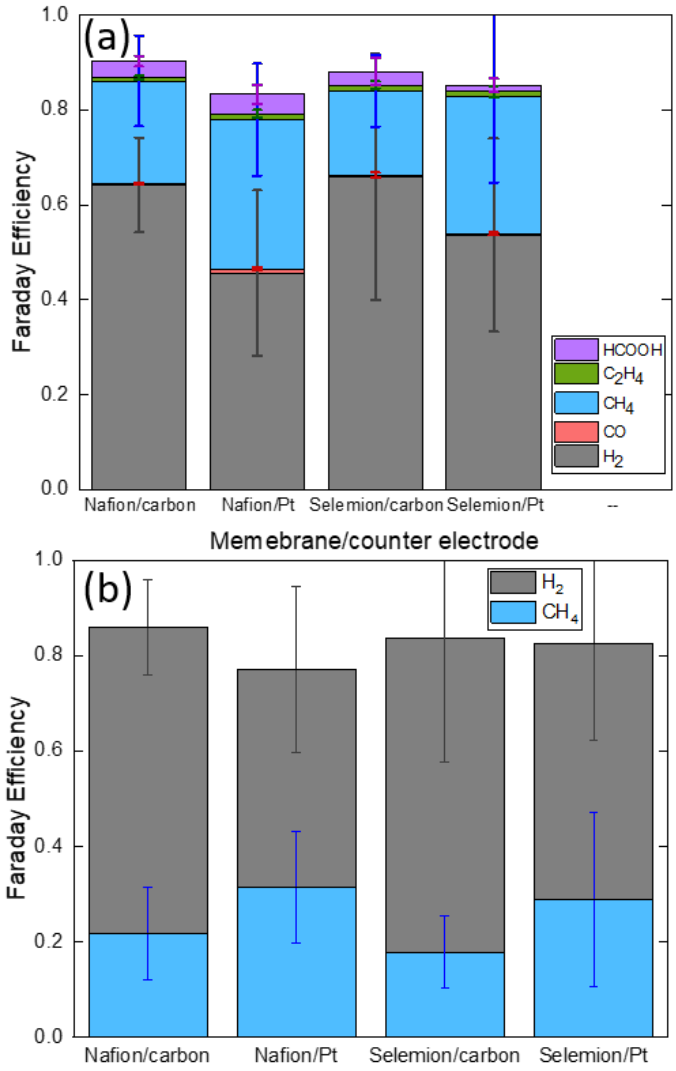

Figure 3-5 Product distribution of Cu CO_2RR with under standard conditions + different combinations of membrane/auxiliary. (a) Faradaic efficiencies of all measured products and (b) emphasis on the Faradaic efficiencies of H_2 and CH_4 for comparison. Potential between –1.55 V and –1.61 V vs Ag/AgCl/KCl(sat.). Error bars are standard deviations from at least 3 independent measurements.

Foil Purity

We also investigated the starting purity of the Cu foil used as the catalyst for the CO_2RR. 99.999%, 99.95%, and 99.8% Cu foils were tested. Each foil was prepared with identical electrochemical polishing pre-treatment in 85% phosphoric acid as described in the experimental section. The Faradaic efficiencies of H_2 and CH_4 generated using foils with different starting purities are summarized in Figure 3-6 and Table 0-19 and Table 0-20. We found that on average, 99.8% purity Cu foils reduces CO_2 to CH_4 with lower Faradaic efficiencies than the higher purity foils. Above purity level of 99.95%, however, the foils show very similar Faradaic efficiencies for CH_4. The amount of trace metal contamination on the Cu surfaces before and after the CO_2RR was measured by etching the foils in 1 M HNO_3 which was analyzed using ICP-MS. The results are summarized in Figure 0-3 and Table 0-21. The most notable metals are Sn (after the electrolysis) and Zn (before and after the electrolysis) which both appear in a higher amount on 99.8% Cu surfaces. Sn and Zn are both active in the CO_2RR with high selectivity towards HCOOH and CO, respectively,[1] although we did not observed significant increases in the associated products when 99.8% Cu foils were used. Nonetheless, our results show that the purity of Cu used will measurably affect the product distribution. In Cu CO_2RR studies, the purity of Cu should be at least 99.95% to avoid unwanted contributions from other metals.

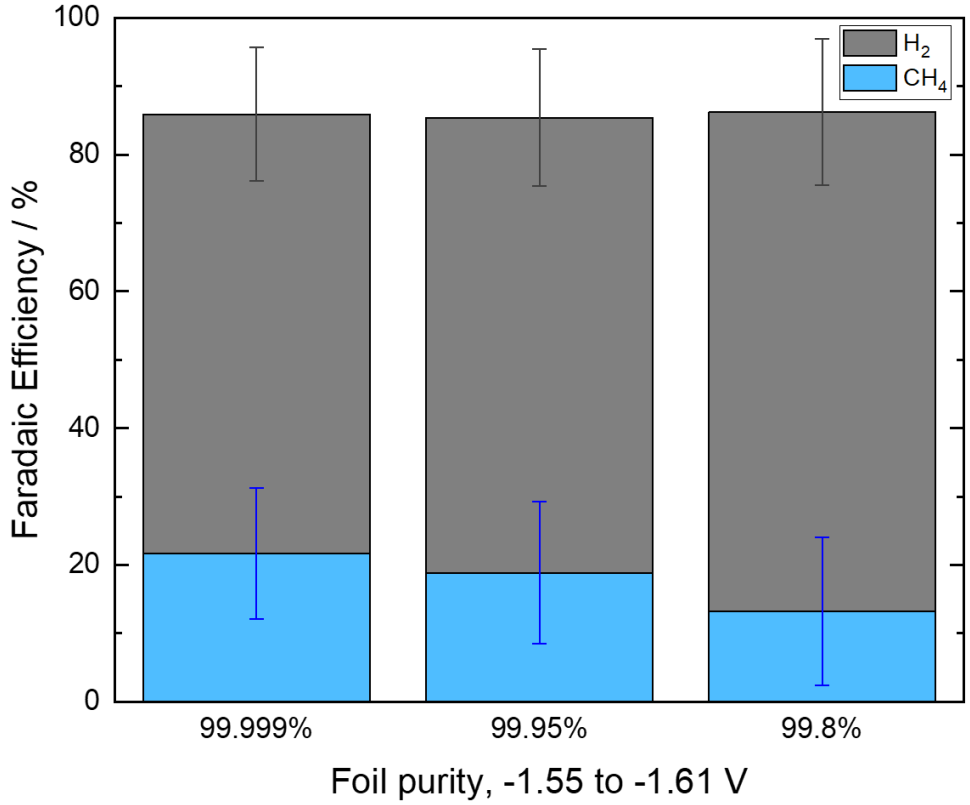

Figure 3-6 Faradaic efficiencies of H_2 and CH_4 of Cu CO_2RR under standard condition + different foil purities. Potential between –1.55 V and –1.61 V vs Ag/AgCl/KCl(sat.). Error bars are standard deviations from at least 3 independent measurements.

Electrolyte starting purity and pre-treatment

Although trace metal contamination in electrolytes and related pre-treatment strategies have been a widely explored research area, it has not been determined whether the same pre-treatment is effective for all different starting purities of an electrolyte salt. We studied the product distribution of the CO_2RR at Cu surfaces and the change in electrolysis current over time for experiments conducted with various starting purities and pre-treatments of the $NaHCO_3$ electrolyte. The salts used to prepare the electrolyte solutions in this study, ranked from highest purity to lowest, were trace metal grade Na_2CO_3, BioXtra grade $NaHCO_3$, HPLC grade $NaHCO_3$, and ACS grade $NaHCO_3$. 0.1 M $NaHCO_3$ electrolytes were prepared using these salts as described in the experimental section. 0.1 M $NaHCO_3$ electrolytes prepared from the salts of various purities were either untreated (used as prepared) or treated with a chelating-resin, a widely adopted pre-treatment strategy that is reported to be an effective way to remove trace metals.[73] The ratio of resin-mass-to-electrolyte-volume in the resin treatment process was held constant regardless of the starting purity of electrolyte salt. For HPLC grade $NaHCO_3$, pre-treatment of electrolyte using pre-electrolysis was also studied.

When comparing resin-treated electrolytes, shown in Figure 3-7, we observed that when using HPLC grade $NaHCO_3$, the CO_2RR shows the highest Faradaic efficiency for CH_4 out of all tested starting purities. We speculate that because the resin can only chelate and remove a fixed amount of trace metals from the electrolyte, electrolytes with lower starting purity will have higher amounts of trace metals present after the resin pre-treatment. It is likely that the relatively clean starting purities (trace metal grade and BioXtra grade) do not contain as many trace metal contaminants after pre-treatments, while HPLC grade would contain an intermediate amount and ACS grade would contain the highest amount of remaining trace metal contaminants. We

originally hypothesized that the small amount of trace metal remaining in the resin-treated HPLC grade electrolyte could promote CH_4 production. However, when we compared the product distributions of resin-treated and untreated electrolytes of all starting purities, shown in Figure 3-8, we observed a more detailed and more complicated trend.

With trace metal grade starting purity, the resin pre-treatment led to decreased Faradaic efficiency for CH_4. Similarly, Cu CO_2RR experiments conducted in BioXtra grade electrolyte also show a slightly lower CH_4 efficiency on average after the resin pre-treatment. In the case of HPLC grade electrolyte, although we did not observe a large difference in the product distribution, the standard deviation of the resin-treated electrolyte is significantly larger than for the pre-electrolysis and untreated electrolyte, suggesting a lower reproducibility when resin pre-treatment is used. When ACS grade electrolyte was resin-treated, higher CH_4 efficiency was observed for the Cu CO_2RR than when using the untreated electrolyte. These results suggest two different trends of the effect of resin pre-treatment on product distribution on different starting purity of the electrolytes. With higher starting purity electrolytes, CH_4 efficiencies are lower with resin pre-treatment. On the contrary, with lower starting purity electrolytes, CH_4 efficiencies remain similar or become higher when resin pre-treatment is used, but with lower reproducibility. Along with the observations discussed earlier, we propose the following explanations for the observed trends in product distribution.

First, for $NaHCO_3$ electrolytes prepared using very high starting purity (trace metal grade), the resin pre-treatment may actually result in more electrolyte impurities than simply using the untreated electrolyte. The introduced metal impurities may cause the lower Faradaic efficiencies for CH_4.

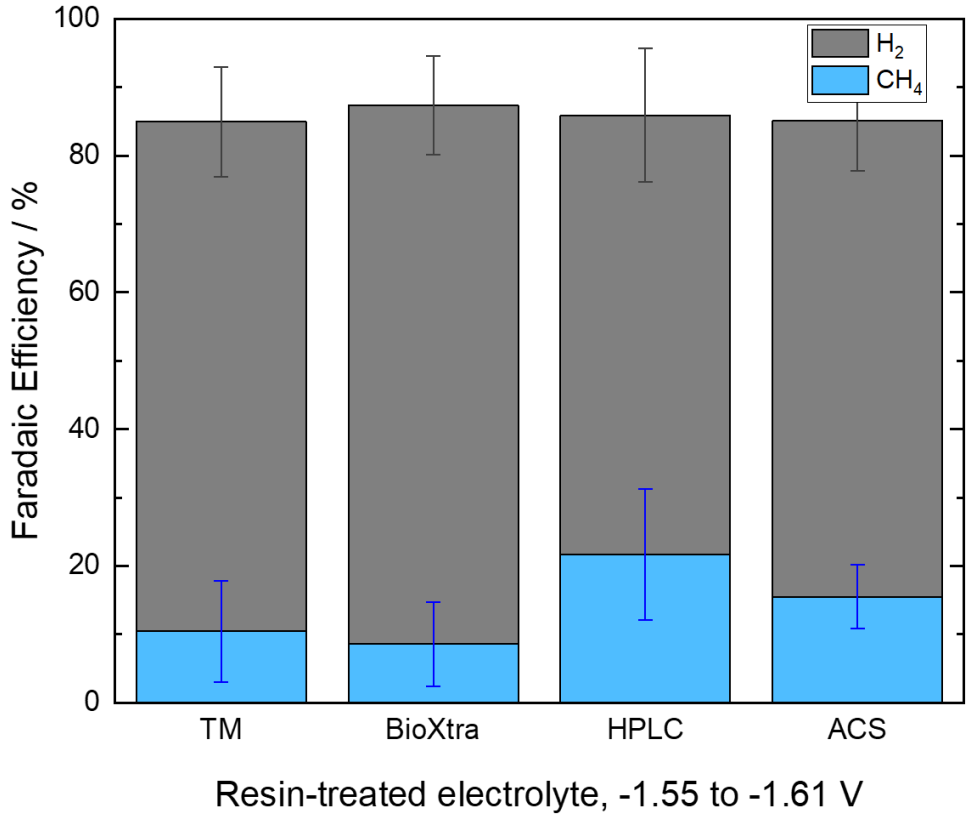

Figure 3-7 Faradaic efficiencies of H_2 and CH_4 from Cu CO_2RR under standard condition + resin-treated electrolyte, different starting grades. Potential between –1.55 V and –1.61 V vs Ag/AgCl/KCl(sat.). Error bars are standard deviations from at least 3 independent measurements.

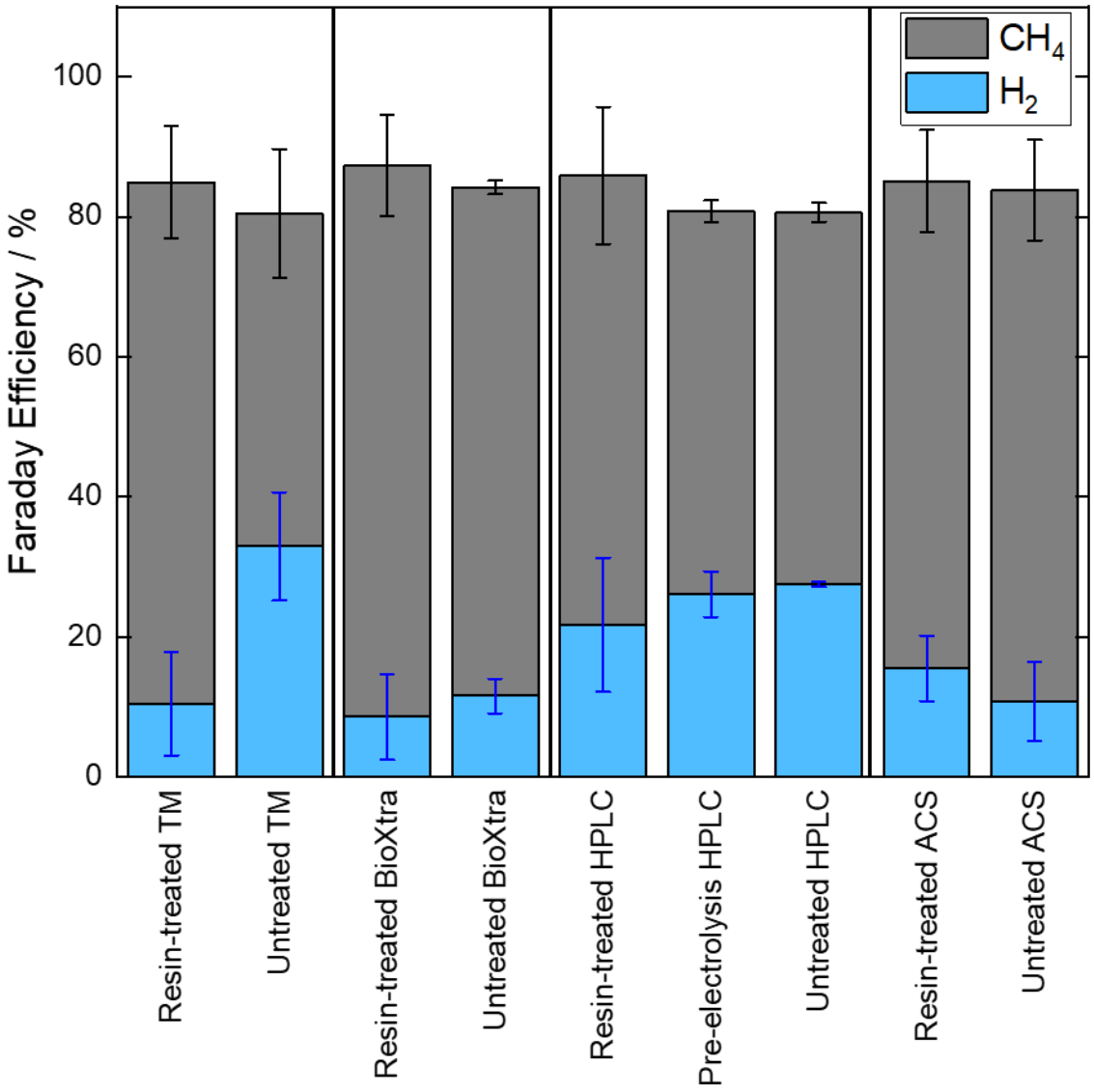

Figure 3-8 Faradaic efficiencies of H_2 and CH_4 from Cu CO_2RR under standard condition + different starting purities and different electrolyte pre-treatments. Potential between –1.55 V and –1.61 V vs Ag/AgCl/KCl(sat.). Error bars are standard deviations from at least 3 independent measurements.

Second, for $NaHCO_3$ electrolytes prepared with very low starting purities, such as ACS grade, most trace metals may be removed during resin treatment and CH_4 efficiencies improve as a result of fewer impurities.

Third, for $NaHCO_3$ electrolytes prepared with intermediate starting purities, the untreated and the resin-treated electrolyte produce similar average product distribution, but the untreated electrolyte shows higher reproducibility of the product distribution within the duration of our experiment (~ 2 h). We suspect that the trace metals that are present in the untreated electrolyte lead to the higher reproducibility. The observation that HPLC grade electrolyte shows the highest CH_4 efficiencies within the resin-treated electrolytes suggests that a small amount of *specific* metal impurities may be beneficial to CH_4 formation, although the reproducibility is lower when compared to untreated HPLC grade electrolyte. The resin-treated trace metal grade electrolytes (which we hypothesize are contaminated during the resin treatment process) show lower CH_4 efficiencies than resin-treated HPLC grade electrolytes (which we hypothesize contain a small amount of specific metal impurities) because the resin-treated trace metal grade electrolyte does not have the specific combination of metals that benefits CH_4 formation.

Overall, the presence of trace metals will lower the efficiency for CH_4, but a specific combination of trace metal impurities may be an exception.

We attempted to measure the amount of trace metals deposited onto the Cu surfaces after the CO_2RR when different electrolytes were used, and these data are summarized in Figure 0-4 and Table 0-30. However, the measurements were inconsistent, and we are not able to draw conclusive analyses from these data. Regardless, our data show that the effect of the resin treatment differs depending on the starting grades. It is therefore important for all investigations across research groups to use the same starting purity of electrolyte in addition to the resin pre-treatment.

Our data showing the change in current over time during the CO_2RR conducted with different electrolyte conditions provides additional insights into the effectiveness of the resin treatment in removing trace metals and preventing catalyst deactivation. Normalized currents, which were calculated by dividing the current at each time point by the initial current, of the Cu CO_2RR using HPLC grade electrolytes with various pre-treatments are shown in Figure 3-9. A normalized current closer to 1 indicates the current remained very similar to the initial current. When electrolyses were conducted using the resin-treated (black trace in Figure 3-9) HPLC grade electrolyte, the normalized current stays at a value close to 1 throughout the course of the electrolysis. However, electrolyses conducted using pre-electrolysis treated (blue trace in Figure 3-9) and untreated (red trace in Figure 3-9) HPLC grade electrolytes both show decreasing normalized currents over time. The same qualitative behavior was observed when comparing normalized currents from CO_2RR electrolyses conducted in resin-treated and untreated electrolytes prepared from BioXtra grade and ACS grade $NaHCO_3$ (Figure 3-10 and Figure 3-11). Electrolyses conducted with trace metal grade electrolytes show relatively stable currents both with and without resin pre-treatment. We speculate that this is due to the extremely low concentration of trace metal contaminants present in the trace metal grade electrolytes when untreated and when resin-treated, leading to a stable normalized current in both cases.

These normalized current measurements further support the argument that resin-treatment is an effective method for removing trace metal contaminants and preventing electrode poisoning and deactivation, while pre-electrolysis is not as effective.[73]

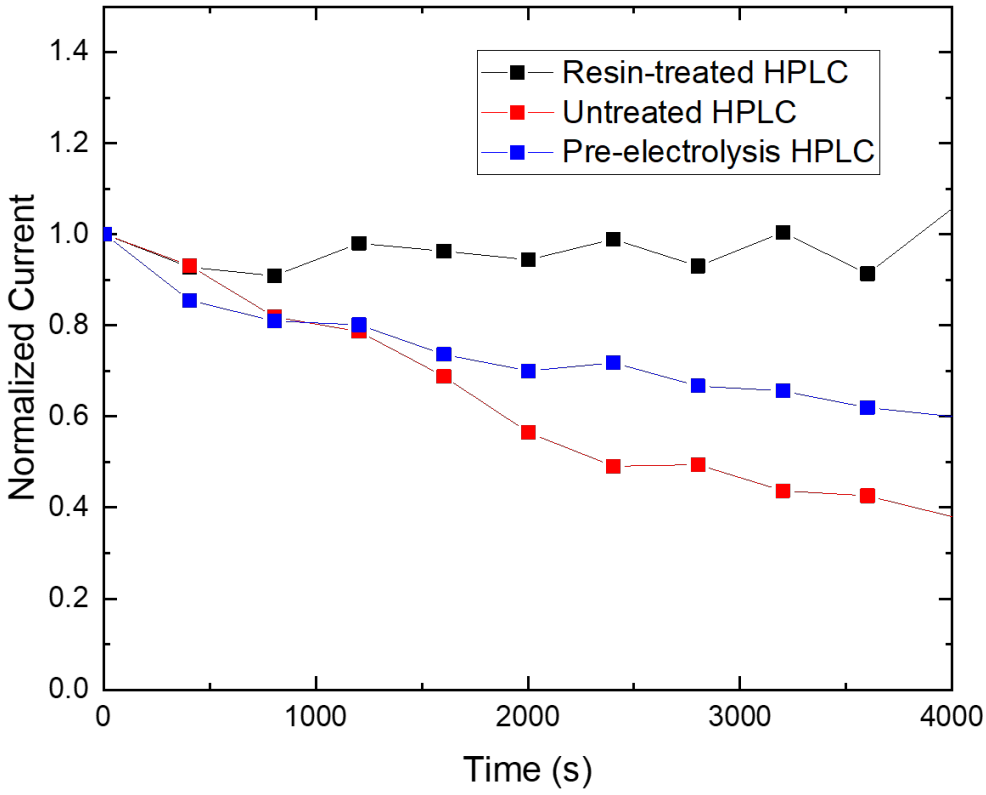

Figure 3-9 Change in current over time during Cu CO_2RR under standard condition + HPLC grade electrolyte with different pre-treatments. A representative sample of each condition is shown. Currents at each time point are normalized to the initial current.

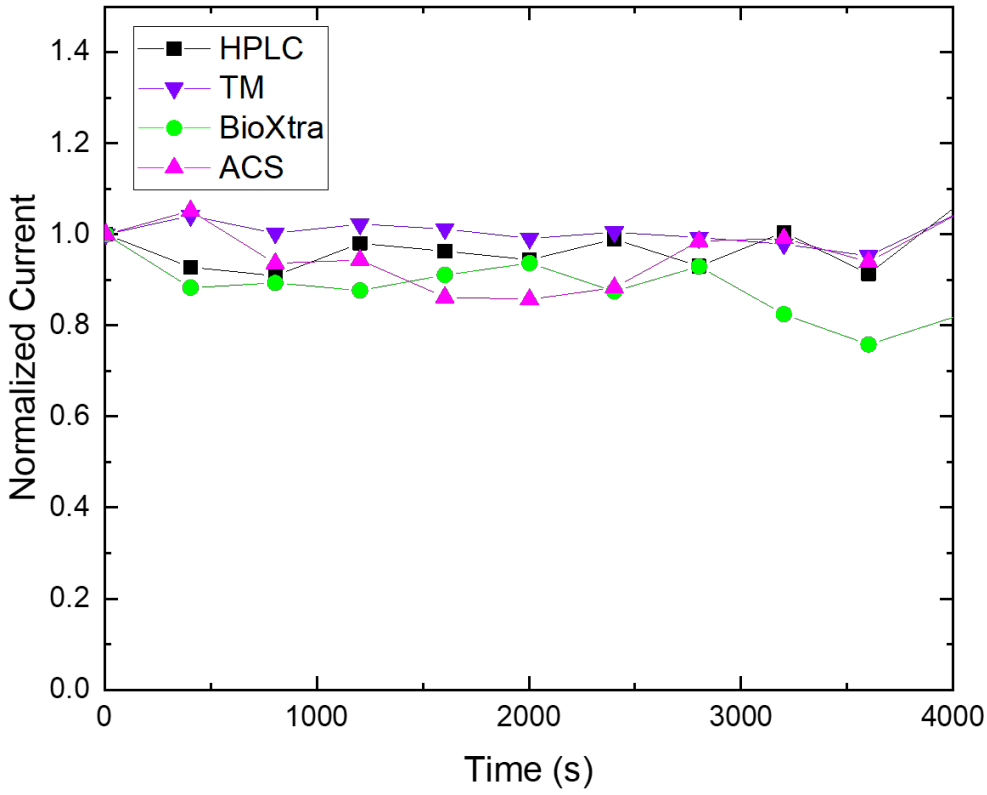

Figure 3-10 Change in current over time during Cu CO_2RR under standard condition + resin-treated electrolyte with different starting purities. A representative sample of each condition is shown. Currents at each time point are normalized to the initial current.

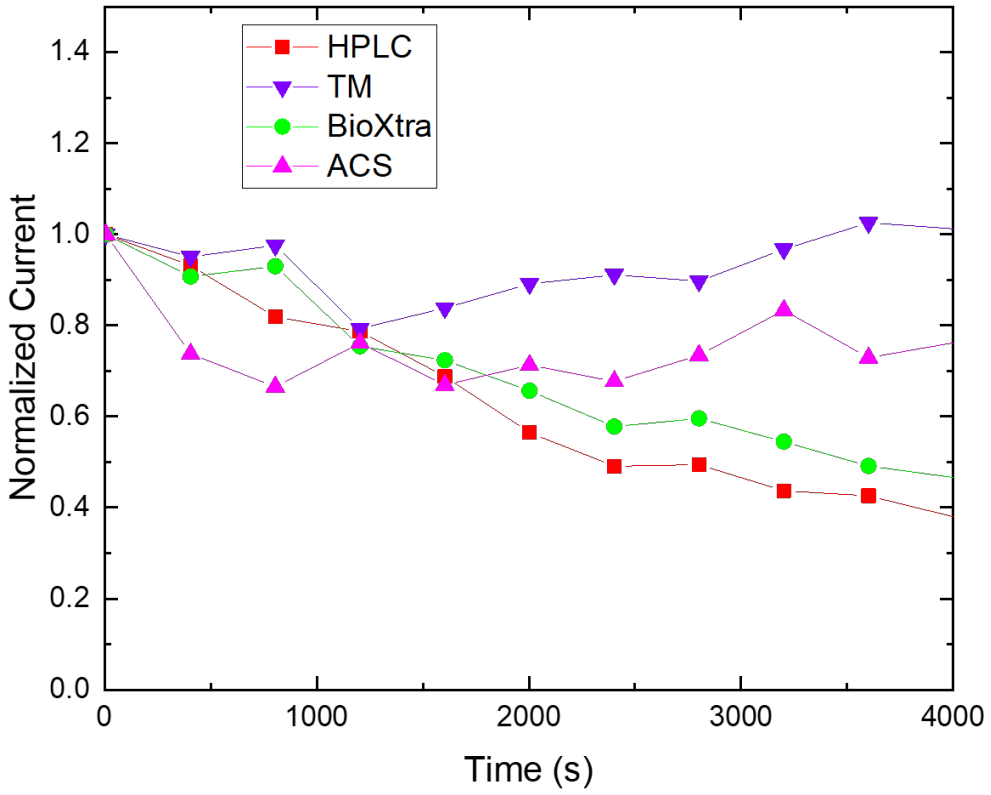

Figure 3-11 Change in current over time during Cu CO_2RR under standard condition + untreated electrolyte with different starting purities. A representative sample of each condition is shown. Currents at each time point are normalized to the initial current.

However, it is important to note that the decrease in current over time cannot and should not be the only indicator of electrode poisoning. In previous studies where we initially added Ag^+ to the electrolyte solution [102], we still observed a stable current for CO_2RR electrolyses when 50 ppb of Ag^+ ions was present in the electrolyte as indicated in Figure 3-12, even though the product distribution at 50 ppb of Ag^+ ions was drastically different than when no Ag^+ ions were added. This example demonstrates that the change in current is a useful indicator of poisoning but cannot be relied on as the *only* indicator of electrode poisoning.

We note that there are some discrepancies between the measurements we report in this study and previously reported results in literature that showed the resin pre-treatment in very high starting purity electrolytes led to higher CH_4 efficiencies than untreated electrolytes.[73] We attribute this difference to the slightly different grades of the electrolyte salt used (≥99.9999% in previous studies compared to 99.999% used in this study), or other minute differences in experimental preparation for which we did not account for. These discrepancies further illustrate the complexity and sensitivity of the Cu CO_2RR systems, as well as the difficulty in controlling all variables within the system.

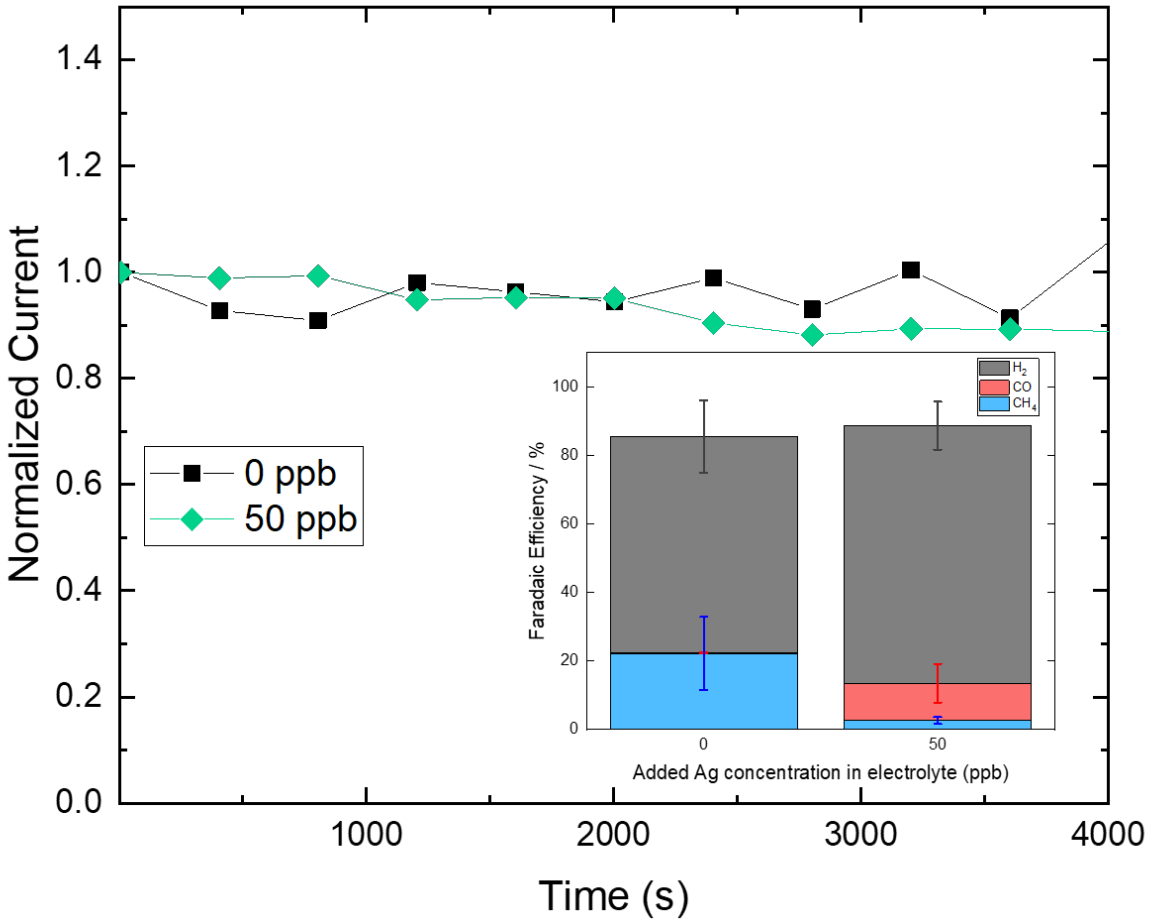

Figure 3-12 Change in current over time during Cu CO_2RR under standard condition + 0 and 50 ppb of externally added Ag ions titrated into the resin-treated HPLC grade electrolyte with different pre-treatments. A representative sample of each condition is shown. Currents at each time point are normalized to the initial current. Inserted bar graph shows the product distribution when 0 an d50 ppb of Ag ions was added.

3.5 Conclusion

In this study, we explored the effect of differences in the membranes, auxiliary electrodes, starting purity of Cu foil, starting purity of electrolyte salts, and electrolyte pre-treatment on CO_2RR product distributions. We found that common choices of membranes and auxiliary electrodes contain trace metal contaminants which are susceptible to leaching into solution and poisoning the electrode surface during electrochemical reactions. Both the starting purity and pre-treatment of materials have noticeable effects on the product distribution. Cu foil with a starting purity of 99.8% shows a slightly lower Faradaic efficiency for CH_4 than Cu foil with starting purity of 99.95% or higher. Electrolyte salts with different starting purities, even with identical resin pre-treatment, show significantly different Faradaic efficiencies for CH_4, with the intermediate starting purity (HPLC grade) electrolytes showing the highest Faradaic efficiency for CH_4. The resin pre-treatment also affects each starting purity electrolyte differently. For electrolytes with higher starting purities, the resin pre-treatment lowers the Faradaic efficiencies for CH_4, while for electrolytes with lower starting purities, the resin pre-treatment results in slightly increased Faradaic efficiencies for CH_4. These results suggest that, although the presence of trace metals generally decreases the Faradaic efficiency for CH_4, a small amount of specific trace metal contaminants could actually benefit the formation of CH_4. When untreated electrolytes were used in our CO_2RR experiments, we observed a change in current during CO_2RR that is consistent with surface poisoning and deactivation. However, it is important to note that the change in current should not be the only indicator of contamination. Overall, our results highlight the complexity and extreme sensitivity of Cu-catalyzed CO_2RR systems to trace metal contamination and demonstrate the need to develop a comprehensive and thorough set of control experiments for

CO_2RR used by all researchers to understand the true nature of their Cu CO_2RR electrochemical systems.

3.6 References

(1) Hori, Y. "Electrochemical CO2 Reduction on Metal Electrodes," *Mod Asp Electrochem* **2008**, 89-189. http://dx.doi.org/Book_Doi 10.1007/978-0-387-49489-0

(8) Hori, Y.; Kikuchi, K.; Murata, A.; Suzuki, S. "Production of Methane and Ethylene in Electrochemical Reduction of Carbon-Dioxide at Copper Electrode in Aqueous Hydrogencarbonate Solution," *Chem Lett* **1986**, 897-898. http://dx.doi.org/DOI 10.1246/cl.1986.897

(11) Kuhl, K. P.; Cave, E. R.; Abram, D. N.; Jaramillo, T. F. "New insights into the electrochemical reduction of carbon dioxide on metallic copper surfaces," *Energy & Environmental Science* **2012**, *5*. http://dx.doi.org/10.1039/c2ee21234j

(14) Liu, Y.; Leung, K. Y.; Michaud, S. E.; Soucy, T. L.; McCrory, C. C. L. "Controlled Substrate Transport to Electrocatalyst Active Sites for Enhanced Selectivity in the Carbon Dioxide Reduction Reaction," *Comments on Inorganic Chemistry* **2019**, 1-28. http://dx.doi.org/10.1080/02603594.2019.1628025

(29) Katsounaros, I.; Meier, J. C.; Klemm, S. O.; Topalov, A. A.; Biedermann, P. U.; Auinger, M.; Mayrhofer, K. J. J. "The effective surface pH during reactions at the solid–liquid interface," *Electrochemistry Communications* **2011**, *13*, 634-637. http://dx.doi.org/10.1016/j.elecom.2011.03.032

(30) Varela, A. S.; Kroschel, M.; Reier, T.; Strasser, P. "Controlling the selectivity of CO 2 electroreduction on copper: The effect of the electrolyte concentration and the importance of the local pH," *Catalysis Today* **2016**, *260*, 8-13. http://dx.doi.org/10.1016/j.cattod.2015.06.009

(31) Hori, Y.; Murata, A.; Takahashi, R. "Formation of Hydrocarbons in the Electrochemical Reduction of Carbon-Dioxide at a Copper Electrode in Aqueous-Solution," *J Chem Soc Farad T 1* **1989**, *85*, 2309-2326. http://dx.doi.org/DOI 10.1039/f19898502309

(45) Dunwell, M.; Lu, Q.; Heyes, J. M.; Rosen, J.; Chen, J. G.; Yan, Y.; Jiao, F.; Xu, B. "The Central Role of Bicarbonate in the Electrochemical Reduction of Carbon Dioxide on Gold," *J Am Chem Soc* **2017**, *139*, 3774-3783. http://dx.doi.org/10.1021/jacs.6b13287

(46) Hori, Y. "Electrochemical CO_2 Reduction on Metal Electrodes," In *Modern Aspects of Electrochemistry*; Vayemas, C. G., Ed.; Springer: New York, 2008; Vol. 42, p 89-189.

(57) Mariano, R. G.; McKelvey, K.; White, H. S.; Kanan, M. W. "Selective increase in CO2 electroreduction activity at grain-boundary surface terminations," *Science* **2017**, *358*, 1187-1191. http://dx.doi.org/10.1126/science.aao3691

(59) Reske, R.; Mistry, H.; Behafarid, F.; Roldan Cuenya, B.; Strasser, P. "Particle size effects in the catalytic electroreduction of CO(2) on Cu nanoparticles," *J Am Chem Soc* **2014**, *136*, 6978-6986. http://dx.doi.org/10.1021/ja500328k

(60) Hori, Y.; Konishi, H.; Futamura, T.; Murata, A.; Koga, O.; Sakurai, H.; Oguma, K. "“Deactivation of copper electrode” in electrochemical reduction of CO2," *Electrochimica Acta* **2005**, *50*, 5354-5369. http://dx.doi.org/10.1016/j.electacta.2005.03.015

(67) He, J.; Huang, A.; Johnson, N. J. J.; Dettelbach, K. E.; Weekes, D. M.; Cao, Y.; Berlinguette, C. P. "Stabilizing Copper for CO2 Reduction in Low-Grade Electrolyte," *Inorg Chem* **2018**, *57*, 14624-14631. http://dx.doi.org/10.1021/acs.inorgchem.8b02311

(70) Klaus, S.; Cai, Y.; Louie, M. W.; Trotochaud, L.; Bell, A. T. "Effects of Fe Electrolyte Impurities on Ni(OH)2/NiOOH Structure and Oxygen Evolution Activity," *The Journal of Physical Chemistry C* **2015**, *119*, 7243-7254. http://dx.doi.org/10.1021/acs.jpcc.5b00105

(71) Trotochaud, L.; Young, S. L.; Ranney, J. K.; Boettcher, S. W. "Nickel-iron oxyhydroxide oxygen-evolution electrocatalysts: the role of intentional and incidental iron incorporation," *J Am Chem Soc* **2014**, *136*, 6744-6753. http://dx.doi.org/10.1021/ja502379c

(73) Wuttig, A.; Surendranath, Y. "Impurity Ion Complexation Enhances Carbon Dioxide Reduction Catalysis," *ACS Catalysis* **2015**, *5*, 4479-4484. http://dx.doi.org/10.1021/acscatal.5b00808

(81) Li, C. W.; Kanan, M. W. "CO2 reduction at low overpotential on Cu electrodes resulting from the reduction of thick Cu2O films," *J Am Chem Soc* **2012**, *134*, 7231-7234. http://dx.doi.org/10.1021/ja3010978

(85) Corrigan, D. A. "The Catalysis of the Oxygen Evolution Reaction by Iron Impurities in Thin-Film Nickel-Oxide Electrodes," *Journal of the Electrochemical Society* **1987**, *134*, 377-384. http://dx.doi.org/Doi 10.1149/1.2100463

(86) Stevens, M. B.; Enman, L. J.; Batchellor, A. S.; Cosby, M. R.; Vise, A. E.; Trang, C. D. M.; Boettcher, S. W. "Measurement Techniques for the Study of Thin Film Heterogeneous Water Oxidation Electrocatalysts," *Chemistry of Materials* **2016**, *29*, 120-140. http://dx.doi.org/10.1021/acs.chemmater.6b02796

(98) Besson, M.; Gallezot, P. "Deactivation of metal catalysts in liquid phase organic reactions," *Catalysis Today* **2003**, *81*, 547-559. http://dx.doi.org/10.1016/s0920-5861(03)00153-6

(99) Twigg, M. V. "<Deactivation of Copper Metal Catalysts for Methanol Decomposition, Methanol Steam Reforming and Methanol Synthesis.pdf>," *Topics in Catalysis* **2003**, *22*, 191-203. http://dx.doi.org/10.1023/a:1023567718303

(100) Kim, C.; Choe, Y.-K.; Won, D. H.; Lee, U.; Oh, H.-S.; Lee, D. K.; Choi, C. H.; Yoon, S.; Kim, W.; Hwang, Y. J.; Min, B. K. "Turning Harmful Deposition of Metal Impurities into Activation of Nitrogen-Doped Carbon Catalyst toward Durable Electrochemical CO2 Reduction," *ACS Energy Letters* **2019**, *4*, 2343-2350. http://dx.doi.org/10.1021/acsenergylett.9b01581

(101) Ullman, A. M.; Liu, Y.; Huynh, M.; Bediako, D. K.; Wang, H.; Anderson, B. L.; Powers, D. C.; Breen, J. J.; Abruna, H. D.; Nocera, D. G. "Water oxidation catalysis by Co(II) impurities in Co(III)4O4 cubanes," *J Am Chem Soc* **2014**, *136*, 17681-17688. http://dx.doi.org/10.1021/ja5110393

(102) Leung, K. Y.; McCrory, C. C. L. "Effect and Prevention of Trace Ag+ Contamination from Ag/AgCl Reference Electrodes on CO2 Reduction Product Distributions at Polycrystalline Copper Electrodes," *ACS Applied Energy Materials* **2019**, *2*, 8283-8293. http://dx.doi.org/10.1021/acsaem.9b01759

(103) Hori, Y.; Kikuchi, K.; Suzuki, S. "Production of Co and Ch4 in Electrochemical Reduction of Co2 at Metal-Electrodes in Aqueous Hydrogencarbonate Solution," *Chem Lett* **1985**, 1695-1698. http://dx.doi.org/DOI 10.1246/cl.1985.1695

(104) Dunwell, M.; Luc, W.; Yan, Y.; Jiao, F.; Xu, B. "Understanding Surface-Mediated Electrochemical Reactions: CO2 Reduction and Beyond," *ACS Catalysis* **2018**, *8*, 8121-8129. http://dx.doi.org/10.1021/acscatal.8b02181

(105) Verdaguer-Casadevall, A.; Li, C. W.; Johansson, T. P.; Scott, S. B.; McKeown, J. T.; Kumar, M.; Stephens, I. E.; Kanan, M. W.; Chorkendorff, I. "Probing the Active Surface Sites for CO Reduction on Oxide-Derived Copper Electrocatalysts," *J Am Chem Soc* **2015**, *137*, 9808-9811. http://dx.doi.org/10.1021/jacs.5b06227

Chapter 4: Conclusion and Future Outlook on Methods to Mitigate Trace Metal Contamination

4.1 Preface

This chapter summarizes the major findings described in my dissertation and outlines future outlooks for Cu CO_2RR research. The extremely sensitivity of Cu CO_2RR systems will be the major challenge for research and commercialization. Therefore, future research should focus on mitigating trace metal contamination by methods such as the polymer-coated electrodes suggested in this chapter. Parts of this section are reprinted with permission from Yingshuo Liu, Kwan Yee Leung, Samuel E. Michaud, Taylor L. Soucy & Charles C. L. McCrory. *Comments on Inorganic Chemistry*, 2019.

4.2 Conclusion and Summary

In this dissertation, the sources and effects of trace metal contamination were investigated. Every electrochemical component, including the reference electrode, membranes, auxiliary electrode, Cu electrode, and electrolyte, was examined. Different configurations of the Ag/AgCl/KCl(sat.) reference electrode and various starting purities and pre-treatments of the other electrochemical components were tested for their effect on trace metal contamination and product distribution. We concluded that the reference electrode is a major source of Ag^+ ion contamination, and that the Cu CO_2RR product distribution is altered with as little as 10 ppb of Ag^+ ion contamination. The membrane and auxiliary electrodes are also found to be sources of trace metal contamination. Even with identical pre-treatment, the starting purity of the Cu foil and electrolyte

salt both affect the product distribution. Cu foils with 99.8% purity show lower CH_4 Faradaic efficiencies than foils with 99.95% or higher purities. Interestingly, using HPLC grade $NaHCO_3$, an "intermediate" grade electrolyte in terms of purity, results in the highest Faradaic efficiency for CH_4 compared to other higher and lower purity electrolytes after identical resin pre-treatment. When comparing the treated and untreated electrolytes, it was observed that the resin pre-treatment affects the different starting purities of electrolytes differently. The highest purity (trace metal grade) shows lower CH_4 efficiencies after resin-treatment, while the lower purities (BioXtra, HLPC, ACS grade) all shows similar or slightly higher CH_4 efficiencies after resin-treatment. The trace metal grade electrolyte is also the only one that does not show a decrease in current over time without resin pre-treatment, unlike the other grades that all display a decrease in current without the resin pre-treatment. It is possible that the resin treatment process might in fact introduce more metal impurities into the higher purity electrolytes. These observations suggest that the effectiveness of the resin pre-treatment depends on the starting purity of the electrolyte, and that a *small amount of specific* metal impurities (present in HPLC grade electrolytes after resin-treatment) might be beneficial for CH_4 production, although further studies are needed to confirm this hypothesis.

This dissertation emphasizes the importance of developing a standard procedure for Cu CO_2RR research. Even within the same laboratory setting, differences in purity and pre-treatment can result in vastly different measured product distributions. Strategies for preventing trace metal contamination are also outlined in this dissertation. Ag^+ ion contamination from the reference electrodes can be effectively prevented for at least 12 h by employing a double-junction configuration. The components of the electrochemical cell should be cleaned with and stored in HNO_3 whenever possible to avoid metal accumulation over time.

4.3 Future outlook

The extreme sensitivity of Cu surfaces towards trace metal contamination will continue to be the major challenge in Cu CO_2RR research and future commercialization. Further studies on the prevention of trace metal contamination on Cu CO_2RR systems can be done using polymer-coated electrodes. Polymer-coated electrodes are a specific subset of overlayer-coated electrodes which have been used to modulate the activity, product distribution, and stability of electrocatalysts for various electrocatalytic reactions including the CO_2RR.[106] An example of an overlayer-coated electrode is illustrated in Figure 4-1. The polymer films can impart significant benefits on the electrocatalysts by controlling substrate transport, stabilizing the reaction intermediate, and protecting against contaminants.[106,107] Coating electrode surfaces with porous overlayers can also play an important role in decreasing transport of contaminants to the electrode surface, thus preventing electrode poisoning and deactivation.[107-109] This is particularly important for the CO_2RR at Cu surfaces, which are extremely susceptible to surface poisoning,[46,74] especially by trace metal contaminants in the electrolyte solutions[60,73,74] and other electrochemical components, as shown in this dissertation. A recent study of CO_2RR by P4VP-coated Cu electrodes for the CO_2RR found that P4VP can act as a sink for heavy-metal contaminants in standard purity (99.7+%) electrolytes, thereby decreasing the effect of the metal contaminants on the electrocatalytic activity and product distribution.[110]

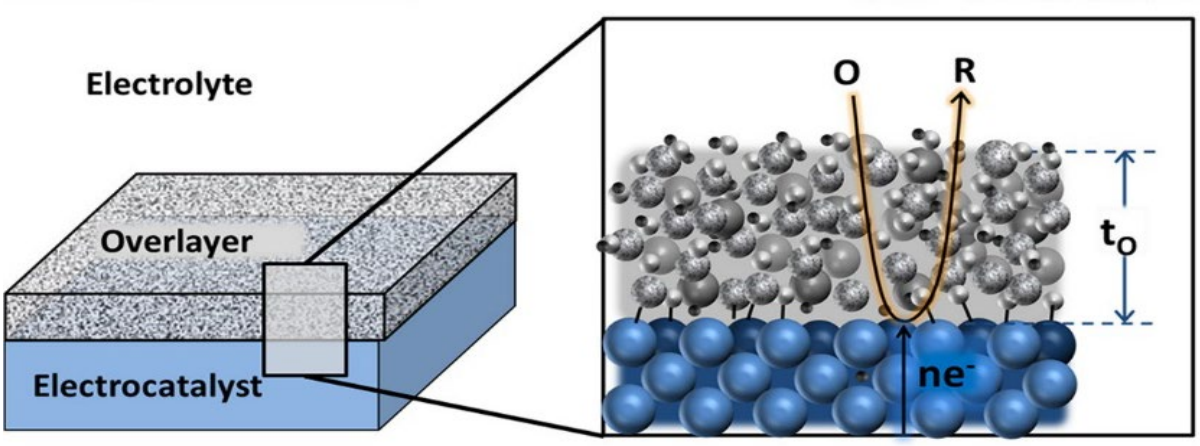

Figure 4-1 An example of overlayer-coated electrode.[111] Adapted with permission from ACS Catal. 2018, 8, 457−465. Copyright (2018) American Chemical Society.

Using a similar concept, trace metal contamination can be mitigated by using an ion-exchange polymer blocking layer coated on the surface of the electrode to prevent metal ions from reaching and therefore poisoning the surface of the electrode. It is hypothesized that when the Cu electrode surface is coated with a cation exchange polymer such as Nafion, the trace metal ions will initially be blocked, and the surface will be protected for some amount of time. However, over time the metal ions will eventually cross over the cation exchange polymer and reach the Cu surface, contaminating the catalyst and altering the product distribution and activity. With an anion exchange polymer such as Fumion or an uncharged polymer such as polystyrene, the polymers will provide prolonged protection and prevent trace metal ions from reaching the Cu surface since there is no method of transport for the positively charged metal cations. However, one challenge will be depositing the polymer layers with uniform thicknesses across samples since the polymer thickness is expected to affect the ability to block metal ions from reaching the electrode. Nonetheless, this study will provide valuable insights into using polymer layers as a viable way to prevent trace metal contamination.

In addition to preventing trace metal contamination, polymers can be used to directly control mass transport of reactive species and fine tune the product distribution of the Cu CO_2RR. As mentioned in **Chapter 1**, the reaction selectivity and product selectivity significantly depend on the local concentration and mass transport of CO_2 and H^+ species. Using specific polymers that facilitate the transport of certain species, the mass transport and local concentration of these particular species can be directly controlled. Blend polymers, which can be prepared by dissolving two or more polymers before depositing them onto an electrode surface, can be used to achieve a control of mass transport and local concentration. A graphical representation of a blend polymer is shown in Figure 4-2.

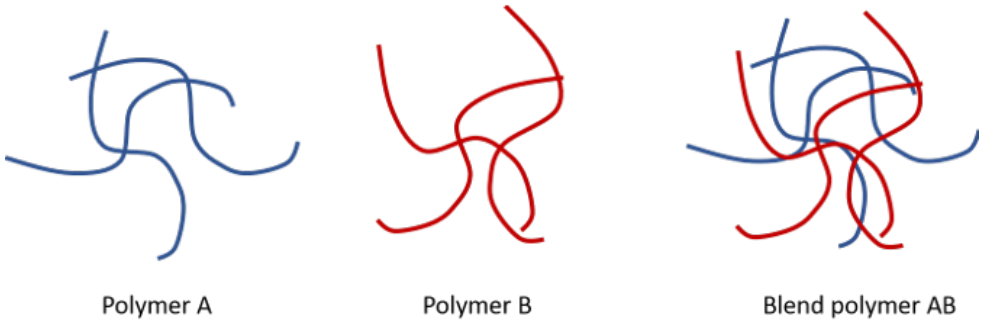

Figure 4-2 Graphical representation of blend polymers. Blend polymer AB can be prepared by blending polymer A and B together before being deposited onto an electrode surface.

By combining different ratios of a CO_2-transport facilitating polymer (such as polyethyleneimines), an H^+-transport facilitating polymer (such as poly-vinyl-imidazole), and a blocking polymer that does not facilitate transport (such as polystyrene) in a blend polymer, the mass transport of CO_2 and H^+ can be directly controlled. The local concentration of CO_2 and H^+, as well as the reaction selectivity and product selectivity, can then be controlled. The blend polymer method could be a valuable way to achieve high degree of control over product distribution in the Cu CO_2RR.

Some preliminary studies using poly-4-vinylpyridine (P4VP), another example of an H^+-transport facilitating polymer, in the Au-catalyzed CO_2RR system were conducted. The goal of the study was to examine the effect of facilitated mass transport of H^+ in CO_2RR using our existing electrochemical set up. Instead of Cu, a Au catalyst system was used because of the relatively simple product distribution, mainly H_2 and CO. P4VP, dissolved in dimethylformamide in various concentrations, was drop cast onto the electrode surface. CO_2RR was then performed on the resulting P4VP-coated surfaces and the product distribution was analysed. There were two types of Au systems studied. One was a solid state planar polycrystalline Au disc, and the other was Au powder drop cast on a glassy carbon disc electrode. Au powder on a glassy carbon electrode was used to understand whether facilitated mass transport would give the same effect for immobilized catalyst systems as for solid state catalyst systems.

In these experiments, the working electrode was an Au disc or a glassy carbon disc electrode. The discs were mechanically polished using MetaDi diamond suspension with sequential grit size (9, 6, 3, 1, 0.1 μm, Buehler) followed by sonication in water. A single junction saturated calomel electrode (SCE) was used as the reference electrode. Nafion was used as the membrane and carbon rod was used as the auxiliary electrode. The electrolyte was 0.1 M untreated

BioXtra grade $KHCO_3$ (Sigma-Aldrich), with CO_2 gas sparged in the electrolyte for 1 h before experiments. The poly-4-vinylpyridine (Sigma-Aldrich) drop cast solution was prepared by dissolving P4VP in dimethylformamide (Sigma-Aldrich). P4VP solutions of 0.04%, 0.1%, and 1% (w/v) were prepared by dissolving 0.004 g, 0.01 g, and 0.1 g of P4VP polymer respectively in 10 mL of DMF. To prepare the solid state polycrystalline Au disc surfaces, 5 µL of the P4VP solution was drop cast onto the Au surface, and the surfaces were place in oven at 60 °C for 10 min to dry. To prepare glassy carbon electrode surfaces with Au powder (GoodFellow, AU006020 Mean Particle size < 2 micron, Purity:99.95%). Au powder was blended into the 0.04% P4VP drop cast solution in 0.02%, 0.16%, and 0.32% concentration by adding 0.002 g, 0.016 g, and 0.032 g Au powder respectively into 10 mL of the drop cast solution. 5 µL of the P4VP with Au powder solution was drop cast onto the glassy carbon electrodes, and the surfaces were place in oven at 60 °C for 10 min to dry. The CO_2RR product distributions using the prepared electrodes are summarized in Table 0-31 through Table 0-39. Example images of the prepared surfaces are shown in Figure 4-3.

In the case of the solid state planar polycrystalline Au disc with a 0.04% P4VP polymer overlayer, the Faradaic efficiency for CO drops from about 71% at -1.6V vs SCE down to 11%. When the P4VP concentration was increased to 1%, the Faradaic efficiency increases back to about 45%. The data suggest that facilitated H^+ transport affects the reaction selectivity of CO_2RR, and the effect is dependent on the concentration or the thickness of the polymer layer. In the case of glassy carbon electrode surfaces with Au powder, CO is not observed except for at the highest Au powder concentration of 0.32%. From the data, the effect of facilitated H^+ transport is inconclusive in the immobilized Au powder systems.

It must be noted that these preliminary data had several significant differences from our other CO_2RR experiments and should not be directly compared to the Cu CO_2RR results from other chapters. For instance, these experiments were completed at a very early stage in my research career and the electrolyte used ($KHCO_3$) was different from the one used in other chapters ($NaHCO_3$). Also, appropriate electrolyte pre-treatments were not used in these studies. Moreover, a single junction SCE reference electrode was used instead of double junction. It is very likely that Hg ions may have contaminated the electrochemical system. There were a few assumptions made when preparing the electrode surfaces with the P4VP polymer layer. It was assumed that the polymer thickness did not change significantly with different concentrations of P4VP and Au powder, and the Au powder was also assumed to be evenly distributed throughout the polymer film. From Figure 4-3 (b) through (e), changes of the polymer layer were observed before and after CO_2RR. It was assumed the change in the polymer during experiment was not significant enough to affect the facilitated mass transport, but a more detailed analysis should be done to confirm this assumption. Furthermore, it is possible that the P4VP polymer and DMF contained trace metals that could contaminate the electrochemical system.

For future CO_2RR studies, these preliminary experiments should be repeated using a double junction Ag/AgCl/KCl(sat.) reference electrode and resin-treated 0.1 M $NaHCO_3$. The P4VP polymer and DMF should also be tested for any trace metal content.

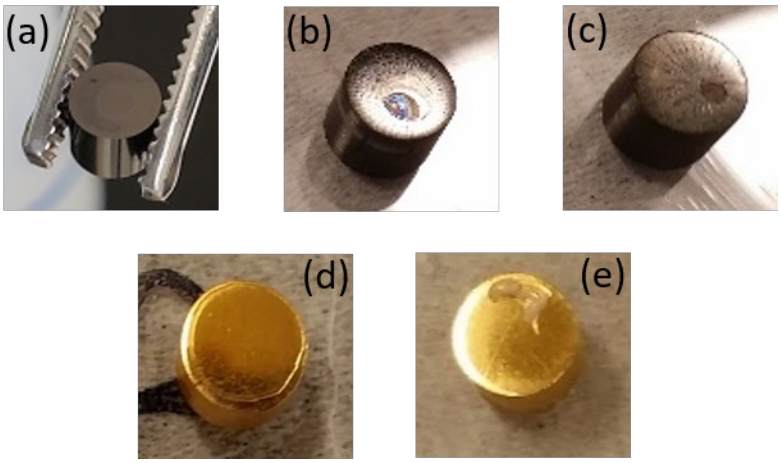

Figure 4-3 Pictures of (a) a polished glassy carbon disc electrode, (b) a glassy carbon disc electrode coated with 0.04% P4VP and 0.16% Au, before CO_2RR, (c) a glassy carbon disc electrode coated with 0.04% P4VP and 0.16% Au, after CO_2RR, (d) a solid state planar polycrystalline Au disc with 1% P4VP, before CO_2RR, (e) a solid state planar polycrystalline Au disc with 1% P4VP, after CO_2RR.

Although popular interest in Cu CO_2RR research focuses on controlling product distribution, particularly towards higher selectivity for hydrocarbons, the results and analyses in this dissertation illustrate the importance of understanding the true nature of the electrochemical system, especially the presence and concentration of trace metal contaminants. The study in **Chapter 2** on trace amounts of Ag leaking from the reference electrode shows that ppb level of metal contaminants can drastically alter the product distribution, an amount much lower than what was previously assumed in literature. **Chapter 3** discusses that even with identical pre-treatment, differences in the starting purity of materials will lead to differences in product distribution. Furthermore, the pre-treatment affected materials of different starting purities differently, illustrating the sensitivity and complexity of the Cu CO_2RR system. Prior to experimenting with new catalyst materials or new methods to alter the product distribution, there is a need for a set of thorough control experiments that carefully examine all possible factors within the electrochemical system to avoid incorrectly attributing the cause of any changes in the product distribution.

This dissertation is, in short, a cautionary narrative of the importance of the basis of the scientific research process—thorough and carefully designed control experiments should be defined as the first steps of all research processes before implementing other experimental variables. This narrative is applicable to all electrochemical systems, including those beyond the CO_2RR. For future advancements in any electrochemical catalysis research, careful analysis of all the sources and effects of contamination must be conducted before meaningful comparison between experiments can be drawn.

4.4 References

(46) Hori, Y. "Electrochemical CO_2 Reduction on Metal Electrodes," In *Modern Aspects of Electrochemistry*; Vayemas, C. G., Ed.; Springer: New York, 2008; Vol. 42, p 89-189.

(60) Hori, Y.; Konishi, H.; Futamura, T.; Murata, A.; Koga, O.; Sakurai, H.; Oguma, K. "“Deactivation of copper electrode” in electrochemical reduction of CO2," *Electrochimica Acta* **2005**, *50*, 5354-5369. http://dx.doi.org/10.1016/j.electacta.2005.03.015

(73) Wuttig, A.; Surendranath, Y. "Impurity Ion Complexation Enhances Carbon Dioxide Reduction Catalysis," *ACS Catalysis* **2015**, *5*, 4479-4484. http://dx.doi.org/10.1021/acscatal.5b00808

(74) Clark, E. L.; Resasco, J.; Landers, A.; Lin, J.; Chung, L.-T.; Walton, A.; Hahn, C.; Jaramillo, T. F.; Bell, A. T. "Standards and Protocols for Data Acquisition and Reporting for Studies of the Electrochemical Reduction of Carbon Dioxide," *ACS Catalysis* **2018**, *8*, 6560-6570. http://dx.doi.org/10.1021/acscatal.8b01340

(106) Ponnurangam, S.; Chernyshova, I. V.; Somasundaran, P. "Nitrogen-containing polymers as a platform for CO2 electroreduction," *Adv. Colloid Interface Sci.* **2017**, *244*, 184-198. http://dx.doi.org/10.1016/j.cis.2016.09.002

(107) Esposito, D. V. "Membrane-Coated Electrocatalysts—An Alternative Approach To Achieving Stable and Tunable Electrocatalysis," *ACS Catal.* **2018**, *8*, 457-465. http://dx.doi.org/10.1021/acscatal.7b03374

(108) Labrador, N. Y.; Songcuan, E. L.; De Silva, C.; Chen, H.; Kurdziel, S. J.; Ramachandran, R. K.; Detavernier, C.; Esposito, D. V. "Hydrogen Evolution at the Buried Interface between Pt

Thin Films and Silicon Oxide Nanomembranes," *ACS Catalysis* **2018**, *8*, 1767-1778. http://dx.doi.org/10.1021/acscatal.7b02668

(109) Oughli, A. A.; Ruff, A.; Boralugodage, N. P.; Rodríguez-Maciá, P.; Plumeré, N.; Lubitz, W.; Shaw, W. J.; Schuhmann, W.; Rüdiger, O. "Dual properties of a hydrogen oxidation Ni-catalyst entrapped within a polymer promote self-defense against oxygen," *Nat. Commun.* **2018**, *9*, 864. http://dx.doi.org/10.1038/s41467-018-03011-7

(110) Ponnurangam, S.; Yun, C. M.; Chernyshova, I. V. "Robust Electroreduction of CO2 at a Poly(4-vinylpyridine)–Copper Electrode," *ChemElectroChem* **2016**, *3*, 74-82. http://dx.doi.org/10.1002/celc.201500421

(111) Esposito, D. V. "Membrane-Coated Electrocatalysts—An Alternative Approach To Achieving Stable and Tunable Electrocatalysis," *ACS Catalysis* **2017**, *8*, 457-465. http://dx.doi.org/10.1021/acscatal.7b03374

Appendix

A.1 Experimental Figures

Figure 0-1 (a) Custom-made single-junction Ag/AgCl/KCl(sat.) reference electrode design. The AgCl-coated Ag wire is enclosed within a glass body filled with saturated KCl(*aq*) and separated from the electrolyte solution by a CoralPor® glass frit. (b) Glass frit which serves as the second junction. Custom-made glass body enclosed with a CoralPor® glass frit (c) Double-junction Ag/AgCl/KCl(sat.)/$NaHCO_3$(0.1 M) reference electrode constructed by placing the single-junction Ag/AgCl/KCl(sat.) reference electrode into the glass body that serves as the second junction. The glass body is filled with electrolyte (resin-treated 0.1 M $NaHCO_3$(*aq*) or 0.1 M H_2SO_4) and separated from the electrolyte solution in the electrochemical cell by a CoralPor® glass frit. A stainless steel rod with an alligator clip is attached to the reference electrode during electrochemical measurements.

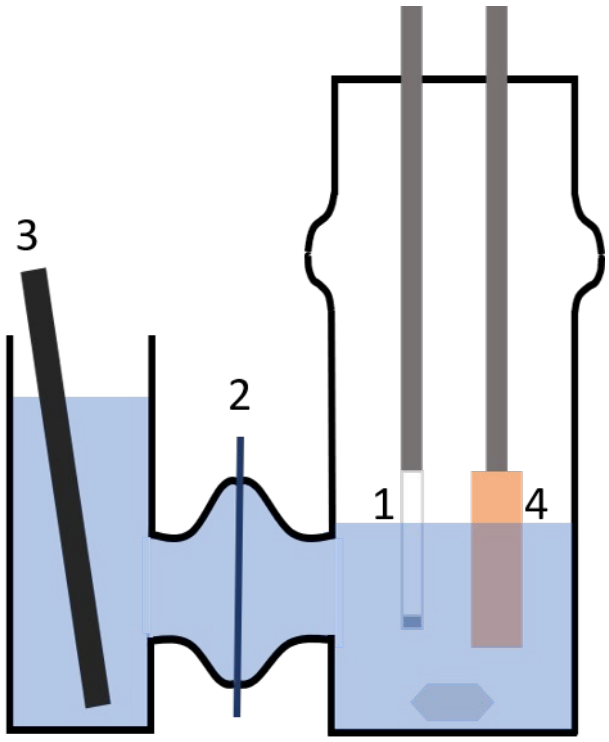

Figure 0-2 Design of glass electrochemical cell filled with electrolyte and stir bar. (1) single-junction Ag/AgCl/KCl(sat.) or double-junction Ag/AgCl/KCl(sat.)/$NaHCO_3$(0.1 M) reference electrode, (2) Nafion membrane, (3) carbon rod as auxiliary electrode, and (4) metal foil working electrode. Stainless steel rods and alligator clips were used for electrical contact for reference electrode and metal foil. Metal foil working electrode was submerged such that ~0.6 cm^2 was exposed to solution during each electrolysis.

A.2 Additional Results and Data

Table 0-1 Product Faradaic efficiencies of Cu CO_2RR under standard conditions, using double-junction Ag/AgCl/KCl(sat.)

Interval range	Avg. potential / V vs Ag/AgCl/KCl(sat.)	H_2	**CO**	CH_4	C_2H_4	HCOOH	Total
–1.51 to –1.53	–1.518	65.1 ± 11.8	**0.4 ± 0.3**	17.4 ± 11.0	0.6 ± 0.6	4.9 ± 0.7	88.3 ± 2.0
–1.53 to –1.55	–1.542	69.0 [a]	**0.2** [a]	16.1 [a]	1.2 [a]	2.5 [a]	88.9 [a]
–1.55 to –1.57	–1.561	67.6 ± 7.5	**0.2 ± 0.1**	20.3 ± 6.0	0.6 ± 0.3	2.8 ± 0.9	91.5 ± 3.9
–1.57 to –1.59	–1.580	64.7 ± 10.8	**0.3 ± 0.2**	20.4 ± 10.6	0.6 ± 0.5	4.0 ± 1.1	89.9 ± 1.7
–1.59 to –1.61	–1.603	59.9 ± 10.5	**0.2 ± 0.1**	25.7 ± 11.4	0.8 ± 0.4	3.4 ± 1.1	90.1 ± 4.3
–1.61 to –1.63	–1.625	68.6 [a]	**0.2** [a]	16.2 [a]	0.4 [a]	1.6 [a]	87.0 [a]
–1.55 to –1.61	–1.581	64.2 ± 10.0	0.25 ± 0.15	21.7 ± 9.6	0.66 ± 0.42	3.5 ± 1.1	90.4 ± 2.9

[a] These values are averages of less than 3 values in the interval range, and so are reported without standard deviation.

Chapter 2 Data

Table 0-2 Product Faradaic Efficiencies of Cu CO_2RR, Single-Junction Ag/AgCl/KCl(sat.)

Interval range	Avg. potential / V vs Ag/AgCl /KCl(sat.)	H_2	**CO**	CH_4	C_2H_4	HCOOH	Total
–1.51 to –1.53	–1.524	85.8 ± 6.6	**1.0 ± 0.007**	3.4 ± 2.5	0 ± 0	0 ± 0	90.2 ± 4.7
–1.55 to –1.57	–1.560	86.4 [a]	**0.4** [a]	4.5 [a]	0 [a]	0 [a]	91.3 [a]
–1.57 to –1.59	–1.580	74.7 ± 11.4	**0.9 ± 0.12**	12.9 ± 10.3	0 ± 0	1.9 ± 2.4	90.5 ± 2.7
–1.59 to –1.61	–1.600	72.6 ± 9.4	**0.7 ± 0.4**	15.1 ± 7.4	0.2 ± 0.4	2.4 ± 1.4	91.0 ± 3.6
–1.61 to –1.63	–1.620	67.3 ± 7.2	**1.1 ± 1.5**	20.7 ± 8.8	0.3 ± 0.5	2.2 ± 1.6	91.6 ± 3.1
–1.63 to –1.65	–1.637	68.9 ± 12.9	**2.5 ± 2.9**	18.1 ± 13.4	0.2 ± 0.4	0.8 ± 0.9	90.5 ± 1.2

[a] These values are averages of less than 3 values in the interval range, and so are reported without standard deviation.

Table 0-3 Amount of Ag^+ leached from Ag/AgCl/KCl(sat.) under no polarization in water for 24 h. Limit of quantification is 0.5 ppb.

Configuration of Ag/AgCl	***Ag^+ concentration (ppb)***
Single-junction (homemade)	52.6 ± 24.0

Double-junction (homemade)	0.61 ± 0.02
Single-junction (commercial)	34.8 ± 2.5
Background (no reference)	0.52 ± 0.10

Table 0-4 Baseline amount of possible Ag^+ contamination in acidic solutions used in the studies. Limit of quantification is 0.5 ppb.

Solutions	***Ag^+ concentration (ppb)***
1 M trace metal grade HNO_3	0.483 ± 0.103
0.1 M trace metal grade H_2SO_4	0.475 ± 0.098

Table 0-5 Baseline amount of possible Ag^+ contamination in electrochemical cell components. Solid samples were etched by 10 mL of 1 M trace metal grade HNO_3. Limit of quantification is 5 ng in 10 mL sample.

Component	***Ag^+ etched from sample (ng)***
Ni foil	7.0 ± 0.2
Nafion	6.2 ± 0.1
Electrochemical cell	6.1
Tygon tubing (for sparging gas)	6.3
Carbon rod (auxiliary electrode)	9.2 ± 7.7
99.999 Cu foil	5.3 ±1.0

Table 0-6 Ag^+ concentration in electrolyte (0.1 M H_2SO_4) in working chamber under polarization after Ni HER. Limit of quantification is 0.5 ppb.

Condition	***Ag^+ concentration (ppb)***
Prior to HER	0.475 ± 0.098
After HER, single-junction Ag/AgCl/KCl(sat.)	6.75 ± 0.13
After HER, double-junction Ag/AgCl/KCl(sat.)	0.588 ± 0.002

Table 0-7 Ag^+ deposited on Ni foil under polarization after Ni HER. Limit of quantification is 5 ng in 10 mL sample.

Condition	***Ag^+ etched from sample (ng)***
Prior to HER	7.0 ± 0.2
After HER, single-junction Ag/AgCl/KCl(sat.)	7.9 ± 1.5
After HER, double-junction Ag/AgCl/KCl(sat.)	6.2 ± 0.0

Table 0-8 Amount of Ag^+ deposited on 99.999% Cu foil during CO_2RR. Limit of quantification is 5 ng in 10 mL sample.

Cu foil Condition	***Ag^+ etched from sample (ng)***
Prior to CO_2RR	5.3 ±1.0
After CO_2RR, single-junction Ag/AgCl/KCl(sat.)	13.0 ± 4.8
After CO_2RR, double-junction Ag/AgCl/KCl(sat.)	6.0 ± 0.4

Table 0-9 Product Faradaic efficiencies of long-term Cu CO2RR, potential between –1.600 and –1.630 V vs Ag/AgCl/KCl(sat.).

Single-junction					
H_2	CO	CH_4	C_2H_4	HCOOH	Total
72.7 ± 6.6	**12.5 ± 4.0**	**2.4 ± 1.2**	0.15 ± 0.13	5.8 ± 1.1	87.8 ± 1.5
Double-junction					
H_2	CO	CH_4	C_2H_4	HCOOH	Total
80.6 ± 4.0	**0.15 ± 0.18**	**11.1 ± 2.34**	0.30 ± 0.08	6.6 ± 1.3	92.1 ± 2.4

Table 0-10 Amount of Ag^+ deposited on 99.999% Cu foil during long-term (12 h) CO_2RR. Limit of quantification is 5 ng in 10 mL sample.

Cu foil Condition	***Ag^+ etched from sample (ng)***
Prior to CO_2RR	5.3 ±1.0
After long-term CO_2RR, single-junction Ag/AgCl/KCl(sat.)	27.3 ± 1.8
After long-term CO_2RR, double-junction Ag/AgCl/KCl(sat.)	4.8 ± 0.7

Table 0-11 Product Faradaic efficiencies of Cu CO2RR using double frit with Ag titration, potential between –1.570 and –1.610 V vs Ag/AgCl.

ppb Ag	**H_2**	**CO**	**CH_4**	**C_2H_4**	**HCOOH**	**Total**
0	63.1 ± 10.5	**0.25 ± 0.17**	**22.2 ± 10.7**	0.67 ± 0.46	3.79 ± 1.11	90.0 ± 3.0
1	70.1 ± 9.7	**0.21 ± 0.01**	**17.5 ± 12.8**	0.56 ± 0.31	3.86 ± 0.54	92.2 ± 3.0
5	76.0 ± 1.0	**0.62 ± 0.45**	**10.8 ± 1.4**	0.22 ± 0.29	4.40 ± 2.26	92.0 ± 1.0
10	64.5 ± 8.1	**2.46 ± 1.93**	**19.6 ± 6.5**	0.57 ± 0.38	4.44 ± 0.96	9.15 ± 1.2
50	75.3 ± 7.0	**10.8 ± 5.7**	**2.63 ± 0.99**	0.00 ± 0.00	1.57 ± 0.71	90.3 ± 0.9
100	73.4 ± 2.5	**16.8 ± 3.2**	**1.04 ± 0.54**	0.00 ± 0.00	1.53 ± 0.29	9.28 ± 1.0
1000	58.8 ± 3.1	**19.8 ± 6.2**	**9.25 ± 4.52**	1.57 ± 0.46	2.19 ± 0.35	91.6 ± 0.9

Table 0-12 Ag^+ deposited on Cu foil after CO_2RR under Ag^+ titration with externally added Ag^+. Limit of quantification is 5 ng in 10 mL sample.

Externally added Ag^+ concentration (ppb)	***Ag^+ etched from sample (ng)***
1	6.1 ± 0.3
5	10.5 ± 0.1
10	37 ± 25
50	141 ± 37
100	235 ± 73
1000	16605 ± 14322

Chapter 3 Data

Table 0-13 Baseline amount of possible metal contamination in ppb in acidic solutions used in the studies. Limit of quantification is 0.5 ppb.

Sample	Ag	Al	Co	Cu	Fe	Mg	Ni	Pb	Pt	Ru	Sn	Zn
1 M TM HNO_3	0.483 ± 0.103	13.672 ± 7.835	0.367 ± 0.204	-1.504 ± 3.080	6.067 ± 5.042	0.929 ± 1.023	-0.220 ± 0.438	0.207 ± 0.191	0.481 ± 0.391	0.992 ± 0.107	0.673 ± 1.092	4.640 ± 3.294
0.1 M TM H_2SO_4	0.475 ± 0.098	9.397 ± 2.127	0.329 ± 0.213	0.966 ± 1.131	5.191 ± 4.537	0.459 ± 0.786	0.078 ± 0.311	0.163 ± 0.165	0.479 ± 0.393	0.993 ± 0.110	0.448 ± 0.813	1.494 ± 1.094

Table 0-14 Baseline amount of possible metal contamination in ng in electrochemical cell components. Solid samples were etched by 10 mL of 1 M trace metal grade HNO_3. Limit of quantification is 5 ng in 10 mL sample (50 ng for Fe).

Sample	Ag	Al	Co	Cu	Fe	Mg	Ni	Pb	Pt	Ru	Sn	Zn
Mechanically polished Ni	7.0 ± 0.2	41.4 ± 14.0	4.8 ± 2.7	17.4 ± 13.5	50.2 ± 46.1	5.5 ± 1.0	Saturated	1.2 ± 0.4	1.4 ± 0.0	34.2 ± 20.5	0.3 ± 0.2	360.2 ± 90.1
Electrochemical cell	6.1	132.9	6.0	-48.9	10.5	15.5	6.9	4.2	0.2	9.0	54.9	184.5
Tygon tubing (for sparging gas)	6.3	512.0	6.2	-25.9	40.7	16.0	4.8	5.8	0.2	9.0	17.8	56.3
1 M TM HNO3	5.0 ± 1.1	142.5 ± 81.6	3.8 ± 2.1	-15.7 ± 32.1	63.2 ± 52.5	9.7 ± 10.7	-2.3 ± 4.6	2.2 ± 2.0	5.0 ± 4.1	10.3 ± 1.1	7.0 ± 11.4	48.3 ± 34.3

Table 0-15 Metal etched in ng from membranes and auxiliary electrodes. Solid samples were etched by 10 mL of 1 M trace metal grade HNO_3. Limit of quantification is 5 ng in 10 mL sample (50 ng for Fe).

Sample	**Ag**	**Al**	**Co**	**Cu**	**Fe**	**Mg**	**Ni**	**Pb**	**Pt**	**Ru**	**Sn**	**Zn**
Nafion	6.2 ± 0.1	538.3 ± 273.0	7.1 ± 0.3	-27.2 ± 10.8	115.3 ± 31.1	42.3 ± 4.9	30.5 ± 9.4	4.8 ± 0.7	0.3 ± 0.0	9.0 ± 0.0	32.0 ± 6.2	69.1 ± 100.1
Nafion, after cleaning with TM HNO_3	6.2 ± 0.1	463.3 ± 199.0	6.1 ± 1.3	-2.7 ± 3.8	90.7 ± 40.1	22.5 ± 6.9	24.5 ± 10.7	5.0 ± 0.2	0.4 ± 0.0	7.6 ± 0.1	28.0 ± 2.6	55.2 ± 10.9
Selemion AMV	6.7 ± 0.2	649.0 ± 92.8	6.3 ± 0.1	-40.1 ± 9.3	38.6 ± 2.9	18.3 ± 2.4	4.6 ± 1.9	4.4 ± 0.1	0.3 ± 0.0	9.0 ±0.0	1403.8 ± 516.1	9.1 ± 1.3
SelemionAMV, after cleaning with TM HNO_3	5.1 ± 0.4	109.6 ± 10.2	2.4 ± 0.3	4.6 ± 2.2	76.2 ± 3.4	43.0 ± 32.6	11.0 ± 3.5	10.5 ± 8.6	7.7 ± 0.0	11.0 ± 0.0	308.8 ± 230.6	49.4 ± 26.1
Carbon rod	9.2 ± 7.7	66.4 ± 34.7	2.4 ± 0.1	323.3 ± 175.4	120.1 ± 25.6	47.0 ± 30.9	69.2 ± 41.2	3.5 ± 0.0	7.4 ± 0.0	11.0 ± 0.0	0.1 ± 0.0	20.5 ± 7.1
Pt gauze	5.2 ± 0.9	32.1 ± 6.9	3.6 ± 2.1	3.9 ± 2.0	46.1 ± 29.8	15.2 ± 12.5	-1.7 ± 7.9	3.2 ± 1.4	5.7 ± 4.0	10.3 ± 1.1	10.2 ± 17.5	72.4 ± 52.1
1 M TM HNO_3	5.0 ± 1.1	142.5 ± 81.6	3.8 ± 2.1	-15.7 ± 32.1	63.2 ± 52.5	9.7 ± 10.7	-2.3 ± 4.6	2.2 ± 2.0	5.0 ± 4.1	10.3 ± 1.1	7.0 ± 11.4	48.3 ± 34.3

Table 0-16 Product Faradaic efficiencies of Cu CO_2RR under standard conditions + different membrane/auxiliary electrode, using double-junction Ag/AgCl/KCl(sat.), potential range –1.55 V to – 1.61 V vs Ag/AgCl.

Membrane/auxiliary electrode	H_2	**CO**	CH_4	C_2H_4	HCOOH	Total
Nafion/carbon rod	64.2 ± 10.0	0.25 ± 0.15	21.7 ± 9.6	0.66 ± 0.42	3.5 ± 1.1	90.4 ± 2.9
Nafion/Pt	45.6 ± 17.5	0.91 ± 0.34	31.4 ± 11.8	1.24 ± 0.80	4.1 ± 2.0	83.3 ± 6.2
Selemion AMV/carbon rod	65.8 ± 25.9	0.48 ± 0.52	17.8 ± 7.6	1.21 ± 0.75	2.9 ± 2.9	88.2 ± 0.4
Selemion AMV/Pt	53.6 ± 20.4	0.31 ± 0.31	28.9 ± 18.1	1.10 ± 1.18	1.3 ± 1.4	85.2 ± 5.2

[a] These values are averages of less than 3 values in the interval range, and so are reported without standard deviation.

Table 0-17 Metal present in working and auxiliary chambers after Ni HER using different membrane/auxiliary electrodes. Limit of quantification is 0.5 ppb.

Sample	Ag	Al	Co	Cu	Fe	Mg	Ni	Pb	Pt	Ru	Sn	Zn
Nafion/carbon rod, working chamber	0.588 ± 0.002	10.813 ± 2.077	0.604 ± 0.007	0.512 ± 0.148	30.282 ± 7.081	1.506 ± 0.047	2872.036 ± 760.456	0.436 ± 0.022	0.024 ± 0.000	0.898 ± 0.006	2.304 ± 0.581	23.202 ± 0.497
Nafion/carbon rod, auxiliary chamber	0.664 ± 0.070	12.945 ± 3.977	0.585 ± 0.003	30.768 ± 6.019	10.247 ± 1.616	4.479 ± 2.051	8.382 ± 1.228	0.595 ± 0.001	0.025 ± 0.002	0.870 ± 0.001	3.563 ± 0.206	25.570 ± 0.211
Nafion/Pt, working chamber	0.598 ± 0.009	11.255 ± 1.436	0.789 ± 0.333	1.715 ± 1.556	38.144 ± 18.267	2.875 ± 2.225	3553.143 ± 1647.513	0.521 ± 0.064	0.137 ± 0.162	0.901 ± 0.020	4.108 ± 2.174	22.459 ± 7.045
Nafion/Pt, auxiliary chamber	0.870 ± 0.135	9.920 ± 0.701	0.601 ± 0.028	1.198 ± 0.169	2.714 ± 0.569	2.037 ± 0.034	33.009 ± 20.400	0.542 ± 0.076	17.719 ± 18.689	0.716 ± 0.205	4.797 ± 1.300	14.594 ± 11.159
Selemion AMV/carbon rod, working chamber	0.593 ± 0.008	12.376 ± 0.900	0.633 ± 0.075	0.357 ± 0.776	21.277 ± 15.447	1.713 ± 0.367	1890.493 ± 1507.500	0.481 ± 0.093	0.027 ± 0.001	0.884 ± 0.015	43.865 ± 13.843	31.901 ± 6.758
Selemion AMV/carbon rod, auxiliary chamber	1.477 ± 1.127	17.792 ± 1.516	0.635 ± 0.067	44.704 ± 40.546	41.077 ± 29.410	6.589 ± 2.436	5.850 ± 1.001	0.855 ± 0.290	0.034 ± 0.009	0.866 ± 0.000	77.147 ± 13.795	43.446 ± 7.179
Selemion AMV/Pt, working chamber	0.588 ± 0.001	12.603 ± 3.374	0.619 ± 0.051	1.842 ± 0.854	22.771 ± 10.345	1.490 ± 0.376	2050.012 ± 970.995	0.435 ± 0.039	0.026 ± 0.000	0.884 ± 0.010	30.310 ± 13.244	27.240 ± 2.058
Selemion AMV/Pt, auxiliary chamber	1.026 ± 0.318	15.205 ± 1.375	0.863 ± 0.382	1.474 ± 0.660	172.062 ± 129.323	10.713 ± 12.127	90.692 ± 145.818	1.455 ± 0.208	31.309 ± 20.887	0.853 ± 0.021	86.557 ± 1.565	38.046 ± 3.024
0.1 M TM H_2SO_4	0.475 ± 0.098	9.397 ± 2.127	0.329 ± 0.213	0.966 ± 1.131	5.191 ± 4.537	0.459 ± 0.786	0.078 ± 0.311	0.163 ± 0.165	0.479 ± 0.393	0.993 ± 0.110	0.448 ± 0.813	1.494 ± 1.094

Table 0-18 Metal etched in ng from Ni after HER using different membrane/auxiliary electrodes. Solid samples were etched by 10 mL of 1 M trace metal grade HNO_3. Limit of quantification is 5 ng in 10 mL sample (50 ng for Fe).

Sample	**Ag**	**Al**	**Co**	**Cu**	**Fe**	**Mg**	**Ni**	**Pb**	**Pt**	**Ru**	**Sn**	**Zn**
Nafion/carbon rod	6.2 ± 0.0	209.2 ± 289.7	21.7 ± 12.0	5.2 ± 8.3	34.5 ± 23.6	10.7 ± 0.7	Saturated	4.3 ± 0.0	0.2 ± 0.0	50.0 ± 31.2	18.8 ± 0.4	10.3 ± 1.2
Nafion/Pt	6.2 ± 0.1	69.5 ± 98.7	18.8 ± 12.3	2.9 ± 3.0	26.4 ± 24.5	9.1 ± 2.4	Saturated	5.0 ± 1.3	0.3 ± 0.2	42.4 ± 32.4	86.7 ± 71.1	85.8 ± 139.4
Selemion AMV/carbon rod	6.2 ± 0.1	59.5 ± 76.0	15.4 ± 9.0	5.5 ± 6.2	21.2 ± 19.7	10.6 ± 3.5	Saturated	3.8 ± 0.2	0.3 ± 0.0	34.2 ± 24.3	198.1 ± 166.4	155.6 ± 256.5
Selemion AMV/Pt	6.2 ± 0.1	41.0 ± 33.3	13.9 ± 6.7	3.9 ± 1.7	17.2 ± 14.6	11.1 ± 6.1	Saturated	4.1 ± 0.3	0.2 ± 0.0	29.6 ± 18.3	315.6 ± 218.3	124.1 ± 203.2
Mechanically polished Ni	7.7 ± 1.1	41.4 ± 14.0	4.8 ± 2.7	17.4 ± 13.5	50.2 ± 46.1	5.5 ± 1.0	1303979.2 ± 253294.4	1.2 ± 0.4	1.4 ± 0.0	34.2 ± 20.5	0.3 ± 0.2	360.2 ± 90.1
1 M TM HNO_3	5.0 ± 1.1	142.5 ± 81.6	3.8 ± 2.1	-15.7 ± 32.1	63.2 ± 52.5	9.7 ± 10.7	-2.3 ± 4.6	2.2 ± 2.0	5.0 ± 4.1	10.3 ± 1.1	7.0 ± 11.4	48.3 ± 34.3

Table 0-19 Product Faradaic efficiencies of Cu CO_2RR under standard conditions + 99.95% Cu, using double-junction Ag/AgCl/KCl(sat.)

Interval range	Avg. potential / V vs Ag/AgCl/KCl (sat.)	H_2	**CO**	CH_4	C_2H_4	HCOOH	Total
–1.45 to –1.47	–1.458	66.7 [a]	0.25 [a]	20.4 [a]	0.54 [a]	1.02 [a]	88.9 [a]
–1.53 to –1.55	–1.538	57.8 [a]	0.19 [a]	30.0 [a]	0.85 [a]	3.36 [a]	92.2 [a]
–1.55 to –1.57	–1.562	66.2 [a]	0.27 [a]	19.3 [a]	0.54 [a]	5.08 [a]	91.4 [a]
–1.57 to –1.59	–1.579	60.6 ± 5.4	0.26 ± 0.02	24.8 ± 8.7	1.25 ± 0.60	3.90 ± 1.25	90.8 ± 4.6
–1.59 to –1.61	–1.599	75.9 [a]	0.18 [a]	9.5 [a]	0.26 [a]	5.00 [a]	90.9 [a]
–1.55 to –1.61	–1.57985	66.6 ± 10.0	0.24 ± 0.07	18.9 ± 10.4	0.76 ± 0.61	4.55 ± 2.22	91.0 ± 2.9

[a] These values are averages of less than 3 values in the interval range, and so are reported without standard deviation.

Table 0-20 Product Faradaic efficiencies of Cu CO_2RR under standard conditions + 99.8% Cu, using double-junction Ag/AgCl/KCl(sat.)

Interval range	Avg. potential / V vs Ag/AgCl/KCl(sat.)	H_2	**CO**	CH_4	C_2H_4	HCOOH	Total
–1.43 to –1.45	–1.435	76.2 [a]	0.13 [a]	13.7 [a]	0.39 [a]	2.79 [a]	93.2 [a]
–1.47 to –1.49	–1.483	67.9 [a]	0.27 [a]	25.1 [a]	0.77 [a]	2.76 [a]	96.8 [a]
–1.51 to –1.53	–1.513	86.0 [a]	0.23 [a]	3.6 [a]	0.00 [a]	2.28 [a]	92.1 [a]
–1.55 to –1.57	–1.560	69.3 ± 12.9	0.29 ± 0.11	17.0 ± 11.9	0.41 ± 0.47	4.15 ± 1.12	91.2 ± 0.8
–1.57 to –1.59	–1.582	75.2 ± 10.0	0.32 ± 0.16	11.0 ± 11.9	0.17 ± 0.27	4.57 ± 0.67	91.3 ± 2.7
–1.59 to –1.61	–1.600	70.2 [a]	0.63 [a]	13.6 [a]	0.49 [a]	5.45 [a]	90.4 [a]
–1.55 to –1.61	–1.575	73.0 ± 10.7	0.33 ± 0.15	13.3 ± 10.8	0.28 ± 0.36	4.40 ± 0.90	91.2 ± 1.8

[a] These values are averages of less than 3 values in the interval range, and so are reported without standard deviation.

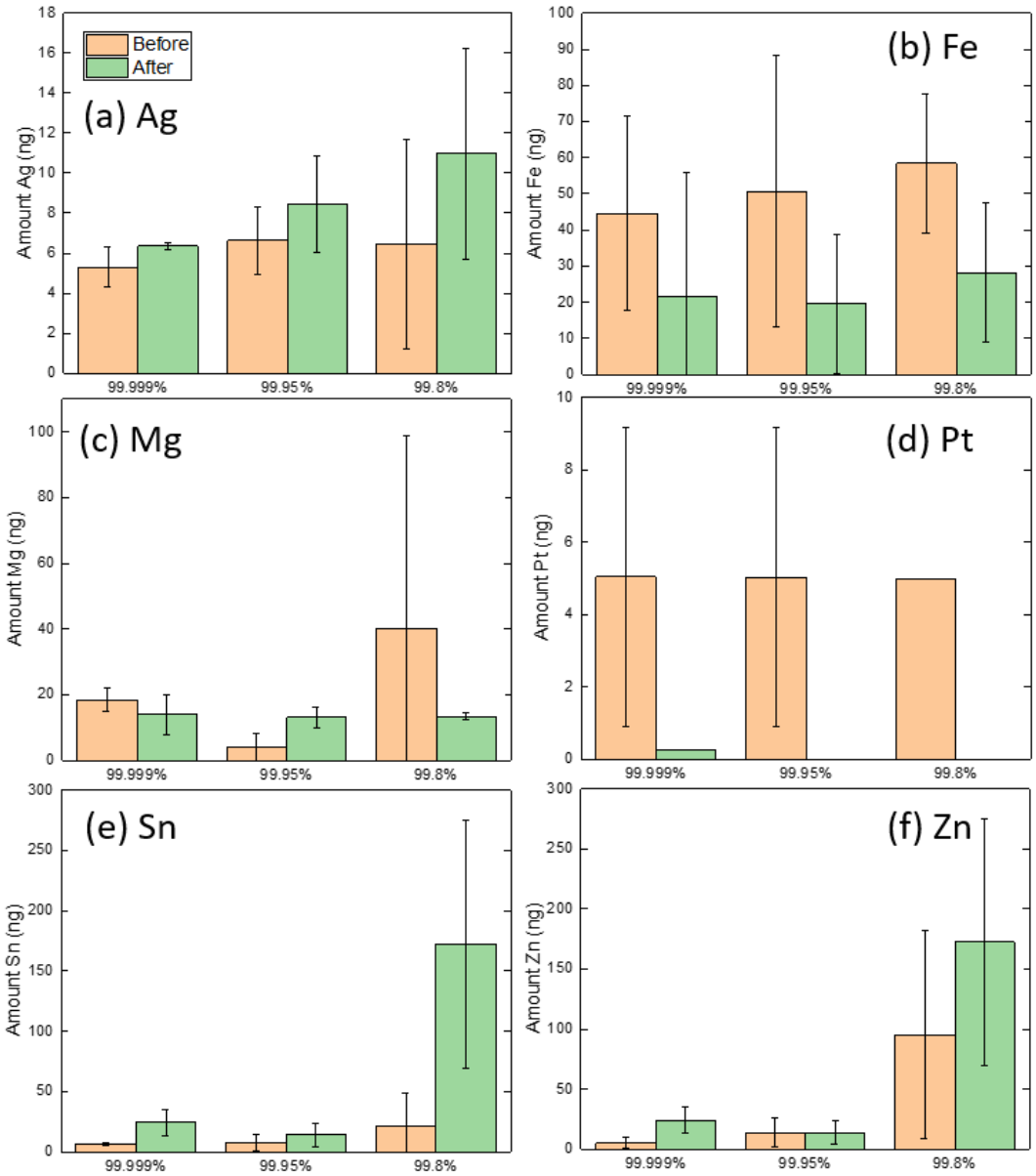

Figure 0-3 (a) Ag (b) Fe (c) Mg (d) Pt (e) Sn and (f) Zn etched from different purities of Cu foils before and after CO_2RR under standard conditions. Error bars are standard deviations from at least 3 independent measurements. Limit of quantification is 5 ng.

Table 0-21 Metal etched in ng from different purity Cu foil before and CO_2RR under standard condition. Solid samples were etched by 10 mL of 1 M trace metal grade HNO_3. Limit of quantification is 5 ng in 10 mL sample (50 ng for Fe).

Sample	**Ag**	**Al**	**Co**	**Cu**	**Fe**	**Mg**	**Ni**	**Pb**	**Pt**	**Ru**	**Sn**	**Zn**
99.999% Before	5.3 ± 1.0	177.4 ± 291.4	3.8 ± 2.6	saturated	44.6 ± 26.8	18.5 ± 3.5	51.3 ± 33.6	1.9 ± 2.0	5.0 ± 4.1	-4.9 ± 11.6	6.4 ± 1.4	5.1 ± 4.4
99.999% After	6.4 ± 0.2	337.6 ± 140.6	6.2 ± 0.1	saturated	21.7 ± 34.2	13.9 ± 6.0	8.4 ± 4.4	6.0 ± 0.8	0.2 ± 0.0	7.7 ± 0.9	24.2 ± 10.7	2.4 ± 8.0
99.95% Before	6.6 ± 1.7	66.4 ± 102.5	3.7 ± 2.1	saturated	50.7 ± 37.7	4.1 ± 4.1	12.6 ± 3.2	6.4 ± 3.3	5.0 ± 4.1	3.0 ± 6.5	7.2 ± 6.9	14.0 ± 12.5
99.95% After	8.5 ± 2.4	399.9 ± 349.3	6.0 ±0.2	saturated	19.6 ± 19.3	13.1 ± 3.1	44.6 ± 30.5	16.1 ± 10.3	-0.4 ± 0.0	-3.8 ± 10.3	13.8 ± 9.4	23.6 ± 13.0
99.8% Before	6.5 ± 0.4	7.3 ± 0.4	4.2 ± 1.7	saturated	58.4 ± 28.7	40.2 ± 58.6	249.8 ± 391.3	10.3 ± 2.7	5.0 ± 4.1	0.1 ±6.7	21.4 ± 27.3	95.3 ± 86.4
99.8% After	11.0 ± 5.3	433.4 ± 156.0	6.4 ± 0.5	saturated	28.1 ± 19.3	13.4 ± 1.1	504.0 ± 264.4	18.3 ± 11.5	-0.4 ± 0.0	-2.3 ± 10.1	172.5 ± 102.9	132.6 ± 82.4
1 M TM HNO_3	5.0 ± 1.1	142.5 ± 81.6	3.8 ± 2.1	-15.7 ± 32.1	63.2 ± 52.5	9.7 ± 10.7	-2.3 ± 4.6	2.2 ± 2.0	5.0 ± 4.1	10.3 ± 1.1	7.0 ± 11.4	48.3 ± 34.3

Table 0-22 Product Faradaic efficiencies of Cu CO_2RR under standard conditions + resin-treated trace metal grade Na_2CO3, using double-junction Ag/AgCl/KCl(sat.)

Interval range	Avg. potential / V vs Ag/AgCl/KCl(sat.)	H_2	**CO**	CH_4	C_2H_4	HCOOH	Total
–1.47 to –1.49	–1.483	66.5 ± 11.1	0.25 ± 0.13	18.8 ± 9.8	0.58 ± 0.37	4.35 ± 1.65	90.5 ± 0.9
–1.55 to –1.57	–1.553	78.8 [a]	0.16 [a]	6.7 [a]	0.20 [a]	1.77 [a]	87.6 [a]
–1.57 to 1.59	–1.581	66.0 [a]	0.27 [a]	17.9 [a]	0.47 [a]	3.69 [a]	88.4 [a]
–1.55 to –1.61	–1.562	74.5 ± 8.0	0.19 ± 0.07	10.4 ± 7.4	0.29 ± 0.26	2.41 ± 1.46	87.8 ± 1.5

[a] These values are averages of less than 3 values in the interval range, and so are reported without standard deviation.

Table 0-23 Product Faradaic efficiencies of Cu CO_2RR under standard conditions + untreated trace metal grade Na_2CO3, using double-junction Ag/AgCl/KCl(sat.)

Interval range	Avg. potential / V vs Ag/AgCl/KCl(sat.)	H_2	**CO**	CH_4	C_2H_4	HCOOH	Total
–1.55 to –1.57	–1.566 [a]	57.8 [a]	0.36 [a]	24.2 [a]	2.85 [a]	4.06 [a]	89.3 [a]
–1.57 to 1.59	–1.577 [a]	44.8 [a]	0.30 [a]	38.9 [a]	1.56 [a]	4.49 [a]	90.0 [a]
–1.59 to –1.61	–1.616 [a]	40.1 [a]	1.12 [a]	35.7 [a]	3.06 [a]	11.0 [a]	91.0 [a]
–1.55 to –1.61	–1.586	47.6 ± 9.2	0.60 ± 0.46	32.9 ± 7.7	2.49 ± 0.81	6.51 ± 3.9	90.1 ± 0.8

[a] These values are averages of less than 3 values in the interval range, and so are reported without standard deviation.

Table 0-24 Product Faradaic efficiencies of Cu CO_2RR under standard conditions + resin-treated BioXtra grade $NaHCO_3$, using double-junction Ag/AgCl/KCl(sat.)

Interval range	Avg. potential / V vs Ag/AgCl/KCl(sat.)	H_2	**CO**	CH_4	C_2H_4	HCOOH	Total
–1.49 to –1.51	–1.504	72.7 [a]	0.27 [a]	11.2 [a]	1.36 [a]	1.11 [a]	86.7 [a]
–1.51 to –1.53	–1.528	82.6 [a]	0.10 [a]	2.9 [a]	0.00 [a]	2.24 [a]	87.9 [a]
–1.53 to –1.55	–1.542	71.1 ± 7.3	0.33 ± 0.16	13.4 ± 4.7	1.68 ± 0.74	1.88 ± 0.82	88.4 ± 1.8
–1.55 to –1.57	–1.561	82.3 [a]	0.46 [a]	5.2 [a]	0.36 [a]	2.52 [a]	90.8 [a]
–1.59 to –1.61	–1.594	75.3 [a]	0.62 [a]	12.0 [a]	1.19 [a]	2.74 [a]	91.8 [a]
–1.55 to –1.61	–1.578	78.8 ± 7.2	0.54 ± 0.18	8.6 ± 6.2	0.77 ± 0.77	2.63 ± 1.00	91.3 ± 0.7

[a] These values are averages of less than 3 values in the interval range, and so are reported without standard deviation.

Table 0-25 Product Faradaic efficiencies of Cu CO_2RR under standard conditions + untreated BioXtra grade $NaHCO_3$, using double-junction Ag/AgCl/KCl(sat.)

Interval range	Avg. potential / V vs Ag/AgCl/KCl(sat.)	H_2	**CO**	CH_4	C_2H_4	HCOOH	Total
–1.45 to –1.47	–1.470	69.9 [a]	0.66 [a]	15.4 [a]	2.47 [a]	1.42 [a]	89.9 [a]
–1.53 to –1.55	–1.537	71.3 [a]	0.57 [a]	11.6 [a]	3.88 [a]	3.04 [a]	90.5 [a]
–1.55 to –1.57	–1.556	72.9 [a]	0.50 [a]	12.0 [a]	1.52 [a]	2.65 [a]	89.5 [a]
–1.59 to –1.61	–1.607	72.7 [a]	1.17 [a]	9.1 [a]	1.26 [a]	3.82 [a]	88.0 [a]
–1.55 to –1.61	–1.569	72.7 ± 1.0	0.51 ± 0.09	11.6 ± 2.5	1.55 ± 0.31	2.95 ± 0.75	89.3 ± 1.2

[a] These values are averages of less than 3 values in the interval range, and so are reported without standard deviation.

Table 0-26 Product Faradaic efficiencies of Cu CO_2RR under standard conditions + pre-electrolysis HPLC grade $NaHCO_3$, using double-junction Ag/AgCl/KCl(sat.)

Interval range	Avg. potential / V vs Ag/AgCl/KCl(sat.)	H_2	**CO**	CH_4	C_2H_4	HCOOH	Total
–1.57 to –1.59	–1.588	53.7 [a]	0.51 [a]	27.1 [a]	0.89 [a]	6.97 [a]	89.1 [a]
–1.59 to –1.61	–1.602	55.2 [a]	0.58 [a]	25.6 [a]	0.75 [a]	7.38 [a]	89.6 [a]
–1.55 to –1.61	–1.604	54.7 ± 1.6	0.56 ± 0.11	26.1 ± 3.2	0.80 ± 0.08	7.24 ± 0.56	89.4 ± 1.3

[a] These values are averages of less than 3 values in the interval range, and so are reported without standard deviation.

Table 0-27 Product Faradaic efficiencies of Cu CO_2RR under standard conditions + untreated HPLC grade $NaHCO_3$, using double-junction Ag/AgCl/KCl(sat.)

Interval range	Avg. potential / V vs Ag/AgCl/KCl(sat.)	H_2	**CO**	CH_4	C_2H_4	HCOOH	Total
–1.57 to –1.59	–1.582	51.2 ± 3.6	0.90 ± 0.21	26.9 ± 4.8	2.22 ± 0.70	8.81 ± 1.38	90.0 ± 2.2
–1.59 to –1.61	–1.604	56.1 [a]	0.88 [a]	28.4 [a]	1.02 [a]	4.17 [a]	90.6 [a]
–1.61 to –1.63	–1.620	43.0 [a]	2.00 [a]	33.6 [a]	5.52 [a]	6.14 [a]	90.3 [a]
–1.55 to –1.61	–1.591	53.1 ± 1.4	0.89 ± 3.74	27.5 ± 0.4	1.74 ± 4.13	6.95 ± 0.97	90.2 ± 2.9

[a] These values are averages of less than 3 values in the interval range, and so are reported without standard deviation.

Table 0-28 Product Faradaic efficiencies of Cu CO_2RR under standard conditions + resin-treated ACS grade $NaHCO_3$, using double-junction Ag/AgCl/KCl(sat.)

Interval range	Avg. potential / V vs Ag/AgCl/KCl(sat.)	H_2	**CO**	CH_4	C_2H_4	HCOOH	Total
–1.45 to –1.47	–1.457	70.8 [a]	0.21 [a]	13.8 [a]	2.3 [a]	2.21 [a]	89.3 [a]
–1.51 to –1.53	–1.516	78.8 ± 0.7	0.29 ± 0.11	9.4 ± 2.0	0.9 ± 0.4	2.45 ± 0.10	91.8 ± 1.7
–1.53 to –1.55	–1.549	69.8 [a]	0.21 [a]	15.0 [a]	1.9 [a]	2.09 [a]	89.0 [a]
–1.57 to –1.59	–1.582	74.5 [a]	0.35 [a]	12.8 [a]	1.5 [a]	3.01 [a]	92.2 [a]
–1.59 to –1.61	–1.598	59.6 [a]	0.27 [a]	21.4 [a]	1.3 [a]	1.12 [a]	83.8 [a]
–1.55 to –1.61	–1.578	69.6 ± 7.3	0.29 ± 0.07	15.5 ± 4.7	1.5 ± 0.3	2.31 ± 0.91	89.3 ± 4.0

[a] These values are averages of less than 3 values in the interval range, and so are reported without standard deviation.

Table 0-29 Product Faradaic efficiencies of Cu CO_2RR under standard conditions + untreated ACS grade $NaHCO_3$, using double-junction Ag/AgCl/KCl(sat.)

Interval range	Avg. potential / V vs Ag/AgCl/KCl(sat.)	H_2	**CO**	CH_4	C_2H_4	HCOOH	Total
–1.57 to –1.59	–1.558	75.1 [a]	0.38 [a]	10.5 [a]	1.10 [a]	2.05 [a]	89.2 [a]
–1.59 to –1.61	–1.602	68.9 [a]	1.45 [a]	11.3 [a]	3.81 [a]	4.14 [a]	89.6 [a]
–1.55 to –1.61	–1.560	73.1 ± 7.2	0.74 ± 0.61	10.8 ± 5.6	2.00 ±1.72	2.75 ± 1.28	89.3 ± 0.4

[a] These values are averages of less than 3 values in the interval range, and so are reported without standard deviation.

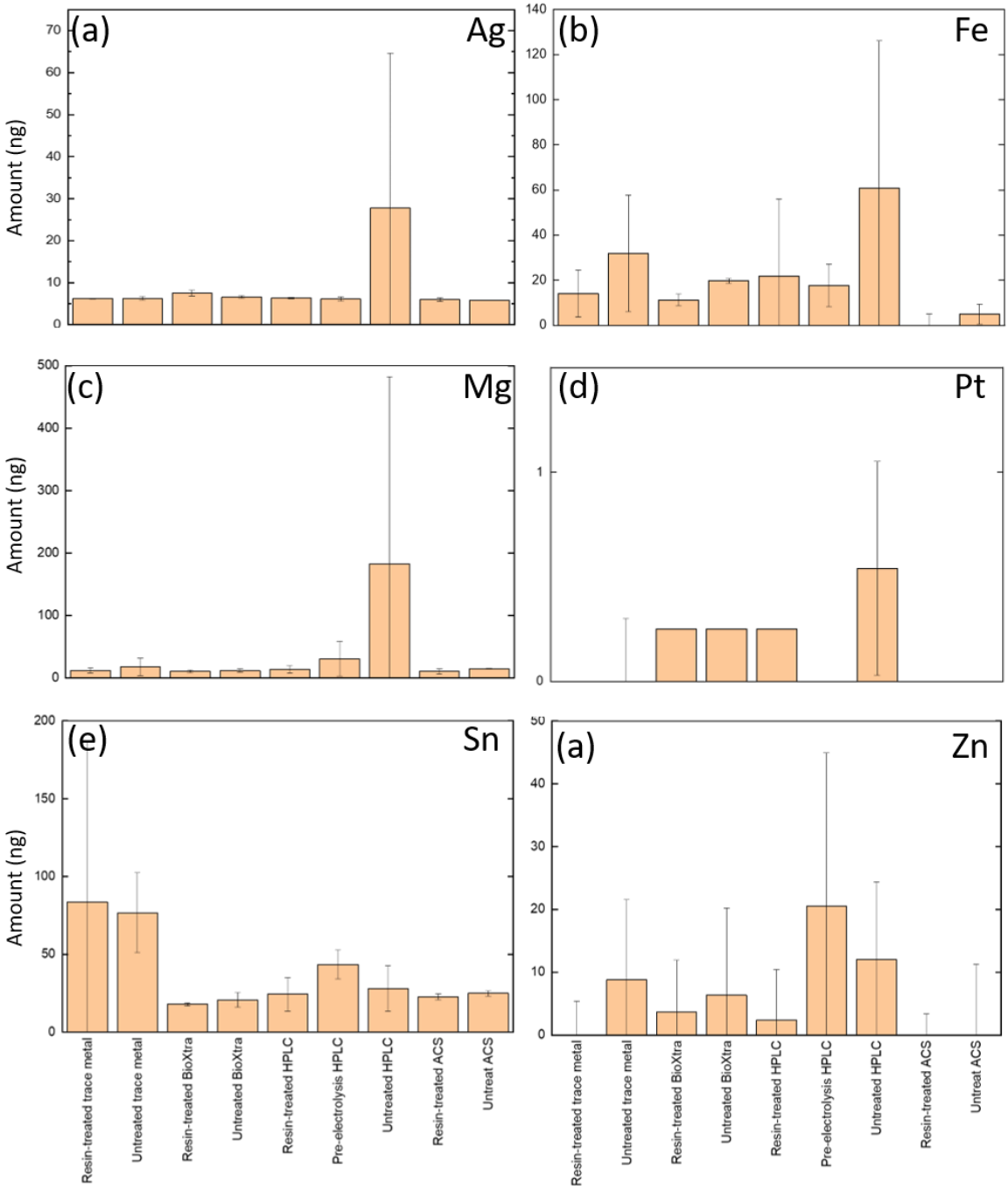

Figure 0-4 (a) Ag (b) Fe (c) Mg (d) Pt (e) Sn and (f) Zn etched from Cu after CO_2RR under standard condition + different purity and pre-treatment of electrolytes. Error bars are standard deviations from at least 3 independent measurements. Limit of quantification is 5 ng.

Table 0-30 Metal etched in ng from 99.999% Cu foil after CO_2RR under standard condition + different purity and pre-treatment of bicarbonate electrolyte. Solid samples were etched by 10 mL of 1 M trace metal grade HNO_3. Limit of quantification is 5 ng in 10 mL sample (50 ng for Fe).

Sample	Ag	Al	Co	Cu	Fe	Mg	Ni	Pb	Pt	Ru	Sn	Zn
Resin-treated trace metal	6.2 ± 0.1	233.0 ± 132.5	6.1 ± 0.0	saturated	14.1 ± 10.3	12.2 ± 4.2	11.5 ± 13.2	6.6 ± 1.3	0.1 ± 0.3	6.0 ± 2.3	83.6 ± 102.9	-1.0 ± 5.4
Untreated trace metal	6.3 ± 0.4	168.7 ± 113.6	6.1 ± 0.1	saturated	31.9 ± 25.8	18.0 ± 14.4	12.6 ± 21.9	5.3 ± 1.2	0.0 ± 0.3	5.8 ± 1.9	76.6 ± 25.6	8.8 ± 12.8
Resin-treated BioXtra	7.5 ± 0.8	262.9 ± 70.5	6.1 ± 0.1	saturated	11.3 ± 2.7	11.0 ± 2.2	1.8 ± 1.1	5.2 ± 0.3	0.2 ± 0.0	-4.5 ± 4.5	17.8 ± 0.9	3.6 ± 8.3
Untreated BioXtra	6.6 ± 0.3	419.2 ± 162.5	6.1 ± 0.1	saturated	19.8 ± 1.1	12.0 ± 2.9	9.0 ± 5.8	6.1 ± 0.4	0.2 ± 0.0	-5.6 ± 6.7	20.6 ± 4.7	6.3 ± 13.9
Resin-treated HPLC	6.4 ± 0.2	337.6 ± 140.6	6.2 ± 0.1	saturated	21.7 ± 34.2	13.9 ± 6.0	8.4 ± 4.4	6.0 ± 0.8	0.2 ± 0.0	7.7 ± 0.9	24.2 ± 10.7	2.4 ± 8.0
Pre-electrolysis HPLC	6.1 ± 0.5	586.3 ± 164.6	6.2 ± 0.0	saturated	17.7 ± 9.4	30.8 ± 27.5	57.1 ± 9.6	5.5 ± 1.3	-0.2 ± 0.1	4.1 ± 4.4	43.4 ± 9.5	20.5 ± 24.4
Untreated HPLC	27.8 ± 36.8	288.7 ±151.3	7.8 ± 3.1	saturated	60.8 ± 65.2	183.2 ± 299.3	8.3 ± 9.1	15.4 ± 14.0	0.5 ± 0.5	-9.3 ± 1.5	28.0 ± 14.5	12.0 ± 12.4
Resin-treated ACS	6.0 ± 0.4	163.7 ± 271.8	6.0 ± 0.1	saturated	0.0 ± 5.0	11.1 ± 4.3	27.2 ± 4.3	5.7 ± 1.2	-0.2 ± 0.0	2.2 ± 3.9	22.6 ± 1.8	11.5 ± 14.7
Untreated ACS	5.8 ± 0.0	564.9 ± 61.5	6.0 ± 0.1	saturated	4.9 ± 4.5	14.9 ± 0.7	53.1 ± 19.3	10.3 ± 2.3	-0.4 ± 0.0	4.8 ± 1.5	24.8 ± 1.9	-0.8 ± 11.3
Cu Before CO_2RR	5.3 ± 1.0	177.4 ± 291.4	3.8 ± 2.6	saturated	44.6 ± 26.8	18.5 ± 3.5	51.3 ± 33.6	1.9 ± 2.0	5.0 ± 4.1	-4.9 ± 11.6	6.4 ± 1.4	5.1 ± 4.4

Chapter 4 Data

Table 0-31 Product Faradaic efficiencies of CO_2RR using glassy carbon electrodes under 0.1 M untreated BioXtra grade $KHCO_3$, with Nafion as the membrane and carbon rod as the auxiliary electrode.

Potential / V vs SCE	H_2	**CO**	Total
–1.60	37.9 ± 7.6	0 ± 0	37.9 ± 7.6

Table 0-32 Product Faradaic efficiencies of CO_2RR using glassy carbon electrodes with 0.04% P4VP under 0.1 M untreated BioXtra grade $KHCO_3$, with Nafion as the membrane and carbon rod as the auxiliary electrode.

Potential / V vs SCE	H_2	**CO**	Total
–1.60	37.4 ± 3.0	0 ± 0	37.4 ± 3.0

Table 0-33 Product Faradaic efficiencies of Au CO_2RR under 0.1 M untreated BioXtra grade $KHCO_3$, with Nafion as the membrane and carbon rod as the auxiliary electrode.

Potential / V vs SCE	H_2	**CO**	Total
–1.40	17.3 ± 9.6	51.5 ± 8.8	68.8 ± 12.5
–1.60	8.74 ± 2.30	70.6 ± 14.1	79.4 ± 12.1
–1.80	14.5 ± 4.5	70.7 ± 15.7	85.1 ± 14.3

Table 0-34 Product Faradaic efficiencies of Au CO_2RR with 0.04% P4VP under 0.1 M untreated BioXtra grade $KHCO_3$, with Nafion as the membrane and carbon rod as the auxiliary electrode.

Potential / V vs SCE	H_2	**CO**	Total
–1.60	25.1 ± 7.7	11.0 ± 6.9	36.1 ± 0.8

Table 0-35 Product Faradaic efficiencies of Au CO_2RR with 0.1% P4VP under 0.1 M untreated BioXtra grade $KHCO_3$, with Nafion as the membrane and carbon rod as the auxiliary electrode.

Potential / V vs SCE	H_2	**CO**	Total
–1.60	7.5 ± 2.5	28.0 ± 4.5	35.4 ± 5.7

Table 0-36 Product Faradaic efficiencies of Au CO_2RR with 1.0% P4VP under 0.1 M untreated BioXtra grade $KHCO_3$, with Nafion as the membrane and carbon rod as the auxiliary electrode.

Potential / V vs SCE	H_2	**CO**	Total
–1.40	11.6 ± 7.2	45.7 ± 17.0	57.3 ± 9.8
–1.60	13.5 ± 5.4	45.3 ± 14.7	58.7 ± 14.5
–1.80	25.2 ± 11.1	37.7 ± 7.8	51.8 ± 18.2

Table 0-37 Product Faradaic efficiencies of CO_2RR using glassy carbon electrodes with 0.04% P4VP and 0.02% Au under 0.1 M untreated BioXtra grade $KHCO_3$, with Nafion as the membrane and carbon rod as the auxiliary electrode.

Potential / V vs SCE	H_2	**CO**	Total
–1.60	32.6 ± 13.3	0 ± 0	32.6 ± 13.3

Table 0-38 Product Faradaic efficiencies of CO_2RR using glassy carbon electrodes with 0.04% P4VP and 0.16% Au under 0.1 M untreated BioXtra grade $KHCO_3$, with Nafion as the membrane and carbon rod as the auxiliary electrode.

Potential / V vs SCE	H_2	**CO**	Total
–1.60	60.0 ± 12.0	0 ± 0	60.0 ± 12.0

Table 0-39 Product Faradaic efficiencies of CO_2RR using glassy carbon electrodes with 0.04% P4VP and 0.32% Au under 0.1 M untreated BioXtra grade $KHCO_3$, with Nafion as the membrane and carbon rod as the auxiliary electrode.

Potential / V vs SCE	H_2	**CO**	Total
–1.60	41.8 ± 0.8	14.9 ± 0.1	56.7 ± 0.7

A.3 References

(11) Kuhl, K. P.; Cave, E. R.; Abram, D. N.; Jaramillo, T. F. "New insights into the electrochemical reduction of carbon dioxide on metallic copper surfaces," *Energy & Environmental Science* **2012**, *5*. http://dx.doi.org/10.1039/c2ee21234j

(73) Wuttig, A.; Surendranath, Y. "Impurity Ion Complexation Enhances Carbon Dioxide Reduction Catalysis," *ACS Catalysis* **2015**, *5*, 4479-4484. http://dx.doi.org/10.1021/acscatal.5b00808